Molecular Beam Epitaxial Growth and Characterization of AlGaN Epilayers for Vertical Deep Ultraviolet LEDs on Silicon

Qihua Zhang

Department of Electrical and Computer Engineering
Faculty of Engineering
McGill University, Montreal

April 2023

A thesis submitted to McGill University in partial fulfillment of the requirements of the degree of Doctor of Philosophy

To my fiancée, Sophia, my Mom and Dad, my Pop-pop and Mee-maw~

TABLE OF CONTENTS

ACKNOWLEDGEMENT

This thesis is and has always been a result of excellent teamwork, which could never have occurred without the support of many great people, who have all stood alongside me during this journey and provided the much-needed help and guidance.

I would first express my ultimate gratitude to my supervisor Prof. Songrui Zhao for his consistent support and guidance, in both research and mentality. He has always made himself available for research discussions, coming up with project ideas, and designing experiments. I am also ultimately grateful for my committee members, Prof. Martin Rochette and Prof. Patanjali Kambhampati, for their insightful suggestions and challenging comments during my course of study.

I would also like to thank Dr. Patrick Daoust of Polytechnique Montréal, for his help on training and providing guidance with the X-ray diffraction facility. Moreover, I would also like to acknowledge many professional staffs of McGill University, including Dr. Zhao Lu, Mr. Jun Li, Mr. Peng Yang, Dr. S Kelly Sears, and Dr. David Liu, who have all provided professional training and suggestions on McGill Nanotools Microfab laboratory and Facility for Electron Microscopy Research.

I would also express my gratitude to many collaborators, Eli Martel and Prof. Thomas Szkopek, for their help and providing the atomic force microscopy, as well as Jenaes Sivasundarampillai and Prof. Matthew J. Harrington for their assistance on the Raman experiments. Additionally, special thanks to Eli for his help on translations of French abstract.

I am more than indebted to my teammates, Xue Yin and Jiaying Lu, for teaching and helping me with photoluminescence experiments, as well as Heemal Parimoo and Mohammad Fazel Vafadar for their generous help on undergoing multiple rounds of device fabrications.

Lastly, I would like to thank my parents, my fiancé, my uncles and aunts, for their generous support and strong belief in me. More importantly, I would like to give my utmost gratitude to my grandfather, who shaped me to become compassionate and resilient; and my grandmother, who is watching from heaven, for teaching me to always stay humble and grateful.

This work was supported by Natural Sciences and Engineering Research Council of Canada (NSERC) and Fonds de Recherche du Quebec – Nature et Technologies (FRQNT).

CONTRIBUTIONS OF AUTHORS

This thesis consists of manuscripts that have been published during the PhD study of the candidate. Each manuscript involves contributions from the candidate and other individuals. The following denotes the detailed contributions of authors for the manuscript-based chapters.

For Chapter 3, the candidate performed sample growths with suggestions from Prof. Songrui Zhao, conducted experiments including scanning electron microscopy, potassium hydroxide etching, photoluminescence, current-voltage characteristics, and electroluminescence. Eli Martel performed atomic force microscopy. Heemal Parimoo fabricated light emitting diode devices. Prof. Songrui Zhao conceived the project idea and supervised the data analysis. The manuscript was written by the candidate and Prof. Songrui Zhao.

For Chapter 4, the candidate performed sample growths with suggestions from Prof. Songrui Zhao, conducted experiments and analysis including X-ray crystallography, scanning electron microscopy, photoluminescence, current-voltage characteristics, and electroluminescence. Heemal Parimoo and the candidate fabricated light emitting diode devices. Jenaes Sivasundarampillai and the candidate performed Raman spectroscopy. Prof. Songrui Zhao conceived the experiments, supervised the data analysis, and led the project. The manuscript was written by the candidate and Prof. Songrui Zhao.

For Chapter 5, the candidate performed sample growths under the guidance of Prof. Songrui Zhao, conducted simulation analysis, and performed characterizations including scanning electron microscopy, photoluminescence, current-voltage characteristics, and electroluminescence. Heemal Parimoo fabricated light emitting diode devices. Eli Martel performed atomic force microscopy. Prof. Songrui Zhao conceived the experiments, supervised the data analysis, and led the project. The manuscript was written by the candidate and Prof. Songrui Zhao.

For Chapter 6, the candidate performed sample growths with suggestions from Prof. Songrui Zhao, conducted experiments including scanning electron microscopy, photoluminescence, current-voltage characteristics, and electroluminescence. Heemal Parimoo and the candidate fabricated light emitting diode devices. Eli Martel performed atomic force microscopy. Xue Yin performed simulations and performed data analysis. Prof. Songrui Zhao conceived the experiments, supervised the data analysis, and led the project. The manuscript was written by the candidate and Prof. Songrui Zhao.

LIST OF TABLES

LIST OF FIGURES

LIST OF SYMBOLS AND ABBREVIATIONS

2DEG	Two-Dimensional Electron Gas
3D	Three Dimension
AFM	Atomic Force Microscopy
BEP	Beam Equivalent Pressure
CIE	Carrier Injection Efficiency
CW	Continuous Wave
DH	Double Heterojunction
DI	De-Ionized
EBL	Electron Blocking Layer
ECR	Electron Cyclotron Resonance
EL	Electroluminescence
ELO	Epitaxial Lateral Overgrowth
EQE	External Quantum Efficiency
FWHM	Full Width at Half Maximum
HEMT	High Electron Mobility Transistor
HT	High Temperature
IQE	Internal Quantum Efficiency
LD	Laser Diode

LED	Light Emitting Diode
LEE	Light Extraction Efficiency
LISA	Laser Interferometer Space Antenna
LLO	Laser Lift-Off
LT	Low Temperature
MBE	Molecular Beam Epitaxy
ML	Monolayer
MME	Metal-Modulated Epitaxy
MOCVD	Metal Organic Chemical Vapor Deposition
MQW	Multiple Quantum Well
NLOS	Non-Line of Sight
NW	Nanowire
PL	Photoluminescence
QCSE	Quantum Confined Stark Effect
RC	Rocking Curve
RF	Radio Frequency
RHEED	Reflection High-Energy Electron Diffraction
RMS	Root Mean Square
SCCM	Standard Cubic Centimeters per Minute

SEM	Scanning Electron Microscopy
SIMS	Secondary Ion Mass Spectroscopy
TDD	Threading Dislocation Density
TE	Transverse Electric
TEM	Transmission Electron Microscopy
TM	Transverse Magnetic
UID	Unintentionally Doped
UV	Ultraviolet
XRD	X-Ray Diffraction

ABSTRACT

Light emitting didoes (LEDs) through vertical current injection offer numerous advantages including excellent heat dissipation and size scalability. Yet it remains difficult to realize AlGaN *deep ultraviolet* (deep UV, wavelength shorter than 300 nm) LEDs through vertical injection. Silicon (Si) substrates, owing to their excellent conductivity, easy to removal by chemical wet etching, and mature manufacturing process, are a promising platform for developing vertical AlGaN deep UV LEDs. Nevertheless, obtaining high quality AlGaN epilayers on Si substrate has remained a challenge due to the large lattice and thermal mismatch between AlN and Si. In this thesis, we demonstrate a nanowire template assisted buffer layer technology on Si that enables high-quality AlGaN epilayers on Si, which further enables vertical AlGaN deep UV LEDs.

We first perform the molecular beam epitaxial growth and characterization of AlN epilayers on Si substrates using the nanowire template. Highly smooth AlN epilayers with root-mean-square (rms) roughness of less than 0.4 nm are obtained. Our detailed comparison between the AlN epilayers grown on the nanowire template and the AlN epilayers directly on Si confirms that the use of the nanowire template can improve the crystalline quality and relax the tensile stress from Si. Using such AlN buffer layer, AlGaN epilayers with Al content varying from 35% to 70% are developed. The internal quantum efficiency (IQE) for such AlGaN epilayers are in the range of 30 - 40% under low excitations.

With these material developments, vertically injected, surface emitting AlGaN deep UV LEDs down to 247 nm are demonstrated, by far the shortest wavelength for deep UV LEDs on Si with AlGaN epilayers. To further improve the device electrical performance, we have explored the polarization doped AlGaN epilayers on Si by grading the Al content along the growth direction. Vertical LEDs emitting around 278 nm are realized, and with using the polarization enhanced

doping, the device series resistance is reduced by a factor of 5. This thesis work provides a viable path not only for vertical semiconductor deep UV LEDs, but also for low-cost ultrawide bandgap semiconductor template, potentially impact both photonics and electronic devices.

ABRÉGÉ

Les diodes électroluminescentes (DEL) par injection de courant verticale offrent de nombreux avantages, notamment une excellente dissipation de la chaleur et une évolutivité de la taille. Cependant, il est difficile de réaliser des DELs d'AlGaN à ultraviolets profonds (UV profonds, longueur d'onde inférieure à 300 nm) par injection verticale. Les substrats en silicium (Si), en raison de leur excellente conductivité, de leur facilité d'élimination par gravure humide chimique et de leur processus de fabrication mature, constituent une plate-forme prometteuse pour le développement de DELs d'AlGaN à UV profondes verticales. Néanmoins, l'obtention d'épicouches d'AlGaN de haute qualité sur un substrat de Si est restée un défi en raison du grand réseau et de l'inadéquation thermique entre l'AlN et le Si. Dans cette thèse, nous démontrons une technologie de couche tampon assistée par modèle de nanofils sur Si qui permet des épicouches d'AlGaN de haute qualité sur Si, ce qui permet en outre des DELs d'AlGaN à UV profondes verticales.

Nous effectuons d'abord la croissance épitaxiale par faisceau moléculaire et la caractérisation des épicouches d'AlN sur des substrats de Si à l'aide de la matrice de nanofils. Des épicouches d'AlN très lisses avec une rugosité quadratique moyenne (rms) inférieure à 0,4 nm sont obtenues. Notre comparaison détaillée entre les épicouches d'AlN développées sur la matrice de nanofils et les épicouches d'AlN directement sur Si confirme que l'utilisation de la matrice de nanofils peut améliorer la qualité cristalline et relâcher la contrainte de traction de Si. En utilisant une telle couche tampon d'AlN, des épicouches d'AlGaN avec une teneur en Al entre 35% et 70% sont développées. L'efficacité quantique interne (IQE) pour ces épicouches d'AlGaN est de l'ordre de 30% à 40% sous de faibles excitations.

Avec ces développements de matériaux, des DELs d’AlGaN à UV profondes à émission de surface injectées verticalement jusqu'à 247 nm sont démontrées, de loin la longueur d'onde la plus courte pour les DELs à UV profondes sur Si avec des épicouches d’AlGaN. Pour améliorer encore les performances électriques du dispositif, nous avons exploré les épicouches d’AlGaN dopées en polarisation sur Si en graduant la teneur en Al le long de la direction de croissance. Des DELs verticales émettant autour de 278 nm sont réalisées, et avec l'utilisation du dopage amélioré par polarisation, la résistance en série du dispositif est réduite d'un facteur 5. Ce travail de thèse fournit une voie viable non seulement pour les DELs à UV profondes à semi-conducteur verticales, mais aussi pour un modèle de semi-conducteur à bande interdite ultra large moins coûteux, impactant potentiellement à la fois la photonique et les appareils électroniques.

CHAPTER 1.

Introduction

Aluminum gallium nitride (AlGaN), a ternary compound of gallium nitride (GaN) and aluminum nitride (AlN) in the III-nitride semiconductor family, has been intensively studied over the past decades due to its ultrawide, tunable, and direct bandgap energy [1-8]. The excellent physical properties make it an excellent candidate for the developments of heterojunction devices such as Schottky diodes [9-11], high electron mobility transistors (HEMTs) [12-14], as well as optoelectronic devices including light emitting diodes (LEDs) [15-21], laser diodes (LDs) [22-25], and photodetectors [26-29]. In addition, owing to the large chemical bonding energies for both Al-N and Ga-N bonds, AlGaN-based devices are also chemically stable, mechanically strong, and thus suitable to operate in extreme and harsh environment [3, 30].

For LED devices, depending on the current injection path, they can be categorized into vertical current injection LEDs or lateral current injection LEDs. Compared to lateral current injection, vertical current injection offers several benefits, such as minimized local heating, excellent chip size scalability, as well as simple packaging process [31-37]. Yet, realizing vertical LEDs in the deep UV range has been extremely difficult due to a number of limitations which will be discussed in Section 1.5.

In this context, silicon (Si) substrate, owing to its easy removal by chemical wet etching and simple manufacturing process, along with cost-related benefits, has been viewed as a promising candidate for realizing vertical AlGaN deep UV LEDs [24, 38, 39]. However, owing to the large lattice and thermal mismatches between the AlGaN alloy and Si substrate, it is highly challenging to obtain high quality AlGaN epilayers on Si. Surface cracks and large threading dislocation densities (TDDs) are often observed in AlGaN epilayers grown on Si. These challenges will be discussed in Section 1.7.

To improve the quality of AlGaN epilayers on Si, various buffer layer technologies have been developed, including AlN buffer layers by epitaxial lateral overgrowth (ELO), AlN/AlGaN superlattice layers, as well as compositionally graded AlGaN buffer layers [40-51]. With these buffer layers, promising results have been demonstrated. Nonetheless, they are all very thick, and require complex fabrication and long growth processes, making them not ideal for the development of vertical AlGaN deep UV LEDs.

Here, we present a promising method to obtain high quality AlGaN epilayers on Si substrate by molecular beam epitaxy (MBE), using a nanowire-assisted buffer layer consisting of GaN nanowires and an AlN epilayer. Using such a buffer layer, vertical LEDs in the deep UV range with AlGaN epilayers are successfully demonstrated.

This chapter is organized as followings. The importance of deep UV light sources is discussed in Section 1.1, followed by the discussion on the need of AlGaN for deep UV LEDs in Section 1.2. The current status of AlGaN-based UV LEDs is reviewed in Section 1.3. Subsequently, the benefits and current status of vertical LEDs are presented in Section 1.4. In Section 0, the challenges of developing vertical AlGaN deep UV LEDs are discussed. The application of Si for the development of vertical AlGaN deep UV LEDs is then discussed in Section 1.6. In Section 1.7, the challenges in obtaining high quality AlGaN epilayers on Si are discussed in detail. Lastly, the overview and the contribution of this thesis are further provided in Section 1.8 and Section 1.9.

1.1 Importance of Deep UV Light and the Need of Deep UV LEDs

Light sources emitting in the deep UV range ($\lambda < 300$ nm) are of great importance for various applications [21, 52]. For example, large-area deep UV lamps are widely utilized in water processing plants, as they have been found highly effective in the deactivation of pathogens and viruses in drinking water. Sterilizations of appliances, medical supplies, public-area surfaces, as well as personal items have also become emerging areas for the application of deep UV light sources. Moreover, deep UV light sources can also be used for sensing of gas, molecule, DNA, making them great assets in the medical and bio-chemical industry. Deep UV light sources have also become increasingly important in the communication industry, for their applications in non-line-of-sight (NLOS) wireless communication as well as Laser Interferometer Space Antenna (LISA).

To date, the majority of deep UV light sources are dominated by mercury lamps and excimer lamps, e.g., krypton fluoride (KrF) and krypton-chloride (KrCl) lamps. However, not only are these light sources highly power-consuming, but also are they with short operating lifetime. The use of Mercury, which is of toxic nature, poses severe hazard to both human and the environment. Although diode-pumped solid state light sources such as neodymium-doped yttrium aluminum garnet (Nd:YAG) lasers can also emit light in the deep UV range through higher harmonic frequency generations, their bulky size and expensive cost severely limit their applications.

Semiconductor devices, on the other hand, have a number of advantages such as compactness, long lifetime, high energy efficiency, and are suitable for mass production. As such, semiconductor deep UV light sources are an appealing form of deep UV light sources. Among various semiconductor materials, AlGaN is one of the best candidates. By changing the Al content in the AlGaN alloy, the wavelength of AlGaN LEDs can be adjusted from 365 nm down to around

210 nm at room temperature, which widely covers UVA (320 – 400 nm), UVB (280 – 320 nm), and UVC (200 – 280 nm). More importantly, without the use of toxic materials, AlGaN LEDs do not pose any burden to the environment.

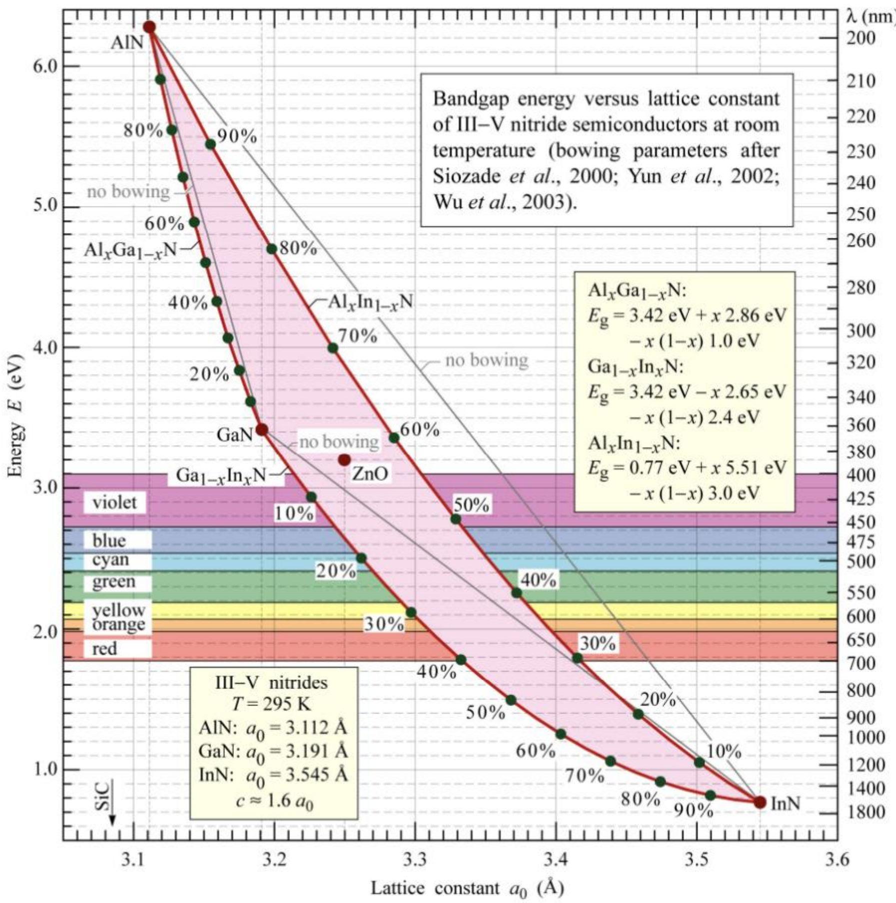

Figure 1-1 Band gap energy vs. lattice constants of III-nitride materials. Reproduced with permission [8]. Copyright 2006, Cambridge University Press.

1.2 Properties of AlGaN and Its Importance for Deep UV LEDs

As a ternary compound alloy in the III-nitride family, AlGaN has a direct energy bandgap. Depending on the Al content (x) of $Al_xGa_{1-x}N$, both the lattice constant and the bandgap energy can be tuned accordingly [2, 52-54]. As illustrated in Figure 1-1, the bandgap energy of $Al_xGa_{1-x}N$ varies from 3.4 eV (GaN, x = 0) up to 6.1 eV (AlN, x = 1) at room temperature. In addition, as the Al content increases, the free exciton (FX) binding energy of AlGaN increases, from 20 meV of GaN up to 80 meV of AlN at room temperature [55-57]. It is also noted that the 80 meV FX binding energy of AlN is also one of the largest among all the bulk materials, which indicates that AlN LED can have a stable emission wavelength at room temperature [58].

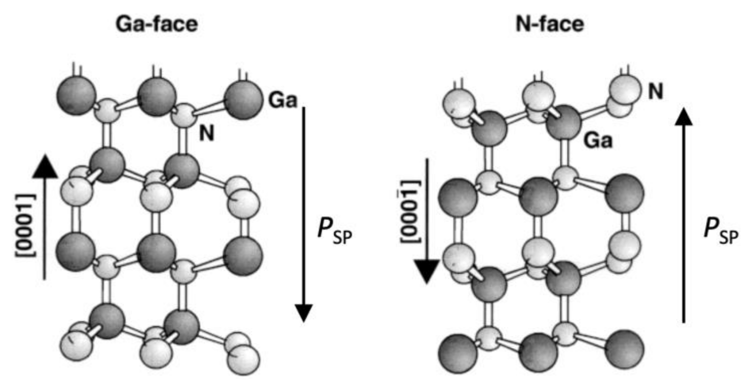

Figure 1-2 Wurtzite GaN structure with metal-polarity (left) and N-polarity (right). The orientation of spontaneous polarization field ($\boldsymbol{P}_{SP}$) is denoted. Reproduced with permission [2]. Copyright 1998, IOP Publishing.

In addition, for wurtzite AlGaN, due to the lack of centrosymmetry, it can have different surface polarities, i.e., whether the surface terminates with metal atoms (Al/Ga) or N. Figure 1-2 illustrates the schematic of wurtzite GaN structure showing metal-polarity (left) or N-polarity (right). In general, the polarity of III-nitrides is dependent on the type of substrate and the growth conditions. For example, the MBE-grown GaN nanowires on Si substrates typically show N-polarity, although mixed polarity has been reported [59-61]. For AlGaN, Al is typically substitutional to Ga site. Depending on the different surface polarity, AlGaN possesses a spontaneous polarization field ($\boldsymbol{P}_{SP}$) either parallel or anti-parallel to the *c*-axis as denoted in Figure 1-2.

The strain (compressive or tensile) of AlGaN further induces a piezoelectric polarization field ($\boldsymbol{P}_{\mathrm{PE}}$) along the c-axis (parallel or anti-parallel), which is related to the strained lattice constant (a), relaxed lattice constant (a_0), piezoelectric constant (e_{33}, e_{31}), and elastic constants (C_{13}, C_{33}) by the following equation [62]:

$$\boldsymbol{P}_{PE} = 2\frac{a - a_0}{a_0}(e_{31} - e_{33}\frac{C_{13}}{C_{33}})$$

Table 1-1 summarizes the spontaneous polarization, piezoelectric and elastic constant for both AlN and GaN. Figure 1-3 demonstrates an example of the direction of $\boldsymbol{P}_{\mathrm{PE}}$ for a metal-polar AlGaN epilayer grown GaN when AlGaN is experiencing a tensile strain.

Table 1-1 Spontaneous polarization, piezoelectric ($\boldsymbol{e_{33}}$, $\boldsymbol{e_{31}}$) and elastic ($\boldsymbol{C_{13}}$, $\boldsymbol{C_{33}}$) constants for AlN and GaN. Values are referenced in [63, 64].

Constant	**AlN**	**GaN**
P_{SP} [C/m^2]	0.081	0.029
e_{33} [C/m^2]	1.46	0.73
e_{31} [C/m^2]	-0.60	-0.49
C_{13} [GPa]	108	103
C_{33} [GPa]	373	405

The net electric polarization is thus $\boldsymbol{P} = \boldsymbol{P}_{\mathrm{PE}} + \boldsymbol{P}_{\mathrm{SP}}$, suggesting the presence of bound charge (σ) at the interface. For example, in the case shown in Figure 1-3, as the net polarization is pointing towards the GaN layer, a positive bound charge (+σ) at the AlGaN/GaN interface is generated. Due to the requirement of charge neutrality, free electrons are thus induced at the AlGaN/GaN interface to compensate +σ, forming two-dimensional electron gas (2DEG). The generation of 2DEG has pioneered important electronic device designs such as HEMTs [12-14].

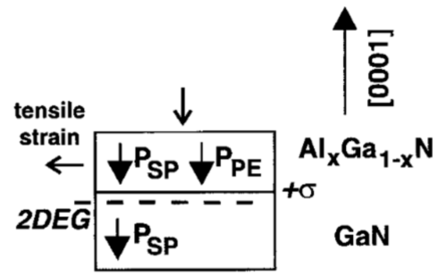

Figure 1-3 Orientation of $\boldsymbol{P}_{SP}$, $\boldsymbol{P}_{PE}$ for metal-polar AlGaN epilayer grown on GaN. Reproduced with permission [62]. Copyright 1999, Wiley-VCH.

Further utilizing these polarization effects, it is possible to obtain free carriers without using impurity doping through grading Al content along the growth direction. Using this polarization doping technique, some of the recent breakthroughs on AlGaN light emitting devices have been achieved, such as the demonstrations of dopant-free polarization-doped AlGaN LEDs [65-68], as well as the first demonstration of deep UV emitting laser diodes [69-71].

1.3 Current Status of AlGaN Deep UV LEDs

To date, AlGaN deep UV LEDs are mainly through *lateral injection*, and their optical performance is typically evaluated by external quantum efficiency (EQE), which is defined as the product of internal quantum efficiency (IQE), carrier injection efficiency (CIE), and light extraction efficiency (LEE). Table 1-2 defines all the four parameters. It is noted that, experimentally, relative EQE, defined as the ratio of the integrated electroluminescence (EL) intensity to the injected current, is also commonly used to study the performance characteristics of LEDs, such as efficiency droop.

Table 1-2 Definitions of EQE, IQE, CIE, LEE of a LED device.

Efficiency	Definition
EQE	$\frac{\#\ photons\ emitted\ into\ free\ space\ per\ second}{\#\ electrons\ injected\ into\ LED\ per\ second}$
IQE	$\frac{\#\ photons\ emitted\ from\ active\ region\ per\ second}{\#\ electrons\ injected\ into\ active\ region\ per\ second}$
CIE	$\frac{\#\ electrons\ injected\ into\ active\ region\ per\ second}{\#\ electrons\ injected\ into\ LED\ per\ second}$
LEE	$\frac{\#\ photons\ emitted\ into\ free\ space\ per\ second}{\#\ electrons\ emitted\ from\ active\ region\ per\ second}$

Figure 1-4 shows the EQE of the current state-of-the-art LEDs covering from the UVA to the UVC spectral range [52]. It is seen that the highest EQE in the deep UV range is 20.3%, which was reported by Takano *et al.* from AlGaN quantum well LEDs emitting at 275 nm [72]. The authors employed a series of light extraction features including using transparent contact layer, Rhodium (Rh) mirror electrode, and encapsulation resin to improve the EQE of the device. On the other hand, this is one of the very few reports in which the EQE is above 10% [72-76]. As the emission wavelength reduces, the EQE generally decreases, and for emission wavelengths shorter than 250 nm, the EQE is typically below 2% [77-83]. Currently, the shortest emission wavelength demonstrated is around 210 nm, which is from AlN p-i-n homojunctions. The peak EQE at this wavelength is extremely low (~10^{-4}%) [84].

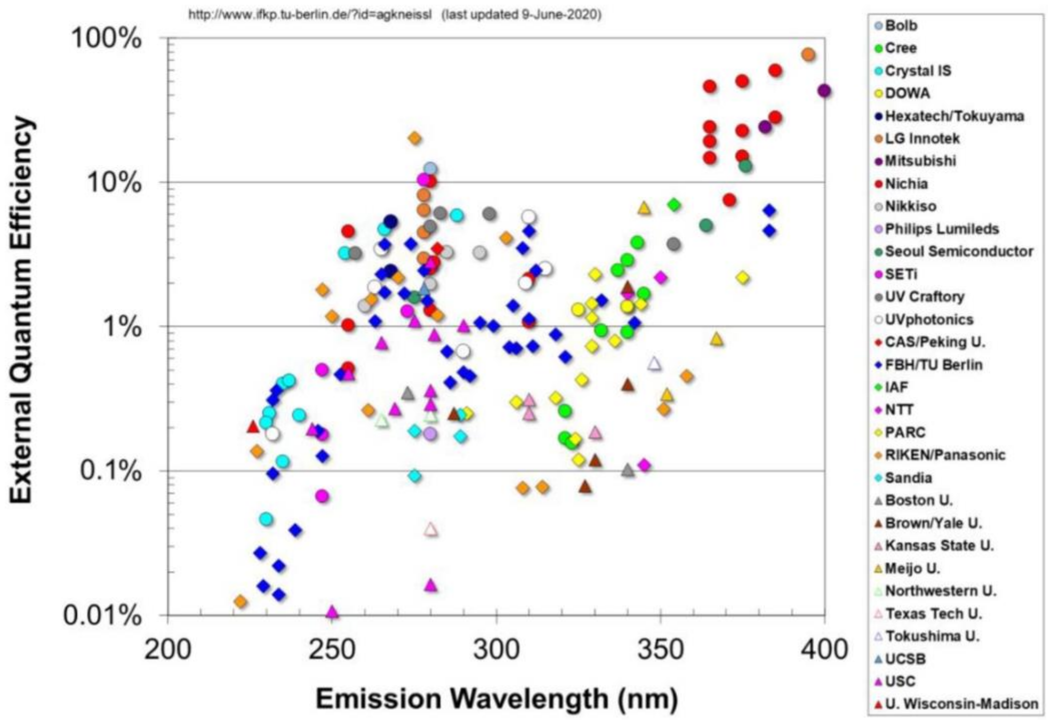

Figure 1-4 Diagram of reported EQEs of LEDs in the UV spectrum. Reproduced with permission [52]. Copyright 2020, IOP Publishing.

There are a number of challenges associated with the efficiency decrease in deep UV range. The primary challenge is the lack of suitable substrates. Currently, the majority of AlGaN LED structures are grown on foreign substrates, e.g., sapphire or silicon carbide (6H-SiC), both of which exhibit large lattice mismatches (as presented in Table 1-3) and thus result in large TDDs in AlGaN epilayers [85-87]. Although commercial bulk AlN substrate has been available, but the extremely high wafer cost is still a penalty at the time of this thesis writing [88]. Moreover, the difficulties to achieve efficient n-type and p-type doping in high Al-content AlGaN epilayers is another major reason to the efficiency decrease. Detailed analysis regarding to the doping challenge is further elucidated in Section 1.5. Lastly, the light polarization change from transverse-electric (TE) to transverse-magnetic (TM) as the wavelength gets shorter also limits the light extraction from the device top surface of the typical *c*-plane LEDs and thus leads to the efficiency decrease. More details will be discussed in Chapter 7.

It is worth noting that, in recent years, significant progress is made in AlGaN nanowire UV LEDs, including AlN nanowire LEDs emitting at 207-210 nm with superior electrical performance [89, 90]. In addition, the use of nanowires as a template for epilayer growth has the potential to improve the crystal quality and relax the lattice strain in AlGaN epilayers. The benefits of nanowires, along with the mechanism of III-nitride nanowire growth, will be discussed in detail in Section 2.3.

Table 1-3 Lattice constant and thermal expansion coefficient of AlN, GaN, Si (111), *c*-plane sapphire, and 6H-SiC. Values are referenced in [2, 5, 17].

Material	AlN	GaN	Si (111)	*c*-plane sapphire	6H-SiC
Lattice constant a_0(Å)	3.112	3.189	3.840	4.758	3.081
Lattice constant c_0(Å)	4.982	5.185	-	12.991	15.117
Thermal expansion coefficient (10^{-6} K^{-1})	4.15	5.59	2.6	7.3	4.46

1.4 Status of Vertical AlGaN Deep UV LEDs

1.4.1 Benefits of LEDs Operating under Vertical Current Injection

A major challenge in LEDs with lateral injection geometry is that they suffer severely from current crowding effect. Figure 1-5(a) shows the schematic structure of LED devices with a lateral current injection geometry. It is seen that the majority of the current crowds at the edge of the p-contact next to the n-type contact. As a consequence, lateral LEDs often suffer severely from local heating as well as nonuniform light emission. On the other hand, devices with a vertical current injection geometry, as schematically shown in Figure 1-5(b), can operate under a much more uniform current injection across the entire mesa area, making them suffer very minimally from the current crowding effect, which further translates to the reduced local heating and uniform light emission [31-33]. Moreover, vertical injection geometry has additional benefits such as reduced device series resistance and improved device lifetime. In addition, for vertical LEDs, the device packaging process is much less complex, and the size of the LED chips can be scaled up to as large as 1×1 mm^2 [34-37].

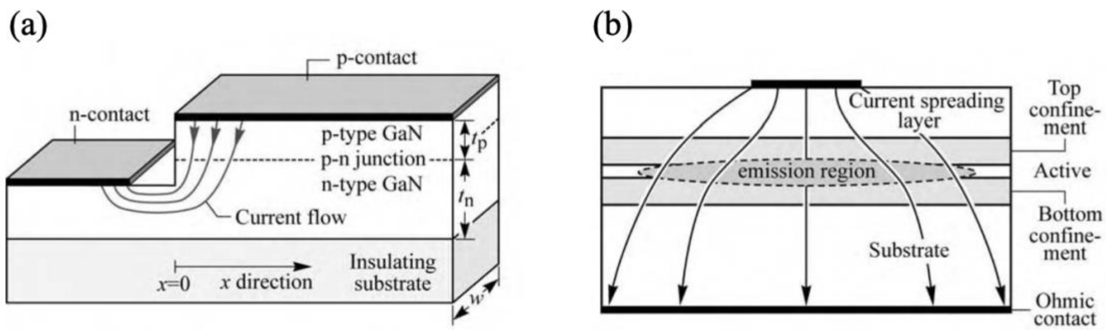

Figure 1-5 Schematics of LEDs with (a) lateral current injection geometry and (b) vertical current injection geometry. (a-b) Reproduced with permission [8]. Copyright 2006, Cambridge University Press.

1.4.2 Current Status of AlGaN Vertical LEDs in Deep UV Range

In general, to realize vertically-injected LEDs, two approaches (considered from electrical conduction viewpoint) can be used: growth of LED structures on conductive substrates and the removal of insulating substrates. The commonly available conductive substrates include n-GaN substrates and n-SiC substrates [87, 91]. However, there is little success in realizing vertical deep UV LEDs on these conductive substrates. For example, there is no report of vertical AlGaN deep UV LED on GaN substrate, whereas on SiC substrate, the only report, to the best of the author's knowledge, is from Liang *et al.*, who demonstrated 288 nm emitting vertically-injected LED, but did not report related device performance [92].

For insulating substrates, the widely used one is sapphire. To further fabricate AlGaN vertical deep UV LEDs, sapphire is removed through a laser lift-off (LLO) process. Compared to using conductive substrates, there have been a few demonstrations of vertical AlGaN deep UV LEDs using sapphire, e.g., Refs. [32, 33, 93, 94]. The first demonstration was reported by Zhou *et al.*, who showed a 280-nm emitting vertical AlGaN LEDs with sub-milliwatt optical output power by removing the GaN buffer layer and sapphire substrate using the LLO process (schematically shown in Figure 1-6(a)) [33]. In addition, several research teams have also demonstrated the LLO process to separate the sapphire substrate from device structure using AlN/AlGaN superlattice as a sacrificial layer [32, 93, 94]. For example, using a 200-nm thick AlN/$Al_{0.5}Ga_{0.5}N$ superlattice as the sacrificial layer for the LLO process, Sung *et al.* reported highly efficient vertical LEDs emitting at 277 nm (schematically shown in Figure 1-6(b)) with an EQE up to 8.61% [93]. Nonetheless, compared to lateral AlGaN deep UV LEDs, vertical LEDs are much less studied, and the shortest emission wavelength has been limited to around 280 nm. The challenges related to the LLO process, as well as the limitations related to the use of conductive substrates, will both be discussed in Section 1.5.3.

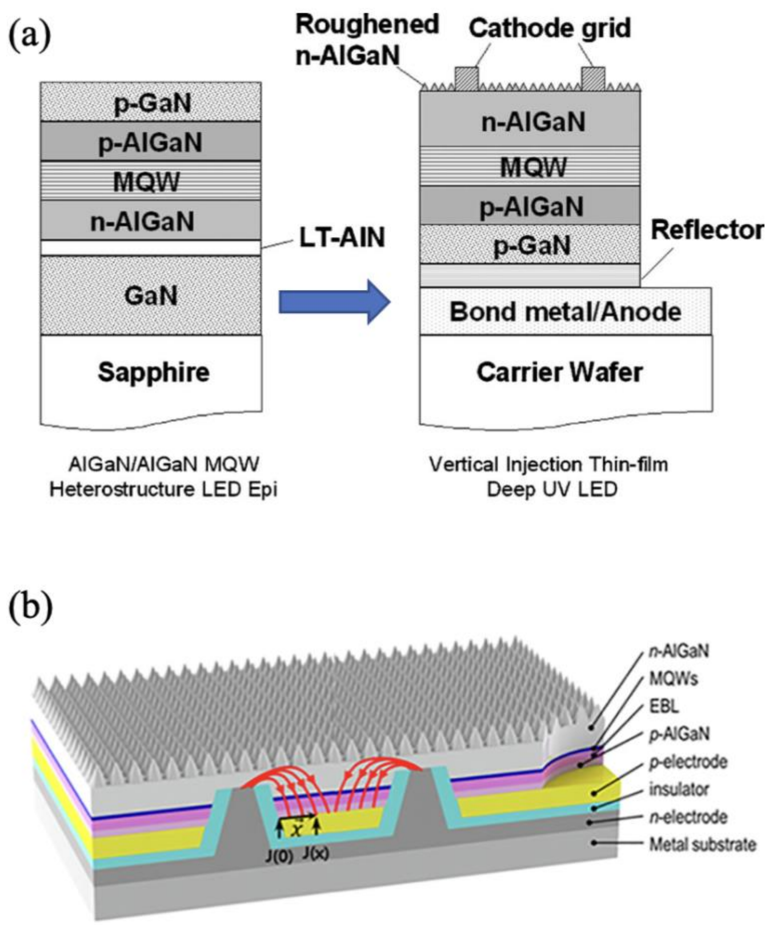

Figure 1-6 (a) Schematic of AlGaN LED structures (left) epitaxially grown on sapphire and (right) fabricated to vertical LEDs using LLO reported by Zhou *et al.* Reproduced with permission [33]. Copyright 2006, AIP Publishing. (b) Schematic of 277 nm emitting vertical LED device reported by Sung *et al.* Reproduced with permission [93]. Copyright 2021, AIP Publishing.

1.5 Challenges in Developing AlGaN Vertical Deep UV LEDs

In this section, challenges related to the material properties of AlGaN, e.g., poor electrical doping, which limits the achieving of highly conductive n-type AlN or high Al-content AlGaN layers, are presented first. The challenge in p-type doping, which not only limits the development of vertical AlGaN deep UV LEDs, but also is a general challenge for AlGaN-based deep UV LEDs, are discussed subsequently. This is followed by the discussion on the fabrication challenges for vertical AlGaN deep UV LEDs, including the limitations of using conductive substrates and the difficulties in performing LLO.

1.5.1 *Doping Challenges for high Al content n-AlGaN*

Although highly conductive n-GaN and low Al-content AlGaN layers have been reported, achieving highly conductive high Al-content AlGaN and AlN epilayers with large free electron concentrations has remained as a challenge [95-98]. For n-type AlGaN epilayers, Si has been widely chosen as the n-type dopant, considering the closely matched atomic radii between Si and Al [99-101]. Figure 1-7 presents the activation energy of Si dopants in high Al-content AlGaN epilayers. It is seen that for AlGaN epilayers with Al contents less than 85 mol%, the Si dopant activation energy remain low, less than 50 meV, meaning a large ratio of dopant ionization and low resistivity can be realized in the epilayer at room temperature. Take n-type $Al_{0.81}Ga_{0.19}N$ epilayer as an example, the Si dopant activation energy is as low as 15 meV, thus large free electron concentrations up to 10^{19} cm^{-3} and resistivity as low as 0.026 Ω·cm can be achieved [97].

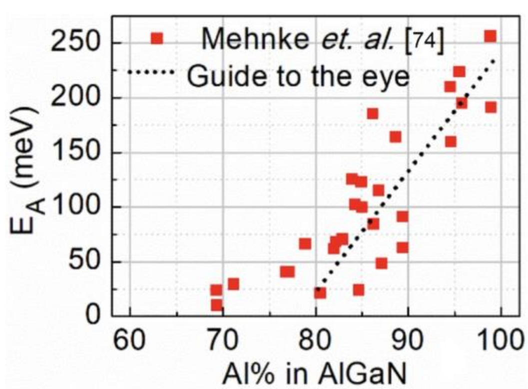

Figure 1-7 Activation energy (E_A) of Si dopant in high Al-content AlGaN epilayers. Reproduced with permission [21]. Copyright 2020, IOP Publishing.

However, for AlGaN epilayers with Al content over 85 mol%, the dopant activation energy increases drastically. For Si-doped AlN, the measured Si dopant activation energy (180 – 280 meV) [96, 102, 103] is significantly higher than the theoretical value, which is in the range of 75 – 95 meV [95, 101]. This huge disagreement is mainly attributed to the presence of point defects related to Al vacancies, such as $(V_{Al})^{3-}$, Al vacancy carrying three negative charges, and $(V_{Al}\ \mathrm{complex})^{2-}$, Al vacancy complex with two negative charges [104, 105]. These defects are considered as deep-level acceptors which reduce the free electron concentrations. It is also reported that at high Si doping levels, Si forms DX center with $(V_{Al})^{3-}$, which results in self-compensation of Si dopant [103]. Worsening the issue, an increase in dislocation densities has led to a higher magnitude of self-compensation [103]. Other defects such as Si_N antistites also possess acceptor-like feature that limit free electron concentrations [106-108]. As such, in the extreme case for Si-doped n-type AlN epilayers, the resistivity remains larger than 10 Ω·cm at room temperature [109].

1.5.2 Doping Challenges for p-AlGaN

The p-type doping in AlGaN epilayers remains as a major challenge, not only for the development of vertical deep UV LEDs, but also for all devices employing p-type AlGaN epilayers. To date, p-type dopants such as magnesium (Mg), beryllium (Be), zinc (Zn), calcium (Ca) have been investigated as the dopant choice for AlGaN alloy [110-114]. Mg remains the most widely-used p-type dopant for AlGaN. However, due to the large hole effective mass in AlGaN, the Mg activation energy is large (up to around 600 meV for AlN) [110, 111]. As such, only a small percentage of Mg dopant can be ionized in p-AlGaN epilayers at room temperature. In Table 1-4**,** a list of free hole concentrations, Mg doping concentrations, Mg dopant activation energy, and room temperature resistivities of p-type AlGaN epilayers with various Al content are summarized.

Table 1-4 Summary of free hole concentrations, Mg doping concentrations, Mg dopant activation energy, and resistivity of p-type AlGaN epilayers with various Al content.

Al content	Mg doping concentration (cm^{-3})	Free hole concentration (cm^{-3})	Dopant Activation Energy (meV)	Resistivity (Ω·cm)	Reference
1	2×10^{19}	1×10^{10}	630	$>1\times10^{8}$	[84]
0.7	5×10^{19}	6×10^{17}	220	1.9	[123]
0.6	2×10^{19}	3×10^{18}	360	10	[124]
0.4	2×10^{19}	4.75×10^{18}	172	Not measured	[125]
0.27	1×10^{20}	2.3×10^{19}	Not measured	1.2	[121]
0	$\sim2\times10^{20}$	1.9×10^{19}	43	0.19	[122]

A number of reasons are associated with the large activation energy in Mg-doped AlGaN epilayers. First, the growth environment of AlGaN epilayers generally incurs a number of impurities such as Carbon (C), Oxygen (O), and hydrogen (H). Both C and O are electron donors for AlGaN, making such epilayers with large background doping concentrations [115-118]. The presence of H in the growth environment also leads to formations of Mg-H complexes, which further suppress the activation of Mg dopants [119]. These issues are found drastically severe in AlGaN epilayers grown by metal-organic chemical vapor deposition (MOCVD); yet for AlGaN grown by MBE, these impurities can be effectively minimized, thus AlGaN epilayers with higher hole concentrations can be obtained [120-123].

Compensating defects are another reason that limit free hole concentration in p-type AlGaN. Nitrogen vacancies carrying three positive charges (V_N^{3+}) are deep-level donors that induce V_N^{3+}-Mg deep-level transitions, which neutralize Mg acceptors and lower the conductivity of p-AlGaN epilayer [118, 126, 127]. The increase in nitrogen vacancies has also been linked to alter the strain of AlGaN epilayers, turning them from compressive-strained to tensile-strained, which further limit Mg incorporation [128]. Furthermore, recent studies have also reported the diffusion of Mg dopants along dislocations, forming Mg-to-screw-dislocation (Mg-TSD) complexes, which turn the p-type epilayer into n-type [129, 130]. Such complexes further lead to large reverse bias leakage current [131]. Worsening the issues, as the doping level of Mg increases, the formations of inversion domains have also been observed, which can cause structural degradation that severely decreases the conductivity of the p-type AlGaN epilayers [132, 133].

It is worthy to note that, very recently, high free hole concentrations of ~3×10^{18} cm^{-3} and a low dopant activation energy (37 meV) were reported in Be-doped AlN epilayers grown by metal-modulated epitaxy (MME) [98, 134], which looks promising for solving the p-type doping challenge.

1.5.3 Fabrication Challenges for Deep UV Vertical LEDs

The unviability of high Al content AlGaN substrates and the electrical doping challenges in high Al content AlGaN essentially limit the choices of substrates to GaN, SiC, and sapphire. However, although n-GaN bulk substrates are highly conductive, there is an up to 2.4% lattice mismatch with AlGaN [2]. The tensile strain induced during the growth of AlGaN epilayers on

GaN leads to additional issues such as crack formation, making it difficult to have high quality device layers. Although these issues might be mitigated by various buffer layers, the highly absorptive nature of GaN in the deep UV range is a decisive parameter that requires the removal of GaN substrates. For SiC, although the lattice mismatch with AlGaN is reduced, the highly absorptive nature of SiC in the deep UV range also requires the removal of SiC. For sapphire substrate, as it is insulating, removal is also a must.

Nonetheless, different from the LLO process of GaN, the LLO process of AlN or high Al content AlGaN (both of which are required for AlGaN deep UV LEDs) is much more difficult. This is because the high temperature decomposition of AlN during the LLO process generates rigid Al metals on the separated layers, which are not only hard to be removed, but also result in cracks and fractures in the separated layers, e.g., active regions. In addition, LLO process was reported to induce additional point defects as well as screw dislocations in the separated LED structures, which lead to an increase in the reverse-bias leakage current [135-137].

In the past, to alleviate various LLO-related issues, different approaches have been proposed, such as the use of low temperature-AlN insertion layer between the GaN buffer layer and device layers, the use of AlN/AlGaN superlattice sacrificial layer for the LLO process between AlN buffer and device layers, nonetheless, as discussed in Section 1.4.2, the device development has been limited, and moreover, a substrate that can be removed easily is preferred.

1.6 Applications of Si to Vertical AlGaN Deep UV LEDs

The issues related to LLO have made Si substrate an attractive platform for vertical AlGaN LEDs. This is because the removal of Si substrate can be achieved by chemical wet etching, avoiding cracking or performance degrading issues related to LLO process [138, 139]. Moreover, it is undeniable that Si owns the most dominant market in the current semiconductor industries, and large-size (up to 12-inch) Si wafers are readily available [24, 38, 39]. Compared to the other substrates such as sapphire, SiC, GaN and AlN substrates, Si substrate can be acquired at a low cost [17, 24, 140-142]. In specific, the production cost for one Si wafer is only 1/10 of that for sapphire, 1/30 of that for SiC, and 1/100 of that for bulk GaN substrate [142]. In addition, compared to sapphire, Si substrate is highly electrically- and thermally-conductive, and both n-type and p-type Si wafers with low resistivity are also available in the market.

In fact, high performance vertical LEDs have already been demonstrated using wet-etching method to remove Si substrates and transferring the GaN-based LED structures onto metal plates or metal substrates [143-146]. For example, Lau *et al.* demonstrated the removal of Si substrates from GaN LED structures (schematically shown in Figure 1-8(a)) using a mixture of acid solutions ($HF:HNO_3:CH_3COOH$) [143]. By transferring the LED structures onto copper (Cu) substrates deposited with reflective metal layers, as shown in Figure 1-8(b), they reported vertical LEDs emitting at around 460 nm. The device optical output power is increased by 5 times compared to that before the transfer process [143]. Recently, using a similar approach for the removal of Si substrates and bonding the LED structures to stacks of metal layers deposited on a new Si wafer, Wang *et al.* reported vertical LEDs emitting at 450 nm with optical output power up to 1 W and a wall plug efficiency (WPE) of 57% [146].

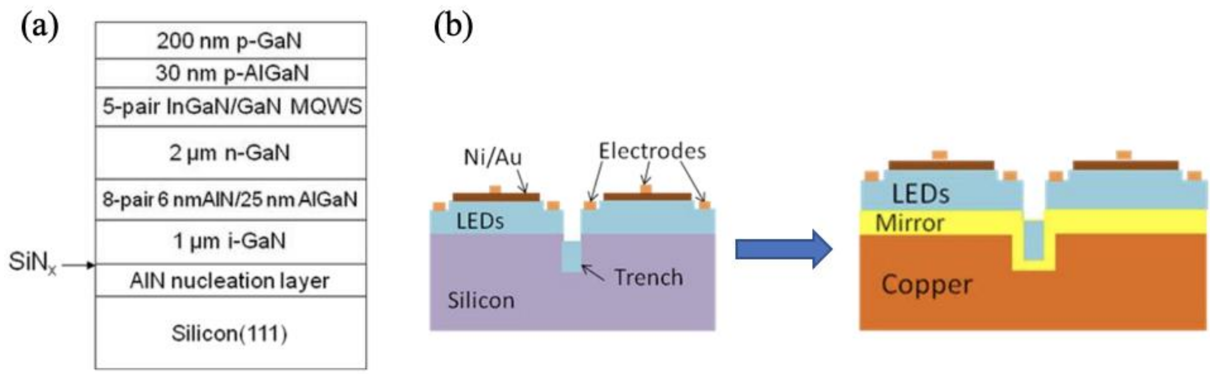

Figure 1-8 (a) Schematic of GaN-based LED structure grown on Si reported by Lau *et al.* (b) Fabrication process for vertical LED devices by bonding the LED structures onto Cu substrate. (a-b) Reproduced with permission [143]. Copyright 2011, Optica Publishing Group.

In addition to being a substrate platform, Si can also serve as a decent light reflector for deep UV light [81, 147]. It is found that, despite Si has a large light absorption coefficient in the deep UV range, the light penetration depth is short (on the order nm range), leading to the majority of deep UV light being reflected rather than absorbed [147, 148]. Substantial improvement in light output power and EQE have been observed by Liu *et al.*, who reported 226 nm emitting AlGaN deep UV LEDs grown on bulk AlN substrates by adopting p-type Si as a reflector [81]. Compared to the LED structure with a 200-nm p-GaN contact layer (Figure 1-9(a)), the LED structure with p-type Si/Al_2O_3/p-GaN heterojunction (Figure 1-9(b)) as the contact layer showed a 60% to 62% improvement in LEE, as demonstrated from the simulated light transmission proportion shown in Figure 1-9(c) [81]. Such device had a maximum output power of 225 μW and a peak EQE of 0.2%, both of which are the highest among LEDs emitting at a similar wavelength.

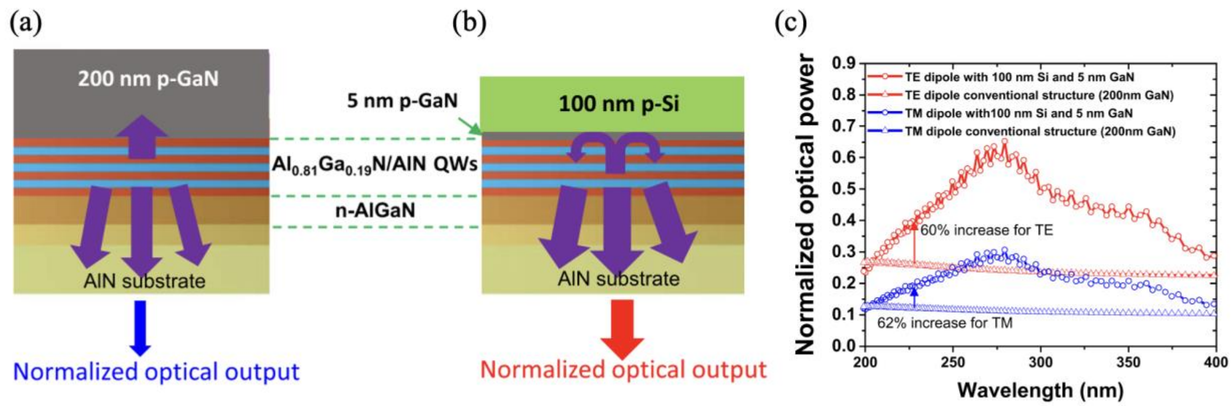

Figure 1-9 (a) Schematic of LED structure with conventional p-GaN contact layer. (b) Schematic of LED structure with p-Si/Al_2O_3/p-GaN as contact layer. (c) Simulated light transmission proportion collected from the bottom (AlN substrate side). (a-c) Reproduced with permission [81]. Copyright 2018, AIP Publishing.

1.7 Challenges of Obtaining High Quality AlGaN Epilayers on Si

Despite of the promises, it remains challenging to obtain high quality AlGaN epilayers on Si substrate. The fundamental limitation is attributed to the large material mismatch, i.e., both the lattice constant and thermal expansion coefficient mismatches between AlGaN alloy and Si. As presented earlier in Table 1-3, the lattice constant mismatch between $Al_xGa_{1-x}N$ and Si (111) substrate ranges from 17% (x = 0) to 19% (x = 1). Tensile strain is generated during the growth of AlGaN epilayers on Si. In addition, a 60% (x = 1) up to 115% (x = 0) mismatch of thermal expansion coefficient exists between AlGaN and Si, which creates more tensile strain during the cooling down process, leading to large TDDs. The typical TDDs are on the order of 10^{10} to 10^{11} cm^{-2} for AlGaN epilayers grown on Si [149-152]. Furthermore, due to the large amount of tensile strain generated, large networks of cracks are also observed on AlGaN epilayers grown on Si substrate [17, 153, 154].

In order to obtain high quality AlGaN epilayers on Si, various buffer layer technologies have been explored [40-51]. Among them, using AlN buffer layers by ELO is by far the most successful one [46-49]. Figure 1-10 describes a detailed wafer preparation process for nano-sized patterns for the ELO-AlN growth [48]. An AlN layer with a thickness of several hundred nm is first grown directly on Si substrates. Subsequently, periodic patterns of various shapes are created on the AlN seed layer. Finally, AlN epilayer is grown on such a patterned substrate by exploiting a coalescence process. Such technique has enabled 2µm-thick ELO-AlN layer on Si with an AlN 0002 XRD rocking curve full-width-at-half-maximum (FWHM) of 499 arcsec [48].

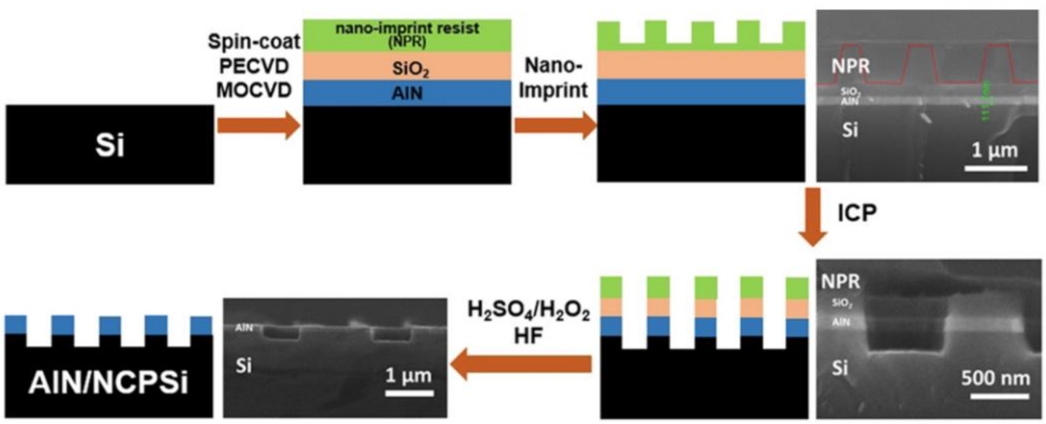

Figure 1-10 Fabrication processes for patterned AlN template for ELO-AlN. Reproduced with permission [48]. Copyright 2020, AIP Publishing.

In the past, ELO-AlN epilayers with low TDDs on the order of 10^7 cm^{-2} and rms roughness of 1.6 nm have also been reported [47, 155]. This has further led to AlGaN deep UV LEDs on Si using such AlN epilayers as buffer layers. For example, using a trench-patterned ELO-AlN buffer layer (Figure 1-11(a)), Mino *et al.* reported AlGaN deep UV LEDs with emission wavelengthes from 278 nm down to 256 nm (Figure 1-11(b)) [51]. It is also notable that 256 nm was by far the shortest emission wavelength from AlGaN deep UV LEDs using AlGaN epilayers on Si prior to this thesis work.

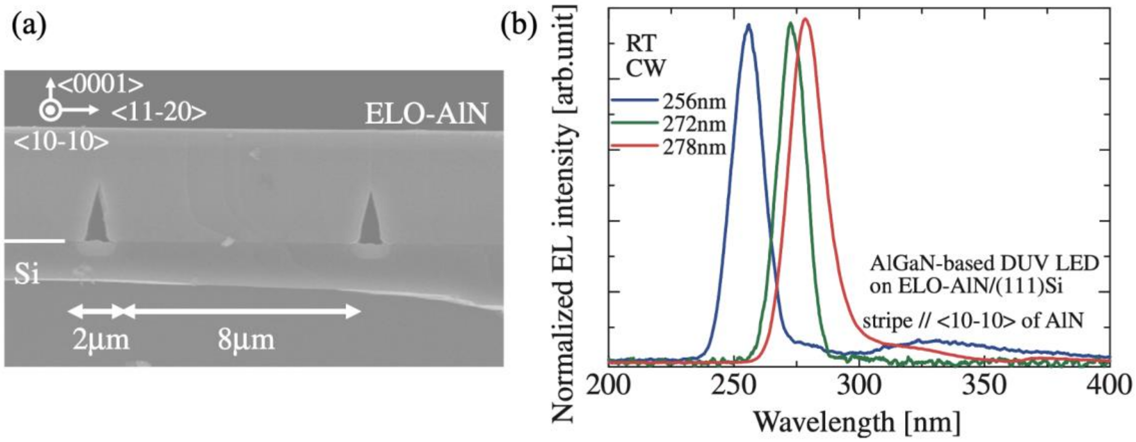

Figure 1-11 (a) SEM image of a trench-patterned ELO-AlN. (b) EL spectra of AlGaN LEDs grown on ELO-AlN buffer layer. Reproduced with permission [51]. Copyright 2011, IOP Publishing.

In addition to ELO-AlN buffer layers, AlN/AlGaN superlattice transitioning layers and compositionally-graded AlGaN layers have also been used and high quality AlGaN epilayers have been reported. For example, using two superlattice transistioning layers consisting of AlN/ $Al_{0.85}Ga_{0.15}N$ and $Al_{0.85}Ga_{0.15}N/Al_{0.6}Ga_{0.4}N$ (schematically shown in Figure 1-12), Huang *et al.* demonstrated a *crack-free* 2-μm-thick $Al_{0.5}Ga_{0.5}N$ epilayer on Si substrate [45]. The as-grown $Al_{0.5}Ga_{0.5}N$ epilayer has a low 0002 rocking curve FWHM of 499 arcsec and a rms roughness of 1.5 nm, both of which are lower than other AlGaN epilayers grown on Si substrate with a similar thickness and Al content [43, 44, 156].

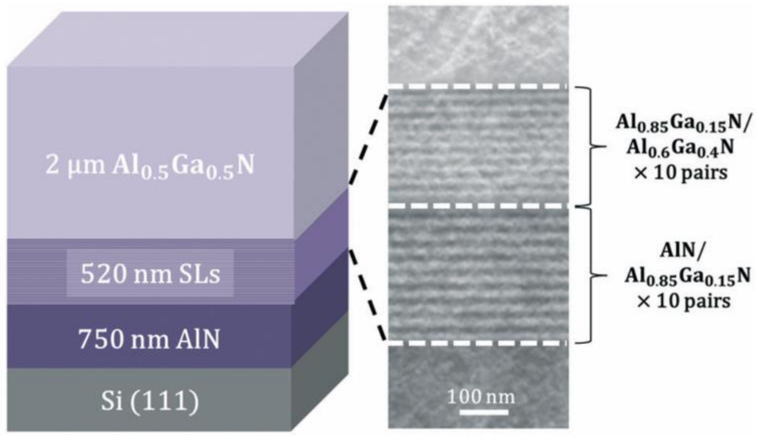

Figure 1-12 Crack-free 2-µm-thick AlGaN epilayer grown on Si using two superlattice transitioning layers. Reproduced with permission [45]. Copyright 2020, ROYAL SOCIETY OF CHEMISTRY.

On the other hand, depsite of the success of these apporaches, they all require thick buffer layers as well as complicated fabrication processes. For example, in the study by Huang *et al.*, a buffer layer (combing AlN and superlattice layers) with thickness over 1µm is used between the top AlGaN epilayer and Si [45], making the growth process highly complicated and time-consuming. In the case of ELO-AlN, several µm thick AlN buffer layer is often required for quality control. For example, the AlGaN LED structures reported by Mino *et al.* are grown on a 4-µm-thick ELO-AlN buffer layer [51]. In addition, the complicated patterned wafer fabrication process is also associated with extra dollar and time costs. As such, a new approach is desirable for the development of vertical AlGaN deep UV LEDs.

1.8 Overview of Thesis

Following the introduction in Chapter 1, in Chapter 2, the main features of MBE system are first discussed. This is followed by a review on AlGaN epitaxy on Si by MBE. The studies on the MBE growth of III-nitride nanowires and their applications to epilayers are also presented.

In Chapter 3, the development of nanowire-assisted AlN epilayers (denoted AlN-on NW) on Si substrate is described. Such AlN epilayer possesses excellent surface morphology, including a highly smooth surface at a near wafer scale (3-inch), with a rms surface roughness of as low as 0.4 nm. Vertically-injected AlGaN deep UV LEDs are further demonstrated on such AlN-on-NW buffer layer. Detailed characterizations on the electrical and optical performance of such AlGaN LEDs are also discussed.

In Chapter 4, the role of nanowires on the crystalline quality and the optical properties of AlN epilayers are further elucidated, by studying AlN-on-NW epilayers under a wide range of growth conditions, in comparison with AlN epilayers grown directly on Si substrate. Various characterizations consistently suggest that, with the use of the nanowire layer, the crystalline quality of AlN epilayers is improved drastically, and the lattice strain of these epilayers can be greatly relaxed. These improved structural properties further transfer to the improved p-type doping and the device performance. The underlying mechanisms are also discussed.

In Chapter 5, the demonstrations of vertical AlGaN deep UV LEDs emitting from 298 nm to 247 nm are presented, through developing AlGaN epilayers with various Al contents on the AlN-on-NW buffer layer.

In Chapter 6, by using polarization doped p-type AlGaN epilayers, AlGaN deep UV LEDs emitting at 278 nm are presented. Enhancements on the electrical performance are also discussed.

In Chapter 7, we further describe the development of far-UVC light emitting AlGaN alloys, given that far-UVC light effectively deactivates pathogens and viruses while is considered safe to human skin exposure. In this regard, both high Al-content (up to 79 mol%) AlGaN epilayers and GaN/AlN stacks are explored. Room temperature far-UVC emissions with wavelength down to 218 nm are demonstrated using GaN/AlN stacks.

In Chapter 8, conclusions are made together with the future developments.

1.9 Contribution of This Thesis Work

In this thesis, a novel approach to obtain high-quality AlN on Si is presented. Using such AlN as buffer layers, device quality AlGaN epilayers are further obtained, which in consequence lead to the demonstrations of vertical AlGaN deep UV LEDs with excellent electrical performance. Moreover, the role of the nanowire template on the crystalline quality and electrical doping properties are elucidated in this thesis.

CHAPTER 2.

Molecular Beam Epitaxial Growths of AlGaN Epilayers on Si

To date, MBE is one of the most widely used growth methods for the synthesis of semiconductor epilayers [16, 23, 99, 157, 158]. In this chapter, the main features of the MBE used in this thesis study are discussed in Section 2.1. A review on the studies of the MBE growth of AlGaN epilayers on Si is presented in Section 2.2. The MBE growth of III-nitride nanowires and their applications to epilayers on Si are described in Section 2.3.

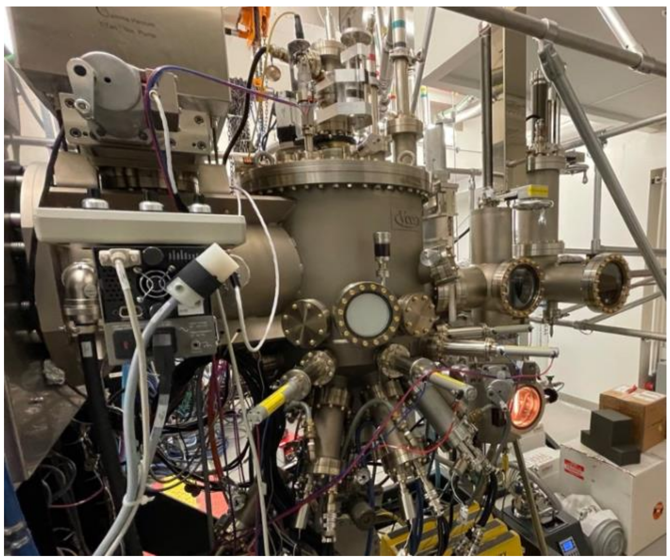

Figure 2-1 Photo of the MBE growth chamber used in this thesis study.

2.1 Main Features of MBE

Figure 2-1 shows a diagram of the MBE growth chamber used in this thesis study. The base pressure is generally held on the order of 10^{-10} to 10^{-11} Torr, which sufficiently limits the incorporation of impurities in the growth chamber. An ion gauge is equipped to monitor the pressure in the growth chamber. To preserve the ultrahigh vacuum (UHV) environment in the growth chamber, vacuum pumps including ion pump and cryogenic pump are equipped. A residual gas analyzer is further integrated to perform the impurity chemical analysis such as CO_2, O_2, and H_2.

Aside from the growth chamber, the load-lock chamber and the buffer chamber are also kept under UHV environment. The load-lock chamber, with a typical pressure on the order of 10^{-8} Torr, is used for loading and unloading the wafers and is the only chamber with direct contact to the ambient environment. It consists of a heating filament which is used to bake the chamber before transferring the wafers into buffer chamber. The buffer chamber is pumped by an ion pump and the pressure is maintained on the order of 10^{-9} Torr. In addition, a substrate heater is equipped in the buffer chamber for wafer outgassing purpose.

Source materials used for MBE growth are of ultra-high purity and controlled individually in the thermal effusion cells, which further minimize any impurity contamination in the growth chamber. Each source material is placed in a crucible within the effusion cell, where the amount of material supply can be controlled by adjusting the cell temperature. A beam flux monitor is also equipped in the growth chamber to measure the amount of material supplied, through measuring the beam equivalent pressure (BEP), often referred to as "flux". Active nitrogen radicals (including neutral atomic N and metastable N_2^*) are generated by electrically discharging ultrahigh purity nitrogen gas through a plasma source [159].

Electron-cyclotron resonance microwave (ECR) [160] and radio-frequency (RF) plasma [161] are the widely used plasma sources for nitrogen. Neutral atomic N, metastable N_2^*, and ionic species are generated in the plasma source [159, 162, 163]. RF plasma source (used in this thesis study) is generally preferred due to the higher neutral atomic N generated for the epitaxial process

[164]. MBE systems integrated with a RF plasma source are often referred as RF plasma assisted MBE (RF-PAMBE).

The MBE system is also integrated with reflection high energy electron diffraction (RHEED), which offers *in-situ* monitoring of the structural evolution during the growth. Figure 2-2 shows the typical geometry of the RHEED component [165]. During the growth, an electron gun sends high energy electron beams to the sample surface at a grazing incident angle. The incident electrons are diffracted from the atoms on the sample surface. A portion of the diffracted electrons interfere constructively and are further captured on the phosphor-coated screen, forming diffraction patterns. In general, RHEED patterns are widely used for multiple analyses such as surface roughness, polarity, growth rate, as well as measurement of the thickness of epilayer [166-169].

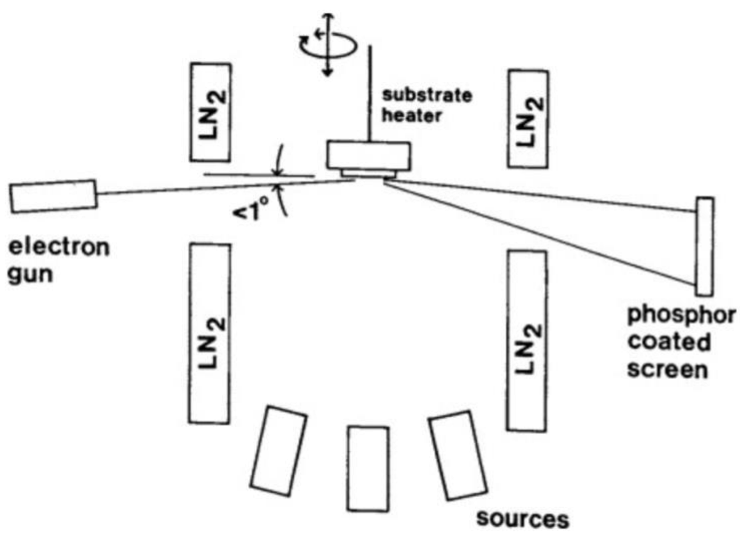

Figure 2-2 Schematic of RHEED geometry. Reproduced with permission [165]. Copyright 1995, Elsevier.

2.2 AlGaN Epitaxy on Si by MBE

The MBE growth of III-nitrides on Si substrates can be traced back to 1989, when Sitar *et al.* demonstrated the growths of polycrystalline GaN on Si (100) substrates using an ECR-MBE system [160]. In the meantime, using ECR-MBE, the research team led by T.D. Moustakas also demonstrated the growth of wurtzite GaN on Si (111) substrates [170-172]. However, such GaN epilayers also exhibited large densities of stacking faults and zinc-blende components as revealed from X-ray diffraction (XRD) scans [172]. Improvement on the crystal quality of GaN epilayer was later reported by Ohtani *et al.*, who demonstrated the growth of crack-free, monocrystalline wurtzite GaN epilayers on Si (111) [173, 174]. Such GaN epilayer also exhibited a PL peak position of 3.46 eV at 10 K, which was among the first demonstrated GaN epilayer on Si that exhibited luminescence [174].

The MBE growth of AlN epilayers on Si substrates was started in the early 1990s by Miyauchi *et al.*, who presented single crystalline AlN epilayers on Si (111) substrates using ECR-MBE [175]. Improvement on the quality of AlN epilayers on Si was then reported by Yasutake *et al.*, who presented a rms roughness as low as 0.3 nm from AlN epilayers grown by RF-PAMBE [161]. The 002 XRD rocking curve FWHM, nonetheless, was broad. At around the same time, Calleja and co-workers studied the effect of both III/V ratio and temperature on the MBE growth of AlN epilayers on Si, and demonstrated a high growth rate up to 500 nm/hr with RF-PAMBE [176, 177].

Using AlN as a buffer layer, AlGaN epilayers as well as UV light emission from LED devices were also reported on Si substrates by MBE [178-184]. Guha and Bojarczuk were among the first to use MBE for the growth of AlGaN epilayers on Si substrates [178]. It is also noted that, using a AlGaN/GaN/AlGaN heterostructure, the same research team further reported UV light emission (λ ~ 360 nm) from the LED device [179, 180]. At around the same time, Garcia *et al.* demonstrated the growth of AlGaN epilayers with various Al contents (from 10% to 76%) on Si substrates [181, 182], and reported UV light emission (λ ~ 365 nm) with an light output power up to 1.5 μW using an n-$Al_{0.15}Ga_{0.85}N$/p-GaN single heterojunction [185].

On a different approach, using ammonia-based gas source MBE system, Nikishin *et al.* studied the effect of V/III ratio on the growth of AlGaN epilayers across the entire composition range with an 130-nm thick AlN buffer layer and a 70-nm thick AlGaN/GaN superlattice layer, and established the bandgap dependence on the Al composition of AlGaN epilayers [183, 184].

2.3 MBE Growths of III-Nitride Nanowires and Their Applications to Epilayers

In addition to epilayers, MBE is an emerging technique for the synthesis of III-nitride nanowires [186-189]. In general, III- nitride nanowires can be spontaneously grown by MBE under N-rich condition [59]. The formation of the nanowires can be explained by a diffusion-induced mechanism which is schematically demonstrated in Figure 2-3. Metal adatoms diffuse on the substrate surface and form metal nucleation sites on the substrate. Because of the lower formation energy on the nanowire top surface, adatoms migrate from the nanowire sidewalls towards the top surface, thus promoting the axial growth [189]. The density of the nanowires can be partially controlled by adjusting the growth parameters including temperature and metal fluxes during the initial nucleation [188]. MBE-grown III-nitride nanowires can be formed without using any foreign metal catalyst on over a wide range of substrates, including Si substrates [59, 189, 190], metal thin films [191-193] and graphene [194-196].

A main benefit of nanowires is their larger surface-area-to-bulk-volume ratio, so that lattice strain can be relaxed more efficiently than planar counterparts. Moreover, dopant incorporation can also be enhanced in nanowires. Using AlGaN nanowires grown by MBE, high electrical efficiency deep UV LEDs [89, 90, 197] and electrically injected deep UV lasers [198-200] have been demonstrated.

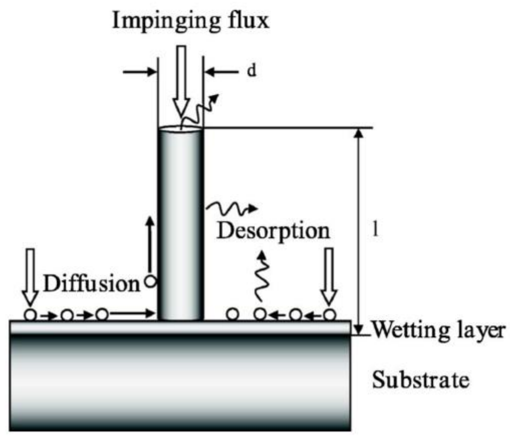

Figure 2-3 Growth process of nanowire via diffusion-induced mechanism. Reproduced with permission [189]. Copyright 2007, AIP Publishing.

In addition, III-nitride nanowires can also be used as a template layer for the growth of III-nitride epilayers, exploiting their excellent strain relaxation characteristics. In the past, multiple studies have been conducted on obtaining GaN epilayers on Si substrates by exploiting the coalescence of GaN nanowires [190, 201-203]. For example, Averett *et al.* demonstrated the lateral epitaxial overgrowth of GaN nanocolumns which exhibited a PL intensity more than two orders of magnitude higher than directly grown GaN epilayers grown on Si substrates [201]. Using a similar approach, Dogan *et al.* further reported that microcrystals obtained from coalescence of GaN nanowires through pendeoepitaxial overgrowth exhibited exceptional structural and optical quality, including a PL peak position at 3.471 eV at 10 K, which was very close to the strain-free value [202]. Nonetheless, the surface morphology of the coalesced GaN epilayers has remained poor, either with a large density of 3D features or with regions showing incomplete coalescence on the surface. It is not until very recently that smooth GaN epilayer with a rms roughness of 0.562 nm was reported by Aiello *et al*. on coalesced GaN nanowires [203]. Light emission at 477 nm was further measured from InGaN quantum dots grown on such GaN buffer layers.

Our group has also conducted the research on obtaining epilayers through a coalescence process, which exploited GaN nanowire template and the coalescence of AlN on Si substrates, and successfully demonstrated both AlN and AlGaN epilayers in N-rich conditions with rms roughness as low as 1.8 nm [204-206], which is comparable to the rms values of typical III-nitride epilayers grown under N-rich conditions [207-209]. In this thesis study, the focus is on metal-rich conditions for the growth of AlN and AlGaN epilayers on Si, and vertical UV LEDs.

CHAPTER 3.

Demonstrations of AlN-on-NW Buffer Layer for Vertically-Injected Deep Ultraviolet LEDs on Si

In this chapter*, AlN epilayers grown on nanowire template (denoted AlN-on-NW) with excellent surface morphology are realized under metal-rich conditions. Further utilizing such AlN-on-NW template as buffer layers, vertically-injected AlGaN deep UV LEDs are demonstrated. The electrical and optical properties of such AlGaN deep UV LED are also analyzed in detail.

3.1 Manuscript

Vertical semiconductor deep ultraviolet light emitting diodes on a nanowire-assisted aluminum nitride buffer layer

Qihua Zhang, Heemal Parimoo, Eli Martel, and Songrui Zhao*

Department of Electrical and Computer Engineering, McGill University, 3480 University Street, Montreal, Quebec H3A 0E9, Canada
**E-mail: songrui.zhao@mcgill.ca*

Keywords: deep ultraviolet, light-emitting diodes, vertical injection, aluminum gallium nitride, silicon

* Section 3.1 is from a manuscript that has been accepted for publication: Q. Zhang, H. Parimoo, E. Martel, and S. Zhao, "Vertical semiconductor deep ultraviolet light emitting diodes on a nanowire-assisted aluminum nitride buffer layer," *Sci. Rep.*, vol. 12, no. 1, p. 7230, 2022, doi: 10.1038/s41598-022-11246-0.

Abstract

Vertical light-emitting diodes (LEDs) have many advantages such as uniform current injection, excellent scalability of the chip size, and simple packaging process. Hitherto, however, technologically important semiconductor aluminum gallium nitride (AlGaN) deep ultraviolet (UV) LEDs are mainly through lateral injection. Herein, we demonstrate a new and practical path for vertical AlGaN deep UV LEDs, which exploits a thin AlN buffer layer formed on a nanowire-based template on silicon (Si). Such a buffer layer enables in situ formation of vertical AlGaN deep UV LEDs on Si. Near Lambertian emission pattern is measured from the top surface. The decent reflectivity of Si in the deep UV range makes such a configuration a viable low-cost solution for vertical AlGaN deep UV LEDs. More importantly, the use of such a thin AlN buffer layer can allow an easy transfer of device structures to other carrier wafers for vertical AlGaN deep UV LEDs with ultimately high electrical and optical performance.

3.1.1 Introduction

Deep UV light sources play a critical role in our everyday life for a wide range of applications in disinfection, UV curing in the production of any personal electronic devices, and bio-chemical sensing. Today, the dominant technologies have remained relying on mercury lamps, which are hazards to both the environment and human health. In this context, a significant effort has been devoted to the development of semiconductor deep UV LEDs based on AlGaN alloys, which are the materials of choice for semiconductor deep UV LEDs[1-12].

In general, there are two schemes for the current injection of a LED device: vertical and lateral. Compared to the lateral scheme, vertical injection offers a number of advantages such as uniform current injection, excellent scalability of the chip size, and simple packaging process[6,13-

[16]. A uniform current injection is also critical for laser devices[17,18]. Nonetheless, realizing vertical AlGaN deep UV LEDs remains to be a challenge in the field; and the majority device demonstrations of AlGaN deep UV LEDs so far are through lateral current injection. The latest review on this topic can be found, e.g., in Ref.[6].

Two common approaches of fabricating vertical LEDs are: 1) using conductive substrates, and 2) substrate removal and bonding to a second carrier wafer. Both approaches, however, are difficult to implement for vertical AlGaN deep UV LEDs. Today, AlGaN deep UV LEDs are mainly on insulating sapphire substrates, precluding the in situ vertical current injection. On the other hand, although n-SiC and n-GaN substrates are conductive, they have a number of limitations. The lattice mismatch between GaN and AlN is a known challenge[6], whereas although the lattice mismatch between SiC (6H) and AlN is small, it faces a substrate cost penalty[19]. More adversely, both n-SiC and n-GaN have a strong deep UV light absorption. As such, in both scenarios, i.e., insulating substrates (sapphire) and conductive substrates (n-GaN, n-SiC), substrate removal is necessary.

Laser lift-off (LLO) has been successful in the fabrication of InGaN visible color LEDs since the first demonstrations around 2000[13,14]. However, the success cannot be transferred to AlGaN deep UV LEDs, due to the need of AlN buffer layers for AlGaN deep UV LEDs. The LLO of AlN is difficult due to the high melting point of AlN, as well as the generation of Al during the LLO process, which can lead to cracks and is difficult to remove[20-25]. This is in addition to a possible device degradation incurred in the LLO process[26,27].

Different from substrates mentioned above, Si substrate can be removed easily by wet etching processes[28,29]. Moreover, Si substrate is available at a large size at a low cost and is thus favorable for mass production. However, growing high quality AlGaN epilayers on Si is a challenge. The large tensile stress in AlN and high-Al content AlGaN alloys, due to their large lattice mismatches with Si (e.g., 19% for AlN), leads to poor material quality (e.g., cracks, poor surface morphology)[30,31]. To mitigate the challenge, various approaches, such as low-temperature (LT)/high-temperature (HT) AlN buffer layers, epitaxial lateral overgrowth (ELO)-AlN buffer layers, AlGaN superlattices (SLs), and graded AlGaN buffer layers, have been developed in order to obtain high quality AlGaN device layers[30-36]. These approaches, however, require the use of complicated and time-consuming substrate patterning processes or growth processes. Moreover, buffer layers of several μm thick are required in order to obtain high quality device layers. The thick, insulating buffer layers used in these approaches only led to laterally injected AlGaN deep UV LEDs[30,33,36,37].

An alternative path for vertical AlGaN deep UV LEDs is to use nanowire structures[38,39]. However, the fabrication of AlGaN nanowire deep UV LEDs is one remaining issue. This is mainly due to the presence of gaps amongst nanowires. For example, due to the presence of gaps, certain planarization is required. Conventionally, this is done by polymer backfill. However, the commonly available polymers absorb deep UV light strongly and degrade under deep UV light illumination. It is ideal to have an AlGaN deep UV LED technology on Si that combines the advantage of nanowires (e.g., better stress relaxation) and epilayers (e.g., manufacturing-compatible device fabrication process).

Recently, we have shown that by using a nanowire template, AlN epilayers can be formed on Si, which have further led to AlGaN epilayers with a relatively high internal quantum efficiency[40-42]. In this work, we further demonstrate vertical AlGaN deep UV LEDs on Si following the idea of nanowire-assisted AlN buffer layer but with modifications: First, to improve the quality of the nanowire template, a pre-nanowire AlN layer is intro- duced to remove any residual tensile stress on the nanowire template from the Si substrate. Second, metal-rich condition, rather than nitrogen-rich condition, is used for the growth of the AlN buffer layer, in order to achieve a smoother surface. The use of metal-rich conditions in general promises a smoother surface compared to using N-rich conditions in a radio-frequency nitrogen-plasma-sourced molecular beam epitaxy (MBE) system. Devices emitting in the deep UV range are demonstrated using such a modified AlN buffer layer in situ on Si. As Si is a decent reflector in the deep UV range[43,44] and highly electrical and thermal conductive, such a configuration could be a possible path of fabricating vertical AlGaN deep UV LEDs and offers a potential benefit of direct integration to other electronic components on Si. More importantly, due to the thickness of the AlN buffer layer is very thin, it can be removed easily by chemical wet etching, which is compatible with the fabrication process of vertical InGaN visible color LEDs on Si substrates[28,29,45,46], allowing for the achievement of vertical AlGaN deep UV LEDs with ultimately high electrical and optical performance.

3.1.2 Results

The MBE growth and characterization of the AlN epilayer is described first. The schematic of the structure is shown in Figure 3-1a, which starts with a thin (1 – 2 nm) AlN layer, followed by a thin (50 – 100 nm) GaN nanowire layer. Figure 3-1b shows the reflection high-energy electron diffraction (RHEED) pattern during the growth of the GaN nanowires. Regularly arranged dots are seen, suggesting a 3-dimensional (3D) growth. This RHEED feature is different from the arcs as often observed from self-organized GaN nanowires, which indicates the improvement of the nanowire vertical alignment with respect to the substrate, due to the use of the thin pre-nanowire AlN layer[47,48].

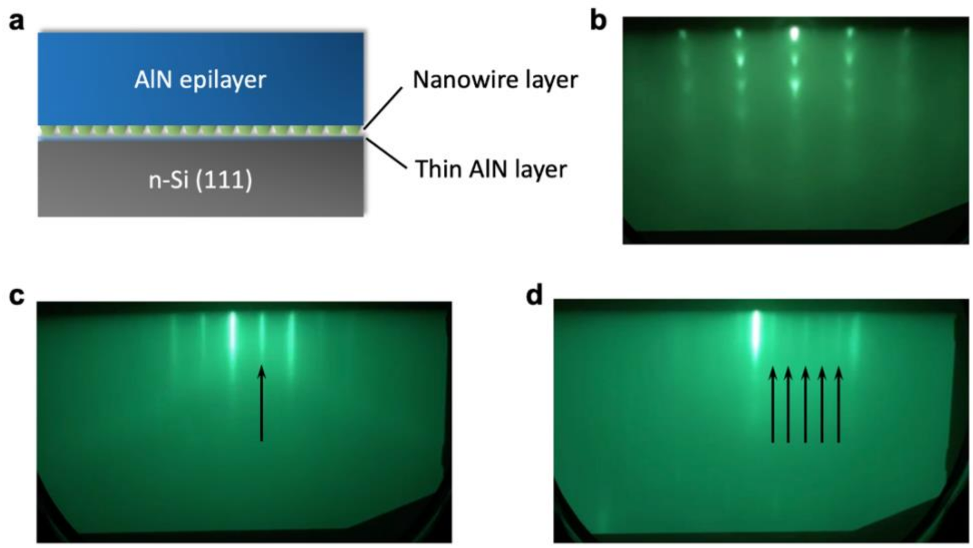

Figure 3-1 (a) Schematic of the growth of the AlN epilayer on Si substrate using a nanowire-based template. (b) RHEED pattern taken during the growth of the nanowires. (c) and (d) RHEED patterns taken along the <11$\bar{2}$0> direction and <1$\bar{1}$00> direction, respectively, during the growth of AlN epilayer. The arrows reflect the 2×6 RHEED reconstruction.

The start of the growth of the AlN epilayer led to the RHEED pattern transition from being spotty to being streaky. The Al-rich growth condition was confirmed by the presence of excess Al through the following observations: (1) the Al shutter open and close test, wherein the close of the Al shutter led to an increase of the RHEED intensity and the opening of the Al shutter led to an intensity decrease; and (2) the observation of the RHEED 2×6 reconstruction (Figure 3-1c and Figure 3-1d) during the growth, which is a signature of Al adlayer[49,50]. Such a RHEED pattern also reflects that the AlN epilayer is Al-polar. In addition, the narrow, bright, and streaky RHEED pattern suggests a highly smooth surface.

Figure 3-2a shows the optical image of the as-grown AlN wafer, an optically smooth surface can be seen. The surface of the as-grown AlN wafer was further examined by scanning electron microscopy (SEM). The images were taken at a tilting angle of 45°. Figure 3-2b shows a typical SEM image, highlighting a very smooth surface. The inset of Figure 3-2b shows an SEM image that manifests the cross section, with the Si substrate, GaN nanowire layer, and AlN epilayer clearly seen. The surface was further examined by atomic force microscopy (AFM). A typical AFM image is shown in Figure 3-2c. For such AlN epilayers, a root-mean-square (RMS) roughness of around 0.4 nm can be obtained, which is comparable to the typical metal-polar AlGaN thin films grown on sapphire and AlN- on-sapphire template[51]. This RMS roughness is also significantly improved compared to our previous studies[41,42].

To confirm the Al-polar polarity of the AlN epilayer, we have performed potassium hydroxide (KOH) etching experiments. In the experiments, 11.2 mol/L KOH solution was heated up to 70 °C, and the sample was entirely placed in the solution, followed by de-ionized (DI) water cleaning. The SEM image of the AlN epilayer after KOH etching is shown in Figure 3-2d. It is seen that hexagonal pits, rather than hillocks, appear on the surface, confirming that the AlN epilayer is Al-polar[52-54]. This Al-polar AlN epilayer can further enable metal-polar AlGaN epilayers grown on top. The benefit is, as the opposite side of the metal-polar surface is N-polar, which can be selectively etched by KOH, it thus enables the removal of unwanted AlGaN epilayers (e.g., additional AlGaN buffer layers for material quality improvement), as well as the roughening of the surface through which the light comes out (for flip-chip devices). Indeed, the AlGaN epilayers to be described below are metal-polar as confirmed by KOH experiments.

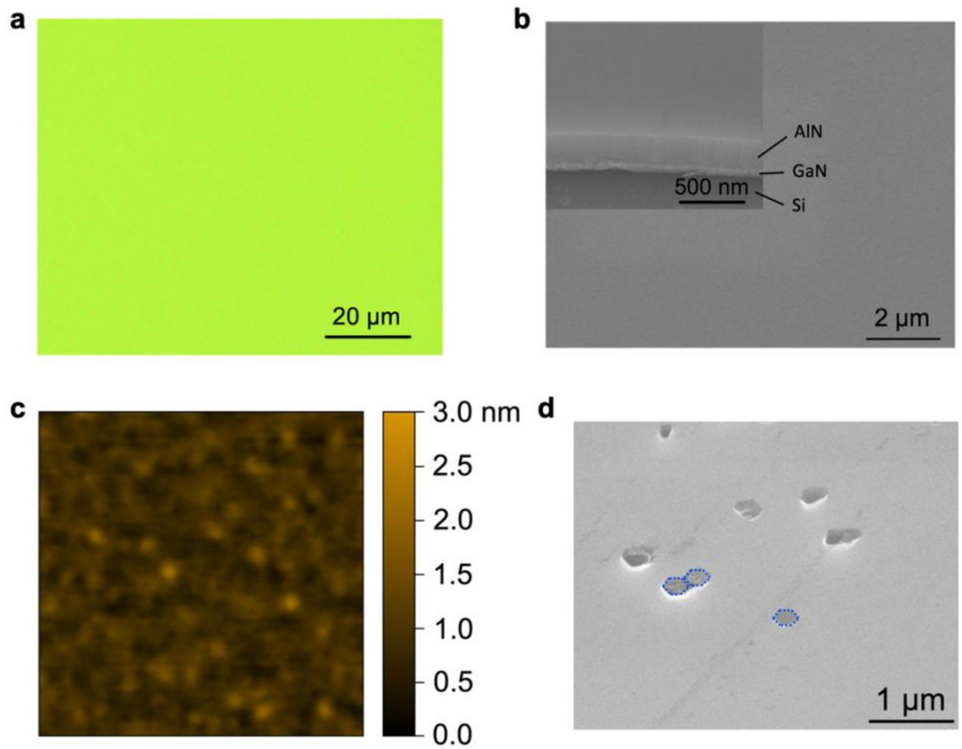

Figure 3-2 (a) An optical image showing the surface of the as-grown AlN epilayer. (b) SEM images of the as-grown AlN epilayer. Inset: An image highlighting the cross-section. (c) An AFM image of the surface of the as-grown AlN epilayer. The image size is 10 μm × 10 μm. (d) An SEM image showing the surface of the etched AlN epilayer by KOH. The dashed lines denote the hexagonal shapes and the network of hexagonal shapes.

We further demonstrate vertical AlGaN deep UV LEDs using such AlN epilayers as buffer layers on Si. The schematic of the device structure is shown in Figure 3-3a, which consists of double heterojunctions (DHs) with an i-$Al_{0.4}Ga_{0.6}N$ active region (~15 nm) and p- and n-$Al_{0.7}Ga_{0.3}N$ cladding layers (~30 nm each). These Al contents were estimated from the room temperature photoluminescence (PL) experiments from AlGaN epilayers grown separately on such AlN buffer layers. Figure 3-3b shows the room temperature PL spectra measured from the AlGaN epilayers intended to be used as the active region and cladding layers for the devices. It is seen that PL emission at around 240 nm and 280 nm are measured. Assuming the PL peak energy approximately to be the bandgap energy and the bowing factor to be 1[55], the Al contents in the active region and cladding layers were estimated to be ~40% and ~70%, respectively. It is also noted that only a single PL emission peak is seen for both the active region and cladding layers, suggesting a uniform alloy composition.

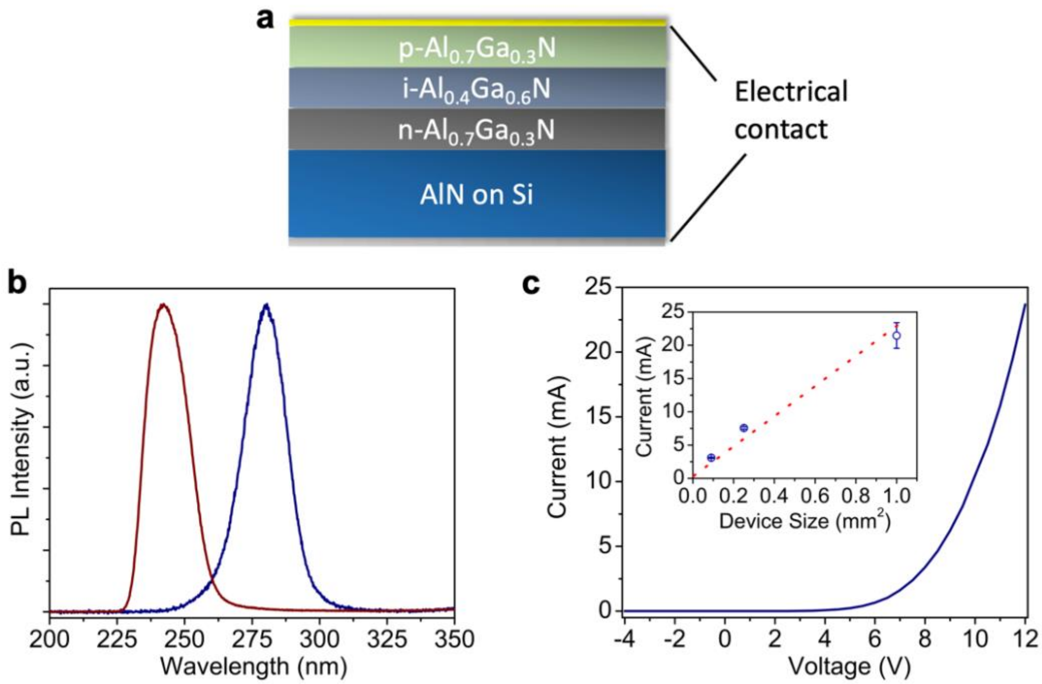

Figure 3-3 (a) Schematic of the AlGaN DH LED structure grown on top of the AlN buffer layer on Si. The electrical contacts are also shown. (b) Room-temperature PL spectra of the AlGaN active region and cladding layers. (c) I-V characteristics of an AlGaN DH LED with a device size of 1 mm × 1 mm. The inset shows the measured forward currents from devices with various sizes at a forward voltage of 12 V. Numerous devices were tested, and the error bars reflect the current variation from devices with the same size.

For device fabrication, we did not use chemical etching to isolate devices with different sizes. The isolation was obtained by the limitation of the current spreading length in the vertical injection scheme. Our calculation indicates that under an injection current density of 0.1 A/cm^2, with the best reported p-AlGaN resistivity (Al content of 70%) and the largest ideality factor[56-58], as well as the present p-AlGaN layer thickness, the maximum current spreading length is on the order of tens of μm. Therefore, by placing p-contact with a separation on the order of several hundred μm, devices can be naturally isolated.

The room-temperature I-V characteristics under a continuous-wave (CW) biasing are shown in Figure 3-3c. At forward voltages of 9 V and 12 V, the forward currents were 6 mA and 23 mA, respectively, which are improved compared to the previously reported laterally injected AlGaN thin film UV LEDs on Si at a similar operating wavelength, e.g., Ref.[33]. Moreover, the device size dependent current further suggests a uniform current injection. Illustrated in the inset of Figure 3-3c is a device size dependent current under a forward voltage of 12 V, and it is seen that the current increase is proportional to the device size increase, indicating a uniform current injection.

The electroluminescence (EL) spectra under different injection currents are shown in Figure 3-4a. It is seen that the EL emission occurs at 298 nm. With the change of the injection current from 2 mA to 20 mA, no noticeable EL emission peak blueshift and full-width-at-half-maximum narrowing are observed. The EL emission wavelength is longer than what we expect, and the reason is being investigated. Figure 3-4b shows the EL spectra measured with a UV-VIS spectrometer, intended to study the defect EL emission. A parasitic EL emission peak at around 400 nm is seen, which could be originated from the deep levels in AlGaN alloys[59,60]. Its intensity, however, is significantly lower compared to the main EL emission peak. Figure 3-4c shows the light output power as a function of the injection current under a CW biasing. A typical LED behavior is seen, i.e., the light output power increases nearly linearly with the injection current. Under an injection current of 100 mA, a light output power of 0.3 μW was measured. An optical image of the light emission is shown in the inset of Figure 3-4c, wherein a bright and uniform emission can be seen.

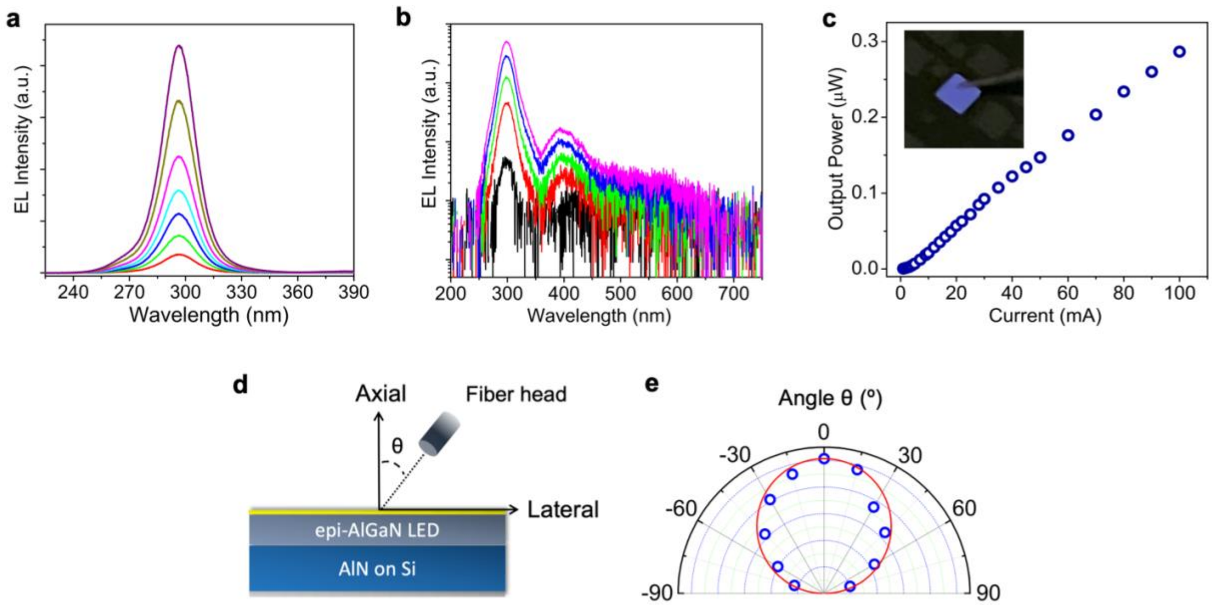

Figure 3-4 (a) Room-temperature EL spectra of an AlGaN DH LED under different injection currents. (b) Room-temperature EL spectra taken up to the visible spectral range with currents varying from 1 mA to 12 mA. (c) Light output power vs. the injected current. The inset shows an optical image of the light emission. (d) Schematic of the setup for the angle dependent EL measurement. (e) Emission pattern with the detection angle θ varying from -75° to 75°. The solid curve denotes the ideal Lambertian pattern. Device size: 1 mm × 1 mm.

The emission pattern of such LEDs is also studied. In this regard, the optical fiber was tilted at various angles with respect to the axial direction (the growth direction) for the light detection, as illustrated in Figure 3-4d. The emission pattern is shown in Figure 3-4e by open circles. The ideal Lambertian emission pattern is also shown by the solid curve. It is seen that the device shows a near Lambertian pattern, suggesting the nature of surface emission.

3.1.3 Discussion

In this work, we have demonstrated vertical AlGaN deep UV LEDs on Si. Such devices are made on a special AlN buffer layer that is formed with the assistance of a nanowire-based template. As Si is a decent reflector in the deep UV range, such vertical devices offer a low-cost solution for vertical semiconductor deep UV LEDs and a potential benefit of in situ integration to other electronics on Si, and are suitable for low-power applications. Further improvement on the electrical performance for such devices is expected by optimizing the electrical doping; and further improvement on the light output power can be expected by optimizing the p-contact and adopting more complicated device designs such as using quantum wells and electron blocking layers. More attractively, as the thickness of the AlN buffer layer is very thin, it can be removed easily by chemical wet etching (same for the nanowires, as the sidewall of nanowires grown by MBE is N-polar, e.g., Ref.[61]), which allows the transfer of device structures grown on top to other carrier wafers for the achievement of vertical AlGaN deep UV LEDs with ultimately high electrical and optical performance. Therefore, this work enables a practical path for high performance vertical semiconductor deep UV LEDs.

3.1.4 Methods

Molecular beam epitaxial growth. All the samples in this work were grown by radio-frequency plasma-assisted molecular beam epitaxy on n-Si (111) substrates. The substrates underwent standard solvent cleaning and in situ thermal outgassing prior to the growth. The Al fluxes for the pre-nanowire AlN layer and the AlN buffer epilayer were 2×10^{-8} Torr and 5×10^{-8} Torr, respectively. For the AlGaN DH LED structure, the Al flux was in the range of $2.8 – 3.5\times10^{-8}$ Torr. The Ga flux was around 1.4×10^{-7} Torr for all layers in this study. A nitrogen flow rate of 0.6 sccm was used for the GaN nanowires, whereas for all the epilayers a nitrogen flow rate of 0.3 sccm was used. A substrate temperature in the range of 720 – 740 °C was used for the AlGaN epilayers; and for the AlN epilayers the substrate temperature was roughly 100 °C higher compared to AlGaN epilayers. The Mg doping concentration in the p-AlGaN layer was 1×10^{18} cm^{-3}, estimated by the secondary-ion mass spectroscopy (SIMS, EAG lab).

Photoluminescence experiments. A 213 nm pulsed laser with a pulse width of 7 ns was used to excite the sample. The emitted light from the sample top surface was collected by an optical fiber, which was further coupled to a deep UV spectrometer.

Device fabrication. Metal bilayer Ni (7 nm)/Au (7 nm) was used for p-contact, which was fabricated by standard photolithography and metallization processes. The size of p-contact defines the size of the device. Colloidal Ag conductive adhesive was used on the backside of n-Si substrate as the n-contact.

Device characterization. The electroluminescence was collected by an optical fiber from the device top surface, and both deep UV and UV–VIS spectrometers were used for the spectral analysis. The light output power was measured by a Si photodetector, which was placed roughly about 5 mm above the device top surface. The device was unpackaged.

References

1 Amano, H. *et al.* The 2020 UV emitter roadmap. *Journal of Physics D: Applied Physics* **53**, doi:10.1088/1361-6463/aba64c (2020).

2 Moustakas, T. D. & Paiella, R. Optoelectronic device physics and technology of nitride semiconductors from the UV to the terahertz. *Reports on Progress in Physics* **80**, 106501, doi:10.1088/1361-6633/aa7bb2 (2017).

3 Kneissl, M., Seong, T.-Y., Han, J. & Amano, H. The emergence and prospects of deep-ultraviolet light-emitting diode technologies. *Nature Photonics* **13**, 233-244, doi:10.1038/s41566-019-0359-9 (2019).

4 Li, D., Jiang, K., Sun, X. & Guo, C. AlGaN photonics: recent advances in materials and ultraviolet devices. *Advances in Optics and Photonics* **10**, doi:10.1364/aop.10.000043 (2018).

5 Fujita, S. Wide-bandgap semiconductor materials: For their full bloom. *Japanese Journal of Applied Physics* **54**, 030101, doi:10.7567/jjap.54.030101 (2015).

6 Crawford, M. Materials challenges of AlGaN-based UV optoelectronic devices. *Semiconductors and Semimetals* **96**, 3-44 (2017).

7 Huang, C., Zhang, H. & Sun, H. Ultraviolet optoelectronic devices based on AlGaN-SiC platform: Towards monolithic photonics integration system. *Nano Energy* **77**, doi:10.1016/j.nanoen.2020.105149 (2020).

8 Liao, Y., Thomidis, C., Kao, C.-k. & Moustakas, T. D. AlGaN based deep ultraviolet light emitting diodes with high internal quantum efficiency grown by molecular beam epitaxy. *Applied Physics Letters* **98**, 081110, doi:10.1063/1.3559842 (2011).

9 Shatalov, M. *et al.* AlGaN Deep-Ultraviolet Light-Emitting Diodes with External Quantum Efficiency above 10%. *Applied Physics Express* **5**, 082101, doi:10.1143/apex.5.082101 (2012).

10 Takano, T. *et al.* Deep-ultraviolet light-emitting diodes with external quantum efficiency higher than 20% at 275 nm achieved by improving light-extraction efficiency. *Applied Physics Express* **10**, 031002, doi:10.7567/apex.10.031002 (2017).

11 Shin, W., Pandey, A., Liu, X., Sun, Y. & Mi, Z. Photonic crystal tunnel junction deep ultraviolet light emitting diodes with enhanced light extraction efficiency. *Optics Express* **27**, doi:10.1364/oe.380739 (2019).

12 Khan, M. A. *et al.* Achieving 9.6% efficiency in 304 nm p-AlGaN UVB LED via increasing the holes injection and light reflectance. *Scientific Reports* **12**, 2591, doi:10.1038/s41598-022-04876-x (2022).

13 Wong, W. S. *et al.* Fabrication of thin-film InGaN light-emitting diode membranes by laser lift-off. *Applied Physics Letters* **75**, 1360 (1999).

14 Wong, W. S. *et al.* InxGa1−xN light emitting diodes on Si substrates fabricated by Pd–In metal bonding and laser lift-off. *Applied Physics Letters* **77**, 2822-2824, doi:10.1063/1.1319505 (2000).

15 Li, C. & Wu, Y. Study on the Current Spreading Effect and Light Extraction Enhancement of Vertical GaN/InGaN LEDs. *IEEE Transactions on Electron Devices* **59**, 400-407, doi:10.1109/TED.2011.2176132 (2012).

16 Kim, H. *et al.* Design of high-efficiency GaN-based light emitting diodes with vertical injection geometry. *Applied Physics Letters* **91**, doi:10.1063/1.2756139 (2007).

17 Aoki, Y. *et al.* A 350-nm-band GaN/AlGaN multiple-quantum-well laser diode on bulk GaN. *Applied Physics Letters* **107**, doi:10.1063/1.4933257 (2015).

18 Taketomi, H. *et al.* Over 1 W record-peak-power operation of a 338 nm AlGaN multiple-quantum-well laser diode on a GaN substrate. *Japanese Journal of Applied Physics* **55**, 05FJ05, doi:10.7567/jjap.55.05fj05 (2016).

19 SaifAddin, B. K. *et al.* AlGaN Deep-Ultraviolet Light-Emitting Diodes Grown on SiC Substrates. *ACS Photonics* **7**, 554-561, doi:10.1021/acsphotonics.9b00600 (2020).

20 Zhou, L. *et al.* Vertical injection thin-film AlGaN∕AlGaN multiple-quantum-well deep ultraviolet light-emitting diodes. *Applied Physics Letters* **89**, 241113, doi:10.1063/1.2408643 (2006).

21 Adivarahan, V. *et al.* Vertical Injection Thin Film Deep Ultraviolet Light Emitting Diodes with AlGaN Multiple-Quantum Wells Active Region. *Applied Physics Express* **2**, doi:10.1143/apex.2.092102 (2009).

22 Aoshima, H. *et al.* Laser lift-off of AlN/sapphire for UV light-emitting diodes. *physica status solidi (c)* **9**, 753-756, doi:10.1002/pssc.201100491 (2012).

23 Kawasaki, K., Koike, C., Aoyagi, Y. & Takeuchi, M. Vertical AlGaN deep ultraviolet light emitting diode emitting at 322nm fabricated by the laser lift-off technique. *Applied Physics Letters* **89**, doi:10.1063/1.2424668 (2006).

24 Sung, Y. J., Kim, D.-W., Yeom, G. Y. & Kim, K. S. Performance of vertical type deep UV light-emitting diodes depending on the Ga-face n-contact hole density. *Applied Physics Letters* **118**, doi:10.1063/5.0052416 (2021).

25 Takeuchi, M. *et al.* AlN/AlGaN short-period superlattice sacrificial layers in laser lift-off for vertical-type AlGaN-based deep ultraviolet light emitting diodes. *Applied Physics Letters* **94**, doi:10.1063/1.3081060 (2009).

26 Sun, Y. *et al.* Microanalyses of the reverse-bias leakage current increase in the laser lift off GaN-based light emitting diodes. *Journal of Applied Physics* **106**, doi:10.1063/1.3159015 (2009).

27 Wu, Y. S., Cheng, J.-H., Peng, W. C. & Ouyang, H. Effects of laser sources on the reverse-bias leakages of laser lift-off GaN-based light-emitting diodes. *Applied Physics Letters* **90**, doi:10.1063/1.2749866 (2007).

28 Jiang, F., Zhang, J., Sun, Q. & Quan, Z. in *Light-Emitting Diodes Solid State Lighting Technology and Application Series* Ch. Chapter 4, 133-170 (2019).

29 Sun, Q. *et al.* GaN-on-Si blue/white LEDs: epitaxy, chip, and package. *Journal of Semiconductors* **37** 044006 (2016).

30 Zhang, Y. *et al.* Near milliwatt power AlGaN-based ultraviolet light emitting diodes based on lateral epitaxial overgrowth of AlN on Si(111). *Applied Physics Letters* **102**, doi:10.1063/1.4773565 (2013).

31 Shen, J. *et al.* High quality AlN film grown on a nano-concave-circle patterned Si substrate with an AlN seed layer. *Applied Physics Letters* **117**, doi:10.1063/5.0010285 (2020).

32 Huang, Y. *et al.* Crack-free high quality 2 μm-thick Al0.5Ga0.5N grown on a Si substrate with a superlattice transition layer. *CrystEngComm* **22**, 1160-1165, doi:10.1039/c9ce01677e (2020).

33 Tran, B. T. & Hirayama, H. Growth and Fabrication of High External Quantum Efficiency AlGaN-Based Deep Ultraviolet Light-Emitting Diode Grown on Pattern Si Substrate. *Scientific Reports* **7**, 12176, doi:10.1038/s41598-017-11757-1 (2017).

34 Li, Y. *et al.* Nucleation layer design for growth of a high-quality AlN epitaxial film on a Si(111) substrate. *CrystEngComm* **20**, 1483-1490, doi:10.1039/C7CE02126G (2018).

35 Feng, M. *et al.* Room-Temperature Electrically Injected AlGaN-Based near-Ultraviolet Laser Grown on Si. *ACS Photonics* **5**, 699-704, doi:10.1021/acsphotonics.7b01215 (2018).

36 Robin, Y. *et al.* High brightness ultraviolet light-emitting diodes grown on patterned silicon substrate. *Materials Science in Semiconductor Processing* **90**, 87-91, doi:10.1016/j.mssp.2018.09.027 (2019).

37 Mino, T., Hirayama, H., Takano, T., Tsubaki, K. & Sugiyama, M. Realization of 256–278 nm AlGaN-Based Deep-Ultraviolet Light-Emitting Diodes on Si Substrates Using Epitaxial Lateral Overgrowth AlN Templates. *Applied Physics Express* **4**, doi:10.1143/apex.4.092104 (2011).

38 Zhao, C. *et al.* III-nitride nanowires on unconventional substrates: From materials to optoelectronic device applications. *Progress in Quantum Electronics* **61**, 1-31, doi:10.1016/j.pquantelec.2018.07.001 (2018).

39 Zhao, S., Lu, J., Hai, X. & Yin, X. AlGaN Nanowires for Ultraviolet Light-Emitting: Recent Progress, Challenges, and Prospects. *Micromachines (Basel)* **11**, doi:10.3390/mi11020125 (2020).

40 Yin, X. & Zhao, S. High Internal Quantum Efficiency AlGaN Epilayer Grown by Molecular Beam Epitaxy on Si Substrate. *ECS Journal of Solid State Science and Technology* **10**, doi:10.1149/2162-8777/ac0f15 (2021).

41 Yin, X., Zhang, Q. & Zhao, S. Molecular Beam Epitaxial Growth of AlN Thin Films on Si through Exploiting Low Al Adatom Migration and the Nitrogen-Rich Environment on a Nanowire Template. *Crystal Growth & Design* **21**, 3645, doi:10.1021/acs.cgd.1c00327 (2021).

42 Zhang, Q., Yin, X., Martel, E. & Zhao, S. Molecular beam epitaxy growth and characterization of AlGaN epilayers in nitrogen-rich condition on Si substrate. *Materials Science in Semiconductor Processing* **135**, doi:10.1016/j.mssp.2021.106099 (2021).

43 Lu, J., Vafadar, M. F. & Zhao, S. Light extraction efficiency of AlGaN nanowire deep ultraviolet light-emitting diodes on Si with different photonic structures. *Journal of Nanophotonics* **15**, 036002 (2021).

44 Liu, D. *et al.* 226 nm AlGaN/AlN UV LEDs using p-type Si for hole injection and UV reflection. *Applied Physics Letters* **113**, doi:10.1063/1.5038044 (2018).

45 Oh, J.-T. *et al.* High-performance GaN-based light emitting diodes grown on 8-inch Si substrate by using a combined low-temperature and high-temperature-grown AlN buffer layer. *Journal of Alloys and Compounds* **732**, 630-636, doi:10.1016/j.jallcom.2017.10.200 (2018).

46 Li, Y. *et al.* High-performance vertical GaN-based near-ultraviolet light-emitting diodes on Si substrates. *Journal of Materials Chemistry C* **6**, 11255-11260, doi:10.1039/c8tc04477e (2018).

47 Lu, J., Zhong, Y. & Zhao, S. Comparative study on the molecular beam epitaxial growth and characterization of AlGaN nanowire structures on AlN buffer layer and on Si. *Journal of Vacuum Science & Technology B* **38**, doi:10.1116/6.0000646 (2020).

48 Songmuang, R., Landré, O. & Daudin, B. From nucleation to growth of catalyst-free GaN nanowires on thin AlN buffer layer. *Applied Physics Letters* **91**, 251902, doi:10.1063/1.2817941 (2007).

49 Lebedev, V., Schroter, B., Kipshidze, G. & Richter, W. The polarity of AlN films grown on Si(111). *Journal of Crystal Growth* **207** 266 (1999).

50 Lee, C. D., Dong, Y., Feenstra, R. M., Northrup, J. E. & Neugebauer, J. Reconstructions of the AlN(0001) surface. *Physical Review B* **68**, doi:10.1103/PhysRevB.68.205317 (2003).

51 Jmerik, V., Toropov, A., Davydov, V. & Ivanov, S. Monolayer-Thick GaN/AlN Multilayer Heterostructures for Deep-Ultraviolet Optoelectronics. *physica status solidi (RRL) – Rapid Research Letters*, doi:10.1002/pssr.202100242 (2021).

52 Li, D. *et al.* Selective etching of GaN polar surface in potassium hydroxide solution studied by x-ray photoelectron spectroscopy. *Journal of Applied Physics* **90**, 4219-4223, doi:10.1063/1.1402966 (2001).

53 Lai, Y.-Y. *et al.* The study of wet etching on GaN surface by potassium hydroxide solution. *Research on Chemical Intermediates* **43**, 3563-3572, doi:10.1007/s11164-016-2430-1 (2016).

54 Guo, W. *et al.* KOH based selective wet chemical etching of AlN, AlxGa1−xN, and GaN crystals: A way towards substrate removal in deep ultraviolet-light emitting diode. *Applied Physics Letters* **106**, doi:10.1063/1.4913705 (2015).

55 Yun, F. *et al.* Energy band bowing parameter in Al[sub x]Ga[sub 1−x]N alloys. *Journal of Applied Physics* **92**, 4837, doi:10.1063/1.1508420 (2002).

56 Liang, Y. H. & Towe, E. Heavy Mg-doping of (Al,Ga)N films for potential applications in deep ultraviolet light-emitting structures. *Journal of Applied Physics* **123**, doi:10.1063/1.5009937 (2018).

57 Lee, K. *et al.* The origin of the high ideality factor in AlGaN-based quantum well ultraviolet light emitting diodes. *physica status solidi (b)* **247**, 1761-1763 (2010).

58 Liao, Y. *et al.* Temperature-dependent study on AlGaN-based deep ultraviolet light-emitting diode for the origin of high ideality factor. *AIP Advances* **11**, 105214, doi:10.1063/5.0059256 (2021).

59 Nepal, N., Nakarmi, M. L., Lin, J. Y. & Jiang, H. X. Photoluminescence studies of impurity transitions in AlGaN alloys. *Applied Physics Letters* **89**, 092107, doi:10.1063/1.2337856 (2006).

60 Nam, K. B., Nakarmi, M. L., Lin, J. Y. & Jiang, H. X. Deep impurity transitions involving cation vacancies and complexes in AlGaN alloys. *Applied Physics Letters* **86**, 222108, doi:10.1063/1.1943489 (2005).

61 Auzelle, T. *et al.* The influence of AlN buffer over the polarity and the nucleation of self-organized GaN nanowires. *Journal of Applied Physics* **117**, doi:10.1063/1.4923024 (2015).

CHAPTER 4.

Role of Nanowire Template on the Quality of AlN Epilayers and Performance of Vertical AlGaN LEDs

In this chapter[†], a series of comparisons are made on the crystallinity and optical properties, including photoluminescence (PL) peak positions and Raman peak shift, of AlN epilayers grown on Si with or without the use of nanowire template over a wide range of growth conditions and thicknesses, in order to evaluate the role of nanowire template on the quality of AlN epilayers. Moreover, properties of Mg-doped AlGaN epilayers grown on AlN-on-NW buffer layers and directly-grown AlN buffer layers are also compared. Finally, the electrical and optical properties of AlGaN LED structures grown on AlN-on-NW buffer layers and directly-grown AlN buffer layers are investigated.

4.1 Manuscript

Nanowire Template Assisted Epitaxy of Ultrawide Bandgap III-Nitrides on Si: Role of the nanowire Template

Qihua Zhang[1], Jenaes Sivasundarampillai[2], Heemal Parimoo[1], and Songrui Zhao[1] **

[1] Department of Electrical and Computer Engineering, McGill University, 3480 University Street, Montreal, Quebec H3A 0E9, Canada

[2] Department of Chemistry, McGill University, 801 Sherbrooke Street West, Montreal, Quebec H3A 0B8, Canada

---

[†] Section 4.1 is from a manuscript that has been accepted for publication: Q. Zhang, J. Sivasundarampillai, H. Parimoo, S. Zhao, "Nanowire Template Assisted Epitaxy of Ultrawide Bandgap III-nitrides on Si: Role of the Nanowire Template," *ACS Applied Optical Materials*, vol. 1, no. 3, p. 652, 2023, doi: 10.1021/acsaom.3c00023.

ABSTRACT: Ultrawide bandgap III-nitrides, including AlN and high Al content AlGaN alloys, are of great importance for applications to deep ultraviolet photonics and radio frequency electronics. However, lack of suitable substrates remains to be a challenge. In this context, we investigate the molecular beam epitaxy of AlN and high Al content AlGaN epilayers on low-cost Si substrates using a nanowire template as an intermediate layer. First, the role of the nanowire template on the quality of AlN is elucidated. By comparing AlN epilayers grown with and without the nanowire template over a wide range of growth conditions, it is found that using the nanowire template can relax the tensile strain in the AlN epilayers, as well as improve the overall crystalline quality. Second, the role of the quality of the AlN epilayer on the quality of the p-AlGaN layer grown on top is further discussed. It is found that the improved quality of AlN, due to the use of the nanowire template, also transfers to the improvement of the p-type doping in the AlGaN epilayers grown on top, which further contributes to a drastic improvement on the electrical performance of AlGaN p-i-n diodes, i.e., a factor of 10^4 reduction on the reverse bias leakage current, as well as a 250× improvement on the light output, comparing the structure with and without using the nanowire template. The study potentially impacts the development of ultrawide bandgap III-nitrides on foreign substrates as well as low-cost ultrawide bandgap III-nitride template technologies for a wide range of electronic and photonic device applications.

KEYWORDS: AlN, AlGaN, molecular beam epitaxy, Si, nanowire, p-n diodes

4.1.1 Main Body

Ultrawide bandgap semiconductors, including AlN and high Al content AlGaN alloys, are considered technologically important for various applications including short wavelength ultraviolet (UV) light emitting, high-electron mobility transistors (HEMTs), and field emission, owing to their ultrawide and direct bandgap energies, large breakdown fields, and chemical stability.[1-7] Moreover, they are widely used as buffer layers for III-nitride electronic and photonic devices.[8-20] However, the lack of native substrate has posed a significant challenge for the development of AlN and high Al content AlGaN based device technologies. The large lattice mismatches with commonly available foreign substrates[21-23] lead to many issues in the epilayers, such as large dislocation densities and cracks. The segregation of dopants to dislocations affects the electrical doping and device performance severely.[24-32] Although single crystalline bulk AlN substrates have been commercially available, they are very costly. A low-cost AlGaN template technology is thus necessary for further device development.

Low-dimensional AlGaN nanowires (NWs) have emerged in the past decade as one way to mitigate the issue of lack of native substrate. In fact, AlGaN NWs can be formed on a wide range of foreign substrates including amorphous layer, metal foil, and graphene, just name a few.[33-37] The main benefit of using NWs is that due to the large surface area to bulk volume ratio, lattice strain can be efficiently relaxed, leading to reduced densities of extended defects such as dislocations, compared to planar counterparts.[38] Moreover, NWs can also be used as strain-relief layer to form device-quality epilayers on top through coalescence processes;[39-43] and transmission electron microscopy studies have confirmed that NWs can reduce dislocation density in the epilayers.[39, 40, 42, 43]

Recently, we have demonstrated nanowire template assisted AlN epilayers on low-cost Si substrates, including vertical AlGaN UV LED demonstrations.[44-49] However, the wafer-scale effect of the nanowire template on relaxing the lattice strain and electrical doping remains unclear. In this study, we carry out this critical and missing study: evaluating the role of the NW template, in the epitaxy of AlN and AlGaN epilayers on Si, using various characterization techniques including X-ray diffraction (XRD), Raman, photoluminescence (PL), current-voltage (I-V) characteristics, and electroluminescence (EL). First, by comparing AlN epilayers grown with and without the NW template over a wide range of growth conditions as well as the thicknesses, it is found that using the NW template can improve the crystalline quality and relax the lattice strain of the AlN epilayer. Moreover, the improved AlN epilayer quality further improves Mg dopant incorporation into AlGaN epilayers grown on top. This study therefore clearly demonstrates the wafer-scale effect of the NW template on the epitaxy of AlN and high Al content AlGaN alloys on Si substrate and represents a critical step towards the integration of ultrawide bandgap III-nitride devices to low-cost foreign substrates as well as low-cost AlN and high Al content AlGaN template technologies.

All the epilayers were grown by plasma-assisted molecular beam epitaxy (MBE) on 3 in. Si (111) substrates. The Si substrates were first cleaned by acetone and methanol and then etched by hydrofluoric solution to remove the nature oxide layer. The growth started with a thin AlN layer (~2 nm) using an Al first approach.[50] This was followed by the growth of a GaN NW layer with a Ga beam equivalent pressure (BEP) of 1.2×10^{-7} Torr, a nitrogen flow rate of 0.6 sccm, and a substrate temperature of 700 °C. Detailed discussions on the nanowire template can be found in our recent publications.[44-46,48,51] The substrate temperature was calibrated using Si (111) 1×1 to 7×7 surface reconstruction during the ramping up process of Si substrates.[52-54] In the end, AlN was grown. Such a NW template based AlN epilayer is schematically shown in the inset of Figure 4-1. Different from the coalescence of GaN NWs to obtain GaN epilayers on top, the coalescence of AlN on GaN NWs requires proper control of NW density so that the stress to AlN due to the formation of a compact GaN epilayer can be minimized. In the past, we have developed such a control process through monitoring the reflection high-energy electron diffraction (RHEED) patterns during the NW growth stage.[44-46]

In this study, a wide range of growth conditions, including nitrogen (N) flow rate, Al BEP, and substrate temperature (T_{AlN}), have been studied for such AlN epilayers. Overall, Al BEP was varied from 3.7×10^{-8} to 1.3×10^{-7} Torr, the N flow rate was either 0.3 or 1.5 sccm, and T_{AlN} was varied from 750°C to 960°C. The detailed parameters for AlN growth will be described together with the results. Figure 4-1 shows representative conditions together with their RHEED patterns. The two curves are guide-for-eyes, denoting the boundary between droplet regime and the intermediate growth regime that is Al-rich but without droplet formation. N-limited growth rates, which correlate to the two N flow rates, are also shown by horizontal lines. Overall, 3 types of RHEED patterns were observed depending on the III/V ratio and T_{AlN}. Pattern (i): Spotty RHEED pattern, correlating to the N-rich or weak metal-deficiency regime. Pattern (ii): Streaky RHEED pattern and strong 2×6 reconstruction, correlating to Al-rich regime but without droplet formation. Pattern (iii): Streaky RHEED pattern but weak 2×6 reconstruction, due to the increased Al adatom desorption or the intentionally reduced Al at the growth front. The samples used in the later characterizations exhibit RHEED patterns close to either (ii) or (iii).

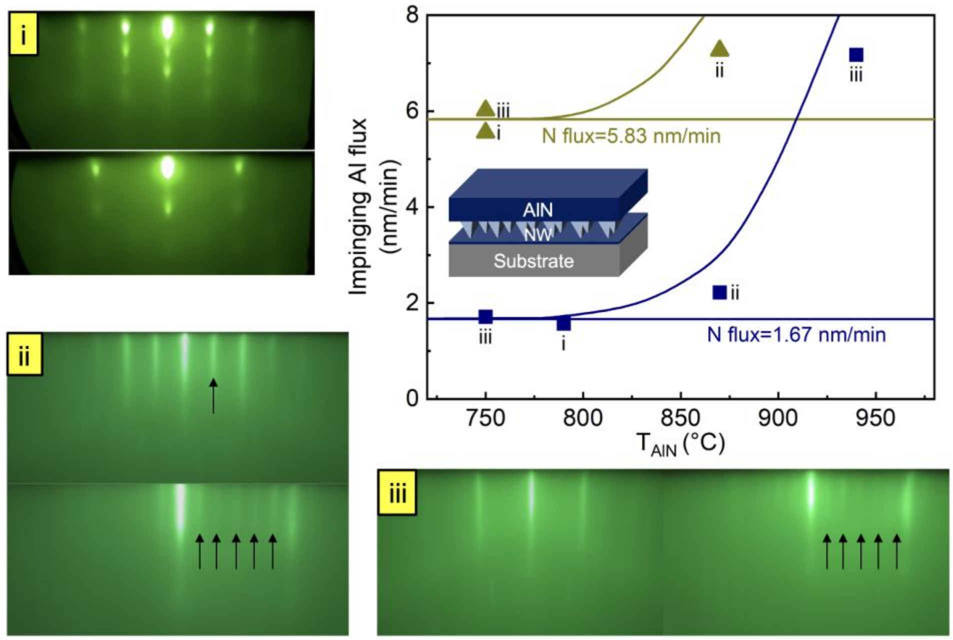

Figure 4-1 Growth diagrams of AlN epilayers on the NW template. Inset: Schematic of the NW template based AlN epilayer. The corresponding RHEED patterns are also shown: (i) spotty RHEED, (ii) bright and clear 2×6 streaky pattern, and (iii) weak 2×6 streaky pattern.

Detailed examination using scanning electron microscope (SEM) at different magnifications and different spots on the wafers further confirm that the wafers are highly smooth, crack-free, and droplet-free at a nearly wafer-scale over a wide range of T_{AlN}. The smooth surface (with a rms roughness of around 0.4 nm) is also confirmed with atomic force microscope (AFM). These surface characteristics are similar to our previous reports.[45,47,49] Nonetheless, for AlN epilayers grown directly on Si, the surface morphology is much worse; the droplet-free, smooth region is only ~ mm^2. The detailed comparison on the surface morphology, as well as comments on the comparison can be found in Supporting Information (Section 4.1.2).

The crystalline quality of the AlN epilayers on the NW template and AlN epilayers grown directly on Si is compared first by XRD rocking curve (RC). The XRD experiments were performed on Bruker D8 Discover high-resolution X-ray diffractometer using a Cu anode, a 1.2

mm divergence slit at the source side, a Ge symmetric four-bounce monochromator, and scintillator detector. Signal calibration was performed by maximizing θ-2θ peak position intensity of the Si (111) plane. Both 002 and 102 reflections were examined; and results of 102 reflection follow the trend of 002 reflection. As such, only 002 reflection RC curves are shown. Figure 4-2(a) shows the full-width-at-half-maximum (fwhm) with respect to the thickness of the AlN epilayer. In this case, T_{AlN} was 870 °C. It is seen that in both sets of samples, with increasing the AlN epilayer thickness, the fwhm reduces, consistent with that thicker epilayers have better crystalline quality.[55-58] Moreover, it is seen that the RC fwhm is reduced by ~800 arcsec for the AlN epilayers on the NW template, suggesting that the use of the NW template can reduce dislocations in the AlN epilayers.

The effect of T_{AlN} on the crystalline quality of the AlN epilayers grown on the NW template is also studied by the 002 reflection RC fwhm. In this case, the thickness of the AlN epilayers was in the range of 0.55 to 1.1 µm, and T_{AlN} was varied from 750 to 960 °C. Shown in Figure 4-2(b), the fwhm decreases as T_{AlN} increases, suggesting an improvement on the crystalline quality. This temperature-dependent crystalline quality improvement can be explained by the dislocation bending and annihilation as the growth temperature increases.[59] Moreover, it is seen that fwhm around 1300 arcsec is obtained at a thickness of 0.55 µm, with the corresponding RC shown in the inset of Figure 4-2(b).

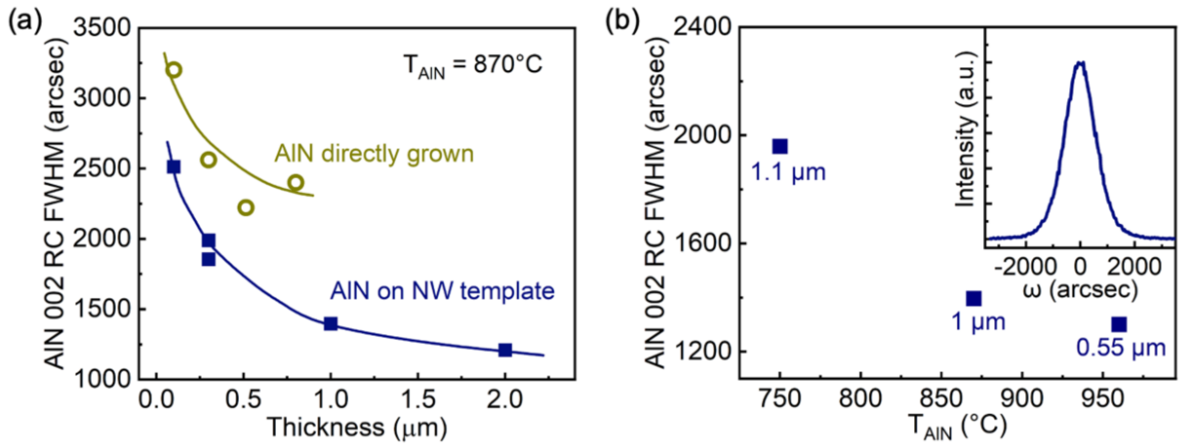

Figure 4-2 (a) fwhm of AlN 002 reflection RC as a function of the AlN layer thickness for AlN epilayers grown on the NW template (filled squares) and directly on Si (open circles). Solid curves are guide-for-eye. (b) Effect of T_{AlN} on the fwhm of AlN 002 reflection RC for AlN epilayers on the NW template. Inset: 002 reflection RC of the 0.55 µm thick AlN.

Hitherto, to improve the AlN epilayer quality on Si, epitaxial lateral overgrowth (ELO) on patterned Si is by far most successful, e.g., refs 23, 60, 61. Nonetheless, in order to obtain device-quality AlGaN epilayers on such AlN buffer layers, several µm thick AlN epilayers are needed. With such thick AlN epilayers, the 002 reflection RC fwhm is in the range of around 500 to 1000 arcsecs.[22, 23, 60-64] In the present study, we approached to this range by using a very thin AlN buffer layer. Moreover, compared to ELO process which requires complicated substrate patterning process, growth control, and relatively long growth duration, our approach is fully epitaxial, easy-to-control, and highly reproduceable at a wafer scale.

Room-temperature (RT) photoluminescence (PL) properties of the AlN epilayers grown on the NW template are further studied. In this regard, 193 nm ArF excimer laser with a repetition rate of 50 Hz and pulse energy of 2 mJ was used as the excitation source. The emitted light was collected from the wafer edge using an optical fiber, which was further coupled to a UV spectrometer. Figure 4-3(a) shows the RT PL spectra for AlN epilayers with a similar thickness of around 1 μm, grown with and without the NW template (T_{AlN} = 750°C). Also shown in Figure 4-3(a) is a RT PL spectrum from a commercial AlN-on-sapphire template. A striking feature is that, both AlN epilayers grown in this study is *free of any defect emission in the whole UV spectral range*. This is in contrast to the commercial AlN-on-sapphire template wherein a strong defect emission at 350 nm (~3.54 eV) is measured, due to deep defect levels related to Al vacancies.[62, 65, 66]

In addition, the three samples show different RT PL peak positions, with the commercial AlN template at 207.2 nm (~5.98 eV), AlN on the NW template at 209.2 nm (~5.93 eV), and AlN directly grown on Si at 212.1 nm (~5.85 eV). Given the same excitation densities for the three samples, the PL peak position difference thus could suggest different strain conditions in the AlN epilayers; that is, the commercial AlN template could be under a slight compressive strain, the AlN directly grown on Si could be under a tensile strain, whereas the AlN on the NW template could be relaxed.[55, 67-70] Figure 4-3(b) further shows the RT PL peak position comparison for AlN epilayers grown with and without the NW template at different thicknesses. It is seen that, regardless of the thickness, the PL peak position is always drastically different comparing AlN epilayers grown with the NW template to those grown without the NW template, again suggesting different strain situations.

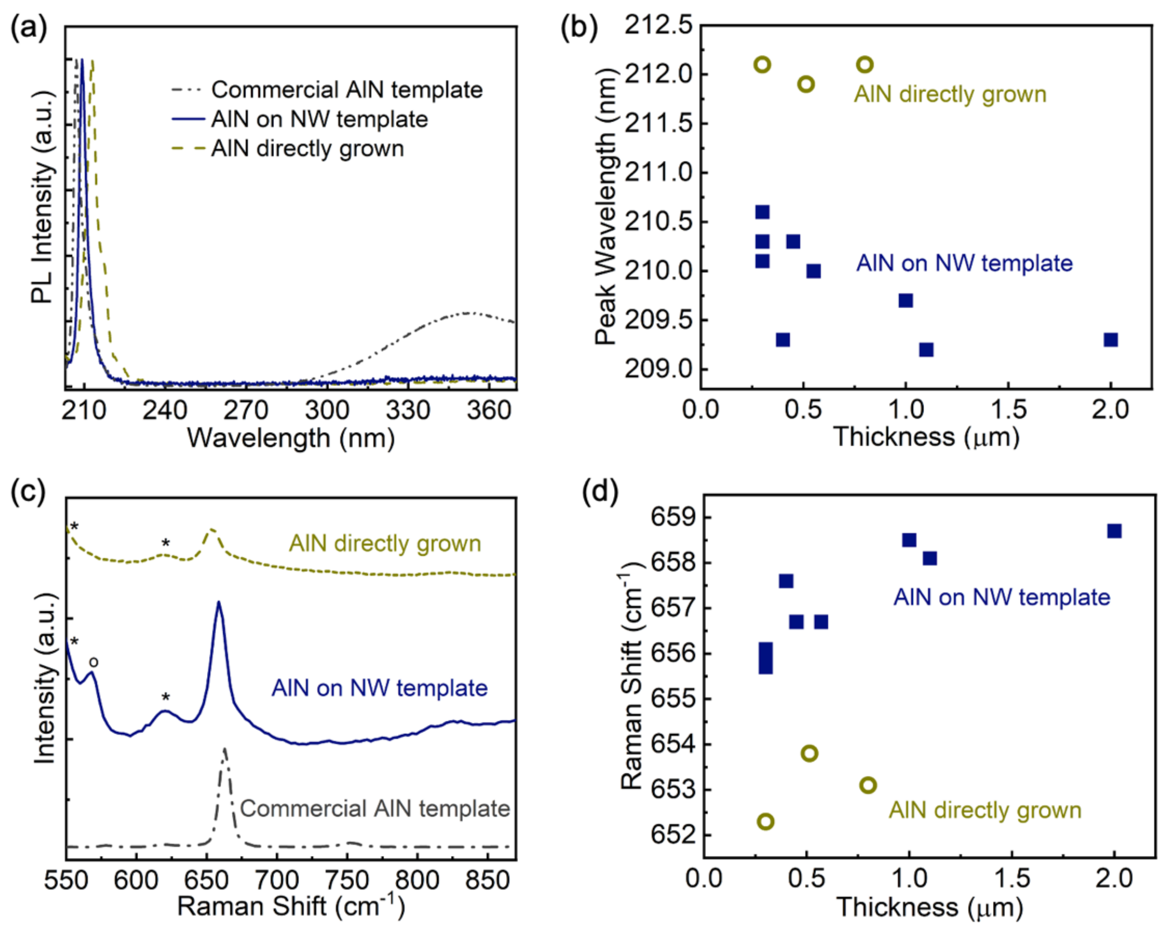

Figure 4-3 (a) Room-temperature PL spectra. (b) PL peak versus the layer thickness for the AlN epilayers grown on the NW template and directly on Si. (c) Room-temperature Raman spectra. Si/SiO_2 related modes are denoted in "⋆". GaN E_2(high) mode is denoted with "o". (d) AlN E_2(high) mode position for AlN epilayers grown on the NW template and directly on Si versus the layer thickness.

The strain in AlN epilayers is further assessed using RT Raman spectroscopy. The AlN E_2(high) mode position in Raman spectroscopy has been widely used to evaluate the strain status of AlN, and the peak position around 657 cm^{-1} at RT typically represents bulk AlN and relaxed AlN epilayers and nanowires.[68, 71-74] In this study, the Raman experiments were conducted by a WITec confocal Raman microscope with a 532 nm laser and a 50× objective lens, under a $z(x\bar{x})\bar{z}$ scattering geometry. A comparison is made between the AlN epilayers with a similar thickness grown on the NW template and directly on Si. Commercial AlN-on-sapphire template is also measured. The results are shown in Figure 4-3(c). It is seen that the AlN E_2(high) mode of the commercial AlN template is at 660.9 cm^{-1}, suggesting that the commercial AlN template is under a compressive strain. For the AlN epilayer grown on the NW template, the AlN E_2(high) mode is at 658.5 cm^{-1}, suggesting that the epilayer is nearly relaxed. Contrarily, the AlN E_2(high) mode for the AlN epilayer grown directly on Si is at 653.1 cm^{-1}, indicating that the epilayer is highly tensile strained.

The AlN E_2(high) mode position for AlN epilayers grown with and without the use of the NW template versus the epilayer thickness is shown in Figure 4-3(d). It is seen that, for the AlN epilayers grown on the NW template, the E_2(high) mode is red-shifted as the layer thickness reduces, but is still within the range of relaxed AlN (by 1 cm^{-1}). In contrast, the AlN epilayers directly grown on Si is always under tensile strain, regardless of the epilayer thickness.

The improved quality of the AlN epilayer further transfers to the dopant incorporation improvement in the AlGaN epilayers grown on top. This is tested by multiple 30 nm thick Mg-doped $Al_{0.7}Ga_{0.3}N$ epilayers with various Mg concentrations grown on the AlN epilayers (250 nm thick) with the NW template (referred to as "AlN-on-NW template") and without the NW template (referred to as "direct AlN"). These Mg-doped $Al_{0.7}Ga_{0.3}N$ epilayers were grown in metal-rich conditions, with an Al BEP of 3.5×10^{-8} Torr, a N flow rate of 0.3 sccm, and a substrate temperature of 725°C. The Mg concentration was measured by Secondary ion mass spectroscopy (SIMS) at EAG Labs and was in the range of 7×10^{17} cm^{-3} to 2×10^{18} cm^{-3}.

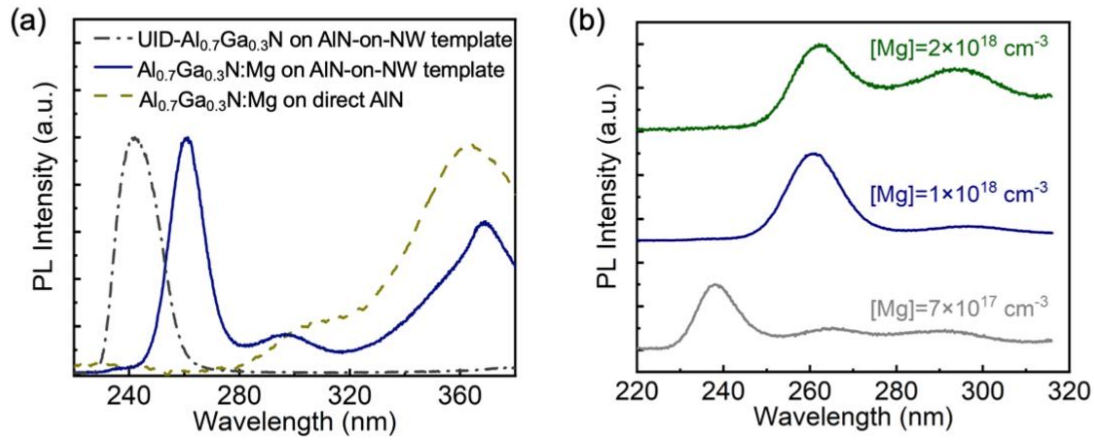

Figure 4-4 (a) Room-temperature PL spectra of various $Al_{0.7}Ga_{0.3}N$ epilayers. (b) Room-temperature PL spectra of $Al_{0.7}Ga_{0.3}N$:Mg epilayers on AlN-on-NW template with different Mg doping concentrations.

Figure 4-4(a) shows the RT PL spectra of such $Al_{0.7}Ga_{0.3}N$:Mg epilayers with Mg doping concentration of 1×10^{18} cm^{-3}. In the RT PL experiments, a solid-state Nd:YAG laser ($\lambda = 213$ nm) with a pulse width of 7 ns was used to excite the samples through the top surface, and the emitted light was collected from the top surface as well by an optical fiber. The RT PL spectrum of an un-doped or unintentionally doped (UID) AlGaN layer on AlN-on-NW template is also shown. It is seen that, for the UID sample, a near band-edge PL peak at 240 nm is measured. Using Vegard's law and a bowing parameter of 1 eV,[75] the corresponding Al content is estimated to be 0.7. For the Mg-doped sample on AlN-on-NW template, the main PL peak is at around 261 nm, with a side peak at 292 nm. These peaks are attributed to transitions from the conduction band minimum to neutral Mg acceptors (CBM-Mg) and deep donor to Mg acceptor pair (DAP), respectively.[76] However, for the Mg-doped sample on direct AlN, with a similar growth condition compared to that on the AlN-on-NW template, only DAP transition is measured, suggesting a poor Mg dopant incorporation and p-type conduction.[76]

Using AlN-on-NW template, the Mg dopant incorporation into AlGaN epilayers can be further controlled. Figure 4-4(b) shows the RT PL spectra of $Al_{0.7}Ga_{0.3}N$:Mg epilayers with various Mg doping concentrations. It is seen that, for the sample with a Mg doping concentration of 7×10^{17} cm^{-3}, the near band-edge transition dominates the PL spectrum, with negligible CBM-Mg and DAP transitions. By further increasing the Mg concentration to 1×10^{18} cm^{-3}, the PL emission is dominated by the CBM-Mg transition, suggesting an increased Mg dopant incorporation. For an even higher Mg concentration (2×10^{18} cm^{-3}), the PL emission related to DAP becomes more pronounced; nonetheless, the overall PL emission characteristics are still dominated by the CBM-Mg transition.

It is also noted that, for the Mg doped samples, the defect PL emission at ~360 nm is measured. This is due to the use of T_{AlN} of 870 °C for all these Mg-doped AlGaN epilayers. Such a defect PL emission peak is found to be suppressed with the use of low T_{AlN} (e.g., 750°C, as shown in Figure 4-3(a)). This could be explained by that, due to the presence of excess Al at the growth front at low T_{AlN}, the formation of Al vacancies can be suppressed. This has been proposed in the previous studies.[77]

The improved Mg dopant incorporation in the AlGaN epilayers further helps to improve the electrical performance of AlGaN p-i-n diodes. In this regard, p-$Al_{0.7}Ga_{0.3}N$/i-$Al_{0.4}Ga_{0.6}N$/n-$Al_{0.7}Ga_{0.3}N$ double heterojunction (DH) p-i-n diodes grown on AlN-on-NW template and direct AlN, as schematically shown in Figure 4-5(a), are compared. All the AlGaN layers were grown in metal-rich conditions, with Al contents controlled by varying Al BEP in the range of 2.8-3.5$\times10^{-8}$ Torr. The N flow rate was 0.3 sccm. Si was used as the n-type dopant. The detailed growth conditions for such AlGaN DHs can be found elsewhere.[45] The only difference for the two structures is with and without the use of AlN-on-NW template. The metallization of such AlGaN p-i-n diodes was realized by Ni (7 nm)/Au (7 nm) as the top p-contact and colloidal Ag conductive adhesive on the backside of n-Si substrate as the n-contact. Figure 4-5(b) shows the I-V characteristics for the two structures under a continuous-wave biasing by a Keithley 2400 source meter. It is seen that nearly no rectification is measured for the structure on direct AlN, due to the very high reverse bias leakage current. With AlN-on-NW template, on the other hand, the reverse bias leakage is reduced by a factor of ~10^4. This dramatic improvement on the electrical performance also improves the light output power, which was collected by an optical fiber from the device top surface. As shown in Figure 4-5(c), no light can be measured at low injection currents (<6 mA) from the structure on direct AlN due to the leakage current, and the light intensity is increased by a factor of ~250 with the use of AlN-on-NW template at a forward current of 20 mA.

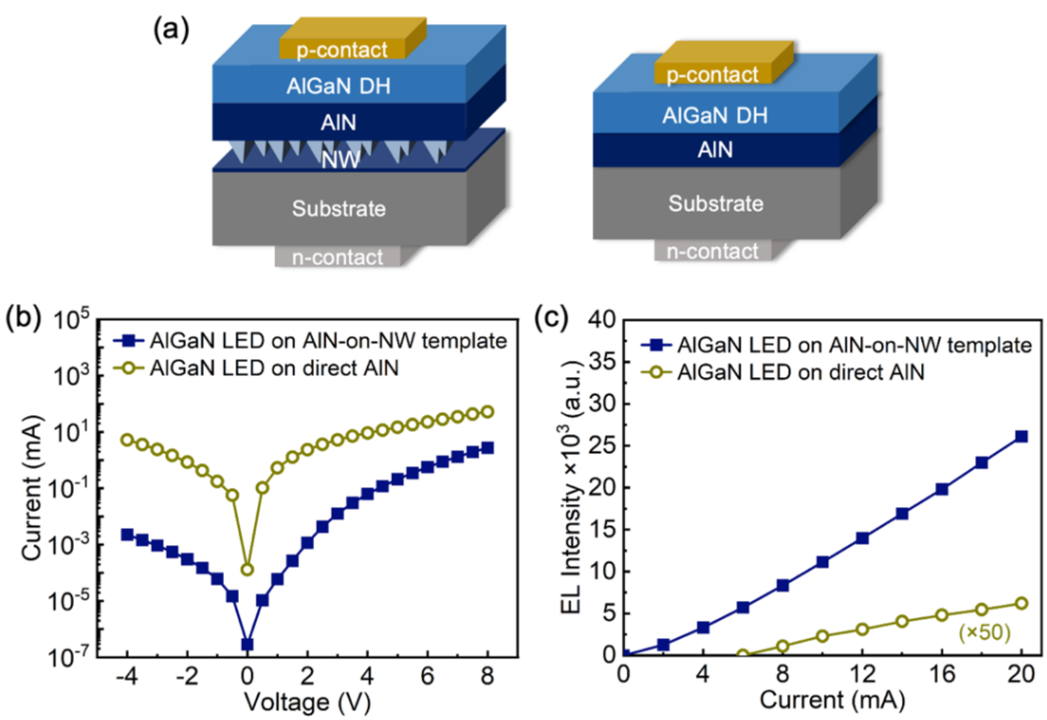

Figure 4-5 (a) Schematics of p-$Al_{0.7}Ga_{0.3}N$/i-$Al_{0.4}Ga_{0.6}N$/n-$Al_{0.7}Ga_{0.3}N$ double heterojunction (DH) p-i-n diodes on AlN-on-NW template (left) and direct AlN (right). (b) and (c) Corresponding I-V characteristics and light output power comparison.

The drastic improvement on the Mg dopant incorporation as well as the diode electrical performance can be explained by the followings. First, as the AlN epilayers grown on the NW template is nearly relaxed as suggested by Raman and PL studies, the continuous growth of thin AlGaN epilayers on top will render a possible compressive strain in the AlGaN epilayers, which favor Mg dopant incorporation.[27,32] Second, as the use of the NW template can improve the crystalline quality of the AlN epilayers (as suggested by XRD experiments), the Mg incorporation into the AlGaN grown on top of such AlN epilayers can be improved, due to the suppression of Mg diffusion along threading dislocations. Lastly, also due to the improvement of the crystalline quality, the formation of donor-type Mg-threading screw dislocations (TSD) complex can be effectively reduced in the AlGaN:Mg epilayers, which significantly reduces the leakage current and improves the rectification ratio of the p-i-n diode.[29-31]

In conclusion, we have investigated the role of the NW template on the epitaxy of AlN epilayers on Si *at a wafer scale* over a wide range of growth conditions. It is found that the use of the NW template can reduce the tensile strain as well as improve the crystalline quality of the AlN epilayer grown on top, as suggested by XRD, PL, and Raman experiments. The improved AlN epilayer quality further transfers into the improved Mg doping in the AlGaN epilayers grown on top of such AlN buffer layers. This further improves the electrical performance of the AlGaN p-i-n diodes, with a 10^4 reduction on the reverse bias leakage current. The light output is also improved by a factor of ~250. It is further worth emphasizing that, as nanowires can be formed virtually on any substrates, this study therefore suggests that it is possible to integrate ultrawide bandgap III-nitride epilayers to other substrates using this approach, and greatly relaxes substrate requirement. Moreover, the easy removal of Si substrate further offers the opportunity to develop free-standing ultrawide bandgap III-nitride templates. As such, this study potentially benefits the development of a wide range of electronic and photonic devices. It should also be noted that, although the approach of using nanowire template to obtain epilayers has been proposed in the past, all studies prior to this work have only focused on the microscopic properties. However, for practical device development, understanding the wafer-scale effect is critical – this missing study limits the practical application of the nanowire template assisted epilayer technology. The present work has filled the gap and provided this missing and critical study, and thus could widen the practical applications of nanowires.

4.1.2 Supporting Information

In this study, we found obtaining smooth, crack-free, droplet-free, and thick AlN epilayer at a large area is much easier using the NW template, compared to without using the NW template. This could be attributed to the modification of growth kinetics with the use of the NW template.

Figure 4-6 shows the SEM images of an AlN on NW template sample grown with T_{AlN} of 870 °C, Al BEP of 5×10^{-8} Torr, and a N flow rate of 0.3 sccm. It is seen that a smooth, droplet-free surface can be obtained. Different spots on the wafer were also examined, providing a similar surface. The droplets were only present on the very edge of the wafer, limited by the substrate heater.

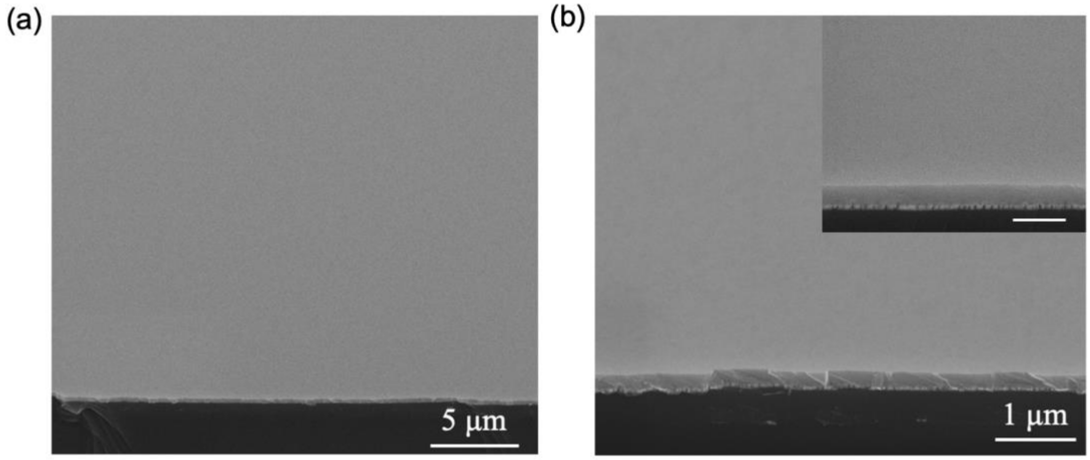

Figure 4-6 SEM images of AlN grown on the NW template. (a), (b), and inset of (b) correlate to different magnifications. The scale bar for the inset of (b) is 500 nm.

Using similar growth parameters, directly growing AlN on Si led to a large variation of surface. As shown in Figure 4-7, over roughly 10 mm variation in the radial direction, the surface changes from a rough surface to a smooth surface but with droplets. Note that Figure 4-7(c) shows a rough AlN surface with droplets. And the droplet region is far away from the wafer edge.

Although it might be possible to obtain smooth, crack-free, droplet-free, and thick AlN epilayers directly on Si with further optimizing growth parameters, such AlN epilayers negate the purpose of the comparison. The purpose of the comparison (including the surface as shown above and other comparisons shown in the main manuscript) is to show the role of the nanowire template; as such, it is more reasonable to use similar growth parameters.

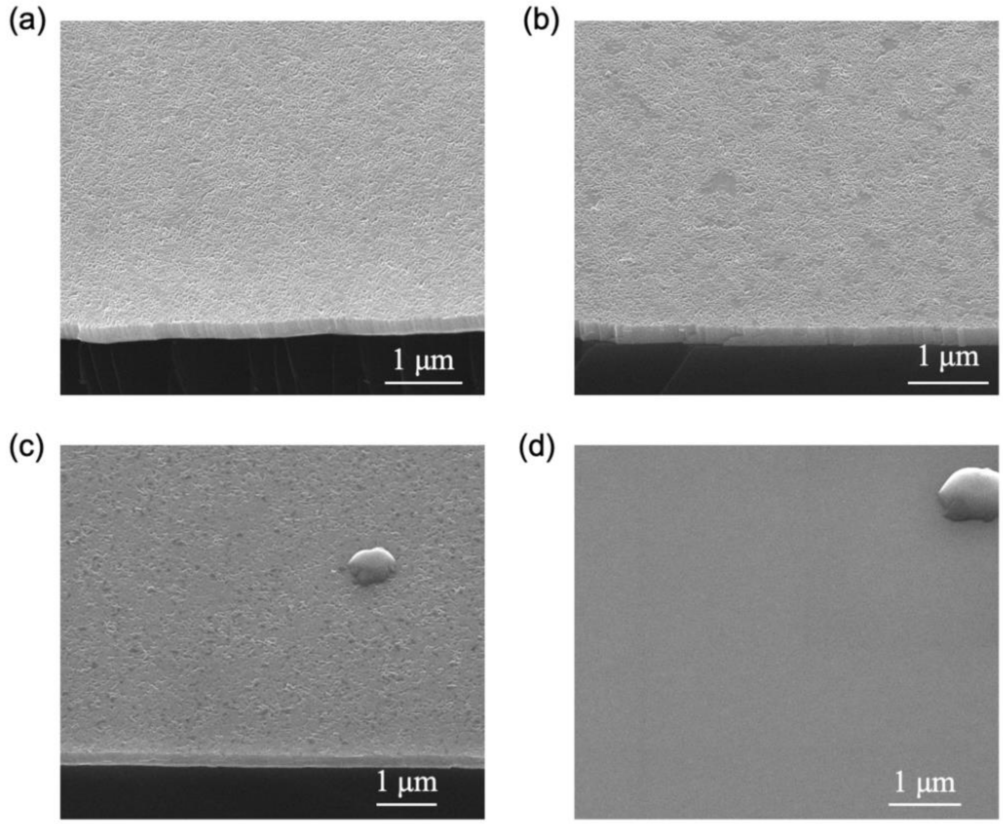

Figure 4-7 SEM images of AlN grown directly on Si on different regions of the wafer. From (a) to (d) it correlates to a slight reduction of the substrate temperature, which led to a smoother surface but with the presence of droplets.

Now, for the comparison between AlN on NW template and other buffer layer technologies on Si, this has been described in the main manuscript; and the NW template method yields AlN epilayers with quality approaching to that of the ELO AlN, but at a much lower dollar- and time-cost; and the growth of AlN using the NW template can be further optimized.

Lastly, it is worth emphasizing that, even today, it has remained challenging to grow smooth, crack-free, droplet-free, and thick AlN on Si. To the best of our knowledge, so far, only ELO and our NW template methods are able to grow such AlN epilayers.

References

(1) Strite, S.; Morkoc, H. GaN, AlN, and InN: a review. *J. Vac. Sci. Technol., B: Microelectron. Nanometer Struct.* **1992**, *10* (4), 1237--1266.

(2) Taniyasu, Y.; Kasu, M.; Makimoto, T. An aluminium nitride light-emitting diode with a wavelength of 210 nanometres. *Nature.* **2006**, *441* (7091), 325-8.

(3) Kaplar, R. J.; Allerman, A. A.; Armstrong, A. M.; Crawford, M. H.; Dickerson, J. R.; Fischer, A. J.; Baca, A. G.; Douglas, E. A. Review—Ultra-Wide-Bandgap AlGaN Power Electronic Devices. *ECS J. Solid State Sci. Technol.* **2016**, *6* (2), Q3061-Q3066.

(4) Taniyasu, Y.; Kasu, M.; Makimoto, T. Field emission properties of heavily Si-doped AlN in triode-type display structure. *Appl. Phys. Lett.* **2004**, *84* (12), 2115-2117.

(5) Shatalov, M.; Gaevski, M.; Adivarahan, V.; Khan, A. Room-Temperature Stimulated Emission from AlN at 214 nm. *Jpn. J. Appl. Phys.* **2006**, *45* (49), L1286-L1288.

(6) Mishra, U. K.; Parikh, P.; Yi-Feng, W. AlGaN/GaN HEMTs-an overview of device operation and applications. *Proc. IEEE.* **2002**, *90* (6), 1022-1031.

(7) Zhao, S.; Connie, A. T.; Dastjerdi, M. H.; Kong, X. H.; Wang, Q.; Djavid, M.; Sadaf, S.; Liu, X. D.; Shih, I.; Guo, H.; Mi, Z. Aluminum nitride nanowire light emitting diodes: Breaking the fundamental bottleneck of deep ultraviolet light sources. *Sci. Rep.* **2015**, *5*, 8332.

(8) Amano, H.; Sawaki, N.; Akasaki, I.; Toyoda, Y. Metalorganic vapor phase epitaxial growth of a high quality GaN film using an AlN buffer layer. *Appl. Phys. Lett.* **1986**, *48* (5), 353.

(9) Chen, P.; Zhang, R.; Zhao, Z. M.; Xi, D. J.; Shen, B.; Chen, Z. Z.; Zhou, Y. G.; Xie, S. Y.; Lu, W. F.; Zheng, Y. D. Growth of high quality GaN layers with AlN buffer on Si(1 1 1) substrates. *J. Cryst. Growth.* **2001**, *225*, 150.

(10) Feng, M.; Liu, J.; Sun, Q.; Yang, H. III-nitride semiconductor lasers grown on Si. *Prog. Quantum Electron.* **2021**, *77*, 100323.

(11) Li, Y.; Xing, Z.; Zheng, Y.; Tang, X.; Xie, W.; Chen, X.; Wang, W.; Li, G. High-efficiency near-UV light-emitting diodes on Si substrates with InGaN/GaN/AlGaN/GaN multiple quantum wells. *J.Mater. Chem. C.* **2020**, *8* (3), 883-888.

(12) Amano, H.; Baines, Y.; Beam, E.; Borga, M.; Bouchet, T.; Chalker, P. R.; Charles, M.; Chen, K. J.; Chowdhury, N.; Chu, R.; De Santi, C.; De Souza, M. M.; Decoutere, S.; Di Cioccio, L.; Eckardt, B.; Egawa, T.; Fay, P.; Freedsman, J. J.; Guido, L.; Häberlen, O.; Haynes, G.; Heckel, T.; Hemakumara, D.; Houston, P.; Hu, J.; Hua, M.; Huang, Q.; Huang, A.; Jiang, S.; Kawai, H.; Kinzer, D.; Kuball, M.; Kumar, A.; Lee, K. B.; Li, X.; Marcon, D.; März, M.; McCarthy, R.; Meneghesso, G.; Meneghini, M.; Morvan, E.; Nakajima, A.; Narayanan, E. M. S.; Oliver, S.; Palacios, T.; Piedra, D.; Plissonnier, M.; Reddy, R.; Sun, M.; Thayne, I.; Torres, A.; Trivellin, N.; Unni, V.; Uren, M. J.; Van Hove, M.; Wallis, D. J.; Wang, J.; Xie, J.; Yagi, S.; Yang, S.; Youtsey, C.; Yu, R.; Zanoni, E.; Zeltner, S.; Zhang, Y. The 2018 GaN power electronics roadmap. *J. Phys. D: Appl. Phys.* **2018**, *51* (16), 163001.

(13) Amano, H.; Collazo, R.; Santi, C. D.; Einfeldt, S.; Funato, M.; Glaab, J.; Hagedorn, S.; Hirano, A.; Hirayama, H.; Ishii, R.; Kashima, Y.; Kawakami, Y.; Kirste, R.; Kneissl, M.; Martin, R.; Mehnke, F.; Meneghini, M.; Ougazzaden, A.; Parbrook, P. J.; Rajan, S.; Reddy, P.; Römer, F.; Ruschel, J.; Sarkar, B.; Scholz, F.; Schowalter, L. J.; Shields, P.; Sitar, Z.; Sulmoni, L.; Wang, T.; Wernicke, T.; Weyers, M.; Witzigmann, B.; Wu, Y.-R.; Wunderer, T.; Zhang, Y. The 2020 UV emitter roadmap. *J. Phys. D: Appl. Phys.* **2020**, *53* (50), 503001.

(14) Kneissl, M.; Seong, T.-Y.; Han, J.; Amano, H. The emergence and prospects of deep-ultraviolet light-emitting diode technologies. *Nature Photonics.* **2019**, *13* (4), 233-244.

(15) Sun, H.; Woodward, J.; Yin, J.; Moldawer, A.; Pecora, E. F.; Nikiforov, A. Y.; Dal Negro, L.; Paiella, R.; Ludwig, K.; Smith, D. J.; Moustakas, T. D. Development of AlGaN-based graded-index-separate-confinement-heterostructure deep UV emitters by molecular beam epitaxy. *J. Vac. Sci. Technol., B: Microelectron. Nanometer Struct.* **2013**, *31* (3), 03C117.

(16) Pandey, A.; Gim, J.; Hovden, R.; Mi, Z. Electron overflow of AlGaN deep ultraviolet light emitting diodes. *Appl. Phys. Lett.* **2021**, *118* (24).

(17) Jmerik, V.; Toropov, A.; Davydov, V.; Ivanov, S. Monolayer-Thick GaN/AlN Multilayer Heterostructures for Deep-Ultraviolet Optoelectronics. *Phys. Status Solidi RRL*. **2021**, *15*, 2100242.

(18) Li, D.; Jiang, K.; Sun, X.; Guo, C. AlGaN photonics: recent advances in materials and ultraviolet devices. *Adv. Opt. Photonics.* **2018**, *10* (1), 43-110.

(19) Huang, C.; Zhang, H.; Sun, H. Ultraviolet optoelectronic devices based on AlGaN-SiC platform: Towards monolithic photonics integration system. *Nano Energy.* **2020**, *77*, 105149.

(20) Shan, M.; Zhang, Y.; Tian, M.; Lin, R.; Jiang, J. a.; Zheng, Z.; Zhao, Y.; Lu, Y.; Feng, Z.; Guo, W.; Dai, J.; Chen, C.; Wu, F.; Li, X. Transverse Electric Lasing at a Record Short Wavelength 244.63 nm from GaN Quantum Wells with Weak Exciton Localization. *ACS Photonics.* **2021**, *8* (5), 1264-1270.

(21) LI, T.; MASTRO, M.; DADGAR, A., III–V compound semiconductors: Integration with silicon-based microelectronics. CRC Press, Taylor & Francis Group: 2011.

(22) Zhang, Y.; Gautier, S.; Cho, C.-Y.; Cicek, E.; Vashaei, Z.; McClintock, R.; Bayram, C.; Bai, Y.; Razeghi, M. Near milliwatt power AlGaN-based ultraviolet light emitting diodes based on lateral epitaxial overgrowth of AlN on Si(111). *Appl. Phys. Lett.* **2013**, *102* (1), 011106.

(23) Shen, J.; Yang, X.; Liu, D.; Cai, Z.; Wei, L.; Xie, N.; Xu, F.; Tang, N.; Wang, X.; Ge, W.; Shen, B. High quality AlN film grown on a nano-concave-circle patterned Si substrate with an AlN seed layer. *Appl. Phys. Lett.* **2020**, *117* (2), 022103.

(24) Schmidt, T.; Siebert, M.; Flege, J. I.; Figge, S.; Gangopadhyay, S.; Pretorius, A.; Lee, T. L.; Zegenhagen, J.; Gregoratti, L.; Barinov, A.; Rosenauer, A.; Hommel, D.; Falta, J. Mg and Si dopant incorporation and segregation in GaN. *Phys. Status Solidi (b).* **2011**, *248* (8), 1810-1821.

(25) Roshko, A.; Brubaker, M.; Blanchard, P.; Harvey, T.; Bertness, K. The role of Si in GaN/AlN/Si(111) plasma assisted molecular beam epitaxy: polarity and inversion. *Jpn. J. Appl. Phys.* **2019**, *58* (SC), SC1050.

(26) Rhode, S. K.; Horton, M. K.; Kappers, M. J.; Zhang, S.; Humphreys, C. J.; Dusane, R. O.; Sahonta, S. L.; Moram, M. A. Mg Doping Affects Dislocation Core Structures in GaN. *Phys. Rev. Lett.* **2013**, *111* (2), 025502.

(27) Soman, R.; Mohan, N.; Chandrasekar, H.; Bhat, N.; Raghavan, S. Dislocation bending and stress evolution in Mg-doped GaN films on Si substrates. *J. Appl. Phys.* **2018**, *124* (24), 245104.

(28) Sang, L.; Ren, B.; Endo, R.; Masuda, T.; Yasufuku, H.; Liao, M.; Nabatame, T.; Sumiya, M.; Koide, Y. Boosting the doping efficiency of Mg in p-GaN grown on the free-standing GaN substrates. *Appl. Phys. Lett.* **2019**, *115* (17), 172103.

(29) Usami, S.; Mayama, N.; Toda, K.; Tanaka, A.; Deki, M.; Nitta, S.; Honda, Y.; Amano, H. Direct evidence of Mg diffusion through threading mixed dislocations in GaN p–n diodes and its effect on reverse leakage current. *Appl. Phys. Lett.* **2019**, *114* (23), 232105.

(30) Usami, S.; Tanaka, A.; Fukushima, H.; Ando, Y.; Deki, M.; Nitta, S.; Honda, Y.; Amano, H. Correlation between nanopipes formed from screw dislocations during homoepitaxial growth

by metal-organic vapor-phase epitaxy and reverse leakage current in vertical p–n diodes on a free-standing GaN substrates. *Jpn. J. Appl. Phys.* **2019**, *58* (SC), SCCB24.

(31) Nakano, T.; Harashima, Y.; Chokawa, K.; Shiraishi, K.; Oshiyama, A.; Kangawa, Y.; Usami, S.; Mayama, N.; Toda, K.; Tanaka, A.; Honda, Y.; Amano, H. Screw dislocation that converts p-type GaN to n-type: Microscopic study on Mg condensation and leakage current in p–n diodes. *Appl. Phys. Lett.* **2020**, *117* (1), 012105.

(32) Kirste, R.; Hoffmann, M. P.; Tweedie, J.; Bryan, Z.; Callsen, G.; Kure, T.; Nenstiel, C.; Wagner, M. R.; Collazo, R.; Hoffmann, A.; Sitar, Z. Compensation effects in GaN:Mg probed by Raman spectroscopy and photoluminescence measurements. *J. Appl. Phys.* **2013**, *113* (10), 103504.

(33) Sun, H.; Li, X. Recent Advances on III-Nitride Nanowire Light Emitters on Foreign Substrates – Toward Flexible Photonics. *Phys. Status Solidi (a).* **2019**, *216* (2), 1800420.

(34) Sarwar, A. T. M. G.; Carnevale, S. D.; Yang, F.; Kent, T. F.; Jamison, J. J.; McComb, D. W.; Myers, R. C. Semiconductor Nanowire Light-Emitting Diodes Grown on Metal: A Direction Toward Large-Scale Fabrication of Nanowire Devices. *Small.* **2015**, *11* (40), 5402-5408.

(35) Kumaresan, V.; Largeau, L.; Madouri, A.; Glas, F.; Zhang, H.; Oehler, F.; Cavanna, A.; Babichev, A.; Travers, L.; Gogneau, N.; Tchernycheva, M.; Harmand, J.-C. Epitaxy of GaN Nanowires on Graphene. *Nano Lett.* **2016**, *16* (8), 4895-4902.

(36) Hetzl, M.; Schuster, F.; Winnerl, A.; Weiszer, S.; Stutzmann, M. GaN nanowires on diamond. *Mater. Sci. Semicond. Process.* **2016**, *48*, 65-78.

(37) Zhao, S.; Kibria, M. G.; Wang, Q.; Nguyen, H. P. T.; Mi, Z. Growth of large-scale vertically aligned GaN nanowires and their heterostructures with high uniformity on SiOx by catalyst-free molecular beam epitaxy. *Nanoscale.* **2013**, *5*, 5283.

(38) Glas, F. Critical dimensions for the plastic relaxation of strained axial heterostructures in free-standing nanowires. *Phys. Rev. B.* **2006**, *74* (12), 121302.

(39) Li, Q.; Lin, Y.; Creighton, J. R.; Figiel, J. J.; Wang, G. T. Nanowire-Templated Lateral Epitaxial Growth of Low-Dislocation Density Nonpolara-Plane GaN onr-Plane Sapphire. *Adv. Mater.* **2009**, *21* (23), 2416-2420.

(40) Yeom, B.-R.; Navamathavan, R.; Park, J.-H.; Ra, Y.-H.; Lee, C.-R. Growth behavior of GaN epilayers on Si(111) grown by GaN nanowires assisted epitaxial lateral overgrowth. *CrystEngComm.* **2012**, *14* (17), 5558-5563.

(41) Fan, S.; Zhao, S.; Liu, X.; Mi, Z. Study on the coalescence of dislocation-free GaN nanowires on Si and SiOx. *J. Vac. Sci. Technol., B: Nanotechnol. Microelectron.: Mater., Process., Meas., Phenom.* **2014**, *32* (2), 02C114.

(42) Wu, Y.; Wang, Y.; Sun, K.; Aiello, A.; Bhattacharya, P.; Mi, Z. Molecular beam epitaxy and characterization of Mg-doped GaN epilayers grown on Si (0 0 1) substrate through controlled nanowire coalescence. *J. Cryst. Growth.* **2018**, *498*, 109-114.

(43) Das, D.; Aiello, A.; Guo, W.; Bhattacharya, P. InGaN/GaN Quantum Dots on Silicon With Coalesced Nanowire Buffer Layers: A Potential Technology for Visible Silicon Photonics. *IEEE Trans. Nanotechnol.* **2020**, *19*, 571-574.

(44) Yin, X.; Zhang, Q.; Zhao, S. Molecular Beam Epitaxial Growth of AlN Thin Films on Si through Exploiting Low Al Adatom Migration and the Nitrogen-Rich Environment on a Nanowire Template. *Cryst. Growth Des.* **2021**, *21* (7), 3645-3649.

(45) Zhang, Q.; Parimoo, H.; Martel, E.; Zhao, S. Vertical semiconductor deep ultraviolet light emitting diodes on a nanowire-assisted aluminum nitride buffer layer. *Sci. Rep.* **2022**, *12* (1), 7230.

(46) Yin, X.; Zhao, S. High Internal Quantum Efficiency AlGaN Epilayer Grown by Molecular Beam Epitaxy on Si Substrate. *ECS J. Solid State Sci. Technol.* **2021**, *10* (7), 076001.

(47) Zhang, Q.; Parimoo, H.; Martel, E.; Yin, X.; Zhao, S. Vertical AlGaN Deep Ultraviolet Light Emitting Diodes with Polarization Enhanced p-AlGaN Epilayer on Si Substrate. *ECS J. Solid State Sci. Technol.* **2022**, *11* (6), 066003.

(48) Zhang, Q.; Yin, X.; Martel, E.; Zhao, S. Molecular beam epitaxy growth and characterization of AlGaN epilayers in nitrogen-rich condition on Si substrate. *Mater. Sci. Semi. Proce.* **2021**, 135, 106099.

(49) Zhang, Q.; Parimoo, H.; Martel, E.; Zhao, S. Molecular Beam Epitaxy of AlGaN Epilayers on Si for Vertical Deep Ultraviolet Light-Emitting Diodes. *ECS J. Solid State Sci. Technol.* **2022**, *11* (11), 116002.

(50) Lu, J.; Zhong, Y.; Zhao, S. Comparative study on the molecular beam epitaxial growth and characterization of AlGaN nanowire structures on AlN buffer layer and on Si. *J. Vac. Sci. Technol. B.* **2020**, *38* (6), 062804.

(51) Zhong, Y; Berikaa, E; Lu, J; Yin, X; Zhao, S. Molecular beam epitaxial growth and optical characterization of AlGaN nanowires with reduced substrate temperature. *AIP Adv.* **2020**, 10, 025022.

(52) Schenk, H. P. D.; Kipshidze, G. D.; Lebedev, V. B.; Shokhovets, S.; Goldhahn, R.; Kräußlich, J.; Fissel, A.; Richter, W. Epitaxial growth of AlN and GaN on Si(111) by plasma-assisted molecular beam epitaxy. *J. Cryst. Growth.* **1999**, *201-202*, 359-364.

(53) Yasutake, K.; Takeuchi, A.; Kakiuchi, H.; Yoshii, K. Molecular beam epitaxial growth of AlN single crystalline films on Si (111) using radio-frequency plasma assisted nitrogen radical source. *J. Vac. Sci. Technol. A.* **1998**, *16* (4), 2140-2147.

(54) Calleja, E.; Sánchez-García, M. A.; Sánchez, F. J.; Calle, F.; Naranjo, F. B.; Muñoz, E.; Molina, S. I.; Sánchez, A. M.; Pacheco, F. J.; García, R. Growth of III-nitrides on Si(111) by molecular beam epitaxy Doping, optical, and electrical properties. *J. Cryst. Growth.* **1999**, *201-202*, 296-317.

(55) Pantha, B. N.; Dahal, R.; Nakarmi, M. L.; Nepal, N.; Li, J.; Lin, J. Y.; Jiang, H. X.; Paduano, Q. S.; Weyburne, D. Correlation between optoelectronic and structural properties and epilayer thickness of AlN. *Appl. Phys. Lett.* **2007**, *90* (24), 241101.

(56) Shen, X.-Q.; Takahashi, T.; Ide, T.; Shimizu, M. High quality thin AlN epilayers grown on Si(110) substrates by metal-organic chemical vapor deposition. *CrystEngComm.* **2017**, *19* (8), 1204-1209.

(57) Yarar, E.; Hrkac, V.; Zamponi, C.; Piorra, A.; Kienle, L.; Quandt, E. Low temperature aluminum nitride thin films for sensory applications. *AIP Adv.* **2016**, *6* (7), 075115.

(58) Tran, B. T.; Hirayama, H.; Maeda, N.; Jo, M.; Toyoda, S.; Kamata, N. Direct Growth and Controlled Coalescence of Thick AlN Template on Micro-circle Patterned Si Substrate. *Sci. Rep.* **2015**, *5* (1), 14734.

(59) Nakarmi, M. L.; Cai, B.; Lin, J. Y.; Jiang, H. X. Three-step growth method for high quality AlN epilayers. *Phys. Status Solidi (a).* **2012**, *209* (1), 126-129.

(60) Tran, B. T.; Hirayama, H. Growth and Fabrication of High External Quantum Efficiency AlGaN-Based Deep Ultraviolet Light-Emitting Diode Grown on Pattern Si Substrate. *Sci. Rep.* **2017**, *7* (1), 12176.

(61) Robin, Y.; Ding, K.; Demir, I.; McClintock, R.; Elagoz, S.; Razeghi, M. High brightness ultraviolet light-emitting diodes grown on patterned silicon substrate. *Mater. Sci. Semicond. Process.* **2019**, *90*, 87-91.

(62) Demir, İ.; Robin, Y.; McClintock, R.; Elagoz, S.; Zekentes, K.; Razeghi, M. Direct growth of thick AlN layers on nanopatterned Si substrates by cantilever epitaxy. *Phys. Status Solidi (a).* **2017**, *214* (4), 1600363.

(63) Mino, T.; Hirayama, H.; Takano, T.; Tsubaki, K.; Sugiyama, M. Characteristics of epitaxial lateral overgrowth AlN templates on (111)Si substrates for AlGaN deep-UV LEDs fabricated on different direction stripe patterns. *phys. status solidi (c).* **2012**, *9* (3-4), 802-805.

(64) Cicek, E.; McClintock, R.; Cho, C. Y.; Rahnema, B.; Razeghi, M. AlxGa1−xN-based solar-blind ultraviolet photodetector based on lateral epitaxial overgrowth of AlN on Si substrate. *Appl. Phys. Lett.* **2013**, *103* (18), 181113.

(65) Nam, K. B.; Nakarmi, M. L.; Lin, J. Y.; Jiang, H. X. Deep impurity transitions involving cation vacancies and complexes in AlGaN alloys. *Appl. Phys. Lett.* **2005**, *86* (22), 222108.

(66) Collazo, R.; Xie, J.; Gaddy, B. E.; Bryan, Z.; Kirste, R.; Hoffmann, M.; Dalmau, R.; Moody, B.; Kumagai, Y.; Nagashima, T.; Kubota, Y.; Kinoshita, T.; Koukitu, A.; Irving, D. L.; Sitar, Z. On the origin of the 265 nm absorption band in AlN bulk crystals. *Appl. Phys. Lett.* **2012**, *100* (19), 191914.

(67) Laleyan, D. A.; Fernández-Delgado, N.; Reid, E. T.; Wang, P.; Pandey, A.; Botton, G. A.; Mi, Z. Strain-free ultrathin AlN epilayers grown directly on sapphire by high-temperature molecular beam epitaxy. *Appl. Phys. Lett.* **2020**, *116* (15), 152102.

(68) Wang, Q.; Zhao, S.; Connie, A. T.; Shih, I.; Mi, Z.; Gonzalez, T.; Andrews, M. P.; Du, X. Z.; Lin, J. Y.; Jiang, H. X. Optical properties of strain-free AlN nanowires grown by molecular beam epitaxy on Si substrates. *Appl. Phys. Lett.* **2014**, *104* (22), 223107.

(69) Feneberg, M.; Leute, R. A. R.; Neuschl, B.; Thonke, K.; Bickermann, M. High-excitation and high-resolution photoluminescence spectra of bulk AlN. *Phys. Rev. B.* **2010**, *82* (7), 075208.

(70) Lee, K.; Page, R.; Protasenko, V.; Schowalter, L. J.; Toita, M.; Xing, H. G.; Jena, D. MBE growth and donor doping of coherent ultrawide bandgap AlGaN alloy layers on single-crystal AlN substrates. *Appl. Phys. Lett.* **2021**, *118* (9), 092101.

(71) Davydov, V. Y.; Kitaev, Y. E.; Goncharuk, I. N.; Smirnov, A. N.; Graul, J.; Semchinova, O.; Uffmann, D.; Smirnov, M. B.; Mirgorodsky, A. P.; Evarestov, R. A. Phonon dispersion and Raman scattering in hexagonal GaN and AlN. *Phys. Rev. B.* **1998**, *58* (19), 12899-12907.

(72) Yang, S.; Miyagawa, R.; Miyake, H.; Hiramatsu, K.; Harima, H. Raman Scattering Spectroscopy of Residual Stresses in Epitaxial AlN Films. *Appl. Phys. Express.* **2011**, *4* (3), 031001.

(73) Lughi, V.; Clarke, D. R. Defect and stress characterization of AlN films by Raman spectroscopy. *Appl. Phys. Lett.* **2006**, *89* (24), 241911.

(74) Hayes, J. M.; Kuball, M.; Shi, Y.; Edgar, J. H. Temperature Dependence of the Phonons of Bulk AlN. *Jpn. J. Appl. Phys.* **2000**, *39* (Part 2, No. 7B), L710-L712.

(75) Yun, F.; Reshchikov, M. A.; He, L.; King, T.; Morkoç, H.; Novak, S. W.; Wei, L. Energy band bowing parameter in Al[sub x]Ga[sub 1−x]N alloys. *J. Appl. Phys.* **2002**, *92* (8), 4837.

(76) Nakarmi, M. L.; Nepal, N.; Lin, J. Y.; Jiang, H. X. Photoluminescence studies of impurity transitions in Mg-doped AlGaN alloys. *Appl. Phys. Lett.* **2009**, *94* (9), 091903.

(77) Ahmad, H.; Engel, Z.; Matthews, C. M.; Lee, S.; Doolittle, W. A. Realization of homojunction PN AlN diodes. *J. Appl. Phys.* **2022**, *131* (17), 175701.

CHAPTER 5.

Vertical AlGaN Deep Ultraviolet LEDs on Si Substrates with Various Emission Wavelengths

With the initial demonstrations of vertical AlGaN deep UV LEDs on Si using AlN-on-NW buffer layers in Chapter 3, as well as elucidating the role of the nanowire template on improving the quality and electrical doping of the epilayers atop in Chapter 4, in this chapter[‡], vertical AlGaN deep UV LEDs widely emitting in the deep UV range are demonstrated. The growths and characterizations of AlGaN epilayers with different Al contents on AlN-on-NW buffer layers are also analyzed in detail.

5.1 Manuscript

Molecular beam epitaxy of AlGaN epilayers on Si for vertical deep ultraviolet light-emitting diodes

Qihua Zhang, Heemal Parimoo, Eli Martel, and Songrui Zhao [z]

Department of Electrical and Computer Engineering, McGill University

3480 University Street, Montreal, Quebec H3A 0E9, Canada

[z] Corresponding Author E-mail Address [songrui.zhao@mcgill.ca]

[‡] Section 5.1 is from a manuscript that is accepted for publication: Q. Zhang, H. Parimoo, E. Martel, and S. Zhao, "Molecular Beam Epitaxy of AlGaN Epilayers on Si for Vertical Deep Ultraviolet Light-Emitting Diodes," *ECS J. Solid State Sci. Technol.*, vol. 11, no. 11, p. 116002, 2022, doi: 10.1149/2162-8777/aca2d9.

Abstract

Silicon (Si) has been an appealing substrate for vertical aluminum gallium nitride (AlGaN) deep ultraviolet (UV) light-emitting diodes (LEDs), toward which, the first step is to demonstrate AlGaN deep UV LEDs on Si. Nonetheless, the epitaxy of AlGaN epilayers on Si remains a challenge. Herein, we demonstrate the molecular beam epitaxy of AlGaN epilayers on Si using a nanowire-based template over a wide Al content range from 35% – 70%. Smooth AlGaN surface down to a rms roughness of 0.4 nm is obtained using this approach. Vertical AlGaN deep UV LEDs emitting down to 247 nm are also demonstrated.

5.1.1 Introduction

AlGaN deep UV LEDs are important photonic light sources that cover a wide range of applications, including disinfection, sensing, material identification, and so on.[1-5] Furthermore, due to the advantages of vertical current injection scheme, such as uniform current in the device active region, easy to scale up, and reduced device fabrication complexity, it is appealing to develop vertical AlGaN deep UV LEDs. Among various substrate choices for vertical AlGaN deep UV LEDs, Si substrate is attractive, not only because the advantages of Si as a substrate such as low cost, readily availability of large substrate sizes, but more importantly, its easy removal compared to other commonly used substrates such as sapphire.[5-7]

The first step to obtain vertical AlGaN deep UV LEDs using Si substrate is to demonstrate AlGaN deep UV LEDs in situ on Si, in order to examine various layers in the device structure. Nonetheless, obtaining AlGaN deep UV LEDs on Si is a challenging task. This is mainly due to the large lattice and thermal mismatches between AlGaN alloys and Si (e.g., 19% lattice mismatch between Si (111) and AlN).[8, 9] The tensile stress from Si often leads to AlGaN epilayers with poor material quality such as cracks and large dislocation densities.

The main approaches, hitherto, used to improve the quality of AlGaN epilayers on Si include using epitaxial lateral overgrowth (ELO)-AlN buffer layers, AlGaN/AlN superlattices, and graded AlGaN buffer layers.[9-17] Even with these efforts, there are only limited reports of AlGaN deep UV LEDs on Si.[8, 18-22] Furthermore, the shortest device operation wavelength reported so far has been limited to 257 nm.[21] Moreover, the thick and insulating buffer layers used in these approaches prevent devices through vertical current injection, regardless of the device operation wavelength.[8, 18-22] In addition, thick and complex buffer layers, as well as substrate patterning, used in these approaches increase growth complexity and time and dollar costs.

An alternative path for AlGaN deep UV LEDs on Si explored so far is using nanowire structures.[23-27] However, the fabrication of AlGaN nanowire deep UV LEDs remains challenging. Recently, we have reported a special approach of growing AlGaN epilayers on Si using a nanowire-assisted AlN buffer layer by molecular beam epitaxy (MBE), which enabled a new AlGaN deep UV LED architecture on Si.[28-32] In this work, we continue to provide detailed studies on the MBE growth and characterization of AlGaN epilayers formed on such AlN buffer layers, and further demonstrate AlGaN epilayers with a wide range of Al contents and vertical AlGaN deep UV LEDs emitting down to 247 nm, shortest wavelength so far for AlGaN deep UV LEDs made with AlGaN epilayers on Si, regardless of the current injection scheme.

5.1.2 Experimental

All the AlGaN epilayers in this study were grown on a nanowire-assisted AlN buffer layer by radio-frequency plasma-assisted MBE. A thin pre-nanowire AlN layer was used prior to the growth of the nanowire template, to relax any residual tensile stress in the nanowire template from the Si substrate. The schematic is shown in Figure 5-1(a). The growth condition of the thin pre-nanowire AlN layer followed an Al-first approach, as described elsewhere.[33] The GaN nanowire layer was grown in N-rich condition,[33] whereas both the AlN buffer layer and AlGaN epilayer were grown in metal-rich conditions. The growth condition of AlGaN epilayers included an Al flux of 2.5×10^{-8} to 3.7×10^{-8} Torr, a Ga flux of 1.2×10^{-7} to 1.4×10^{-7} Torr, and a nitrogen flow rate of 0.3 standard cubic center meter (sccm). The substrate temperature was varied from 720 °C to 740 °C. The temperature was calibrated using the Si substrate reflection high-energy electron diffraction (RHEED) 7×7 reconstruction.

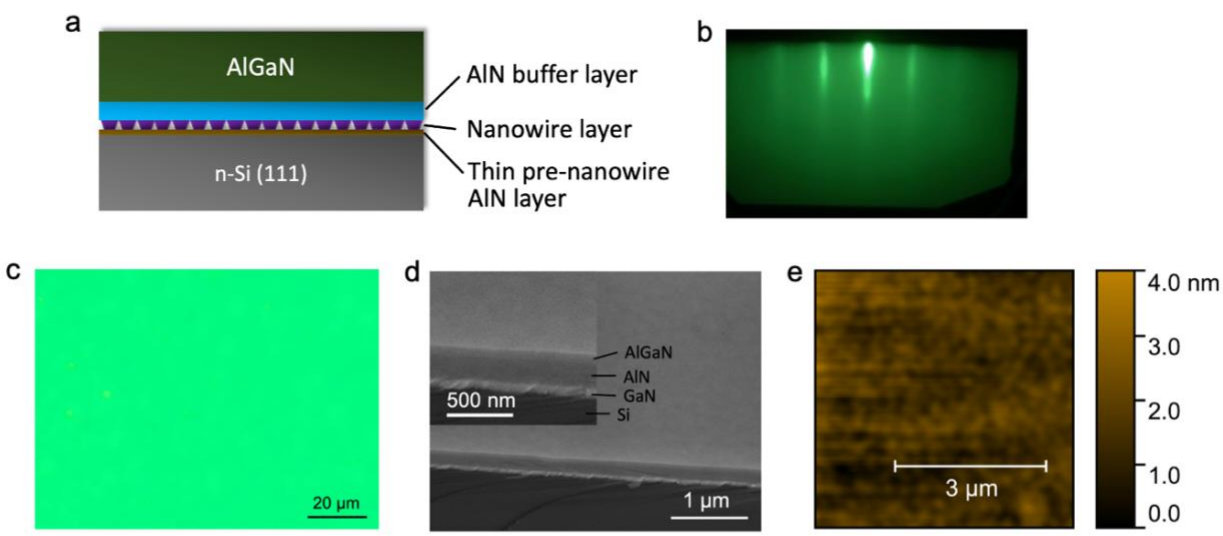

Figure 5-1 (a) Schematic of the AlGaN epilayer grown on the nanowire-assisted AlN buffer layer on Si. (b) RHEED pattern captured during the growth of the AlGaN epilayer. (c) An optical image of the AlGaN epilayer surface. (d) An SEM image of the as-grown wafer, with the inset highlighting the cross-section. (e) An AFM image of the AlGaN epilayer surface.

5.1.3 Results and Discussion

The metal-rich conditions in this study are confirmed by the RHEED intensity change when the metal shutter open/close test was performed. Figure 5-1(b) shows the typical RHEED pattern during the growth of AlGaN epilayers. Streaky RHEED pattern was observed throughout the growth, suggesting a relatively smooth surface. This smooth surface has also been confirmed by the optical image (Figure 5-1(c)) and the scanning electron microscope (SEM) image taken at a tilting angle of 45° (Figure 5-1(d)). The SEM image contrast at the cross-section (inset of Figure 5-1(d)) manifests the GaN nanowire layer, AlN buffer layer, and AlGaN epilayer. Atomic force microscopy (AFM) was further carried out to examine the surface of the as-grown AlGaN epilayer. Figure 5-1(e) shows a typical AFM image. A root-mean-square (rms) roughness of as low as 0.4 nm was obtained in this study. The as-grown surface was further etched by potassium hydroxide (KOH, 11.2 mol L^{-1} at 70 °C). Hexagonal-shaped pits, rather than hillocks, were observed in the etched surface, confirming that the AlGaN epilayers are metal-polar.

Optical properties of the AlGaN epilayers were further investigated by photoluminescence (PL) experiments. In this regard, the samples were excited by a 213 nm pulsed laser. The emitted light was collected from the sample top surface through an optical fiber, which was further coupled to a deep UV spectrometer. Figure 5-2(a) shows the room-temperature PL spectra. It is seen that PL emission from 242 nm to 300 nm is measured. The Al content is further estimated using the room-temperature PL peak wavelength λ, with the equation $E_{PL}(x) = hc/\lambda \approx E_g(AlGaN) = (1-x)E_g(GaN) + xE_g(AlN) - bx(1-x)$, where x is the Al content, *h* is the Planck's constant, *c* is the speed of light, E_g is the bandgap energy, and *b* is the bowing parameter. Bandgap energies E_g of 3.4 eV and 6.2 eV (for GaN and AlN, respectively) and bowing parameter b of 1 eV[34] were used in the estimation. Shown in Figure 5-2(b) is the PL peak wavelength vs. the Al content for various samples. It is seen that Al contents in the range of ~35% to 70% are obtained. It is further noted that, only a single PL emission peak is present, suggesting a relatively uniform compositional distribution in the present AlGaN epilayers.

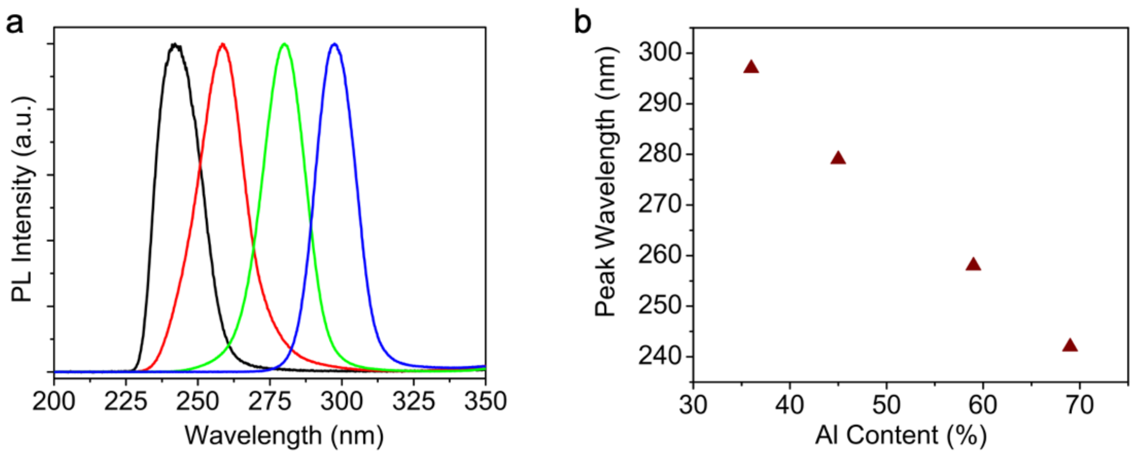

Figure 5-2 (a) Room temperature PL spectra of AlGaN epilayers with various Al contents grown on Si substrate. (b) PL peak wavelength vs. the Al content.

Our estimation of the room-temperature internal quantum efficiency (IQE) using the ABC model[35] further indicated that, for such AlGaN epilayers, IQEs of around 30 – 40 % can be obtained at low excitation conditions. These IQE values are improved compared to the bulk AlGaN epilayers grown on sapphire, e.g., Refs. 36, 37, and suggest that such AlGaN epilayers are suitable for making LEDs devices. It is noted, though, the improved IQE does not necessarily reflect a significant reduction on threading dislocation densities.

We further demonstrate vertical deep UV LEDs using such AlGaN epilayers. Figure 5-3(a) shows the device schematic, which consists of the special AlN buffer layer and AlGaN p-i-n double-heterojunctions (DHs). The thicknesses for the active region and cladding layers were 15 and 30 nm, respectively. Al contents were adjusted in the DH LED structures in order to obtain different emission wavelengths. Roughly the Al content difference in the active region and cladding layer was around 15%. The Mg doping concentrations in p-AlGaN cladding layers were in the range of 1-5×10^{18} cm^{-3}, estimated from the secondary-ion mass spectroscopy (SIMS), performed at EAG Labs. In the present study, the Mg doping neither degrades the surface quality of the epilayer nor incurs polarity inversion due to the moderate doping level.

In the device fabrication process, the limitation of the current spreading length in the vertical injection scheme was used to define and isolate devices with different sizes. The current spreading length L_S was estimated by $L_s = \sqrt{(tnkT/e\rho J_0)}$, where t is the thickness of the current spreading layer (in this work, it is the thickness of the p-AlGaN layer), n is the ideality factor, ρ is the resistivity of the p-AlGaN layer, and J_0 is the forward current density. Additionally, k, T, and e stand for the Boltzmann constant, temperature, and unit charge, respectively. A wide range of ideality factors of group-III nitride LEDs from previous reports were considered.[38-40] The resistivity of the p-AlGaN layer (with an Al content of around 70%) was taken from the best reported so far (assuming that our p-layer is inferior to the state-of-the-art number).[41] Figure 5-3(b) shows the calculated current spreading length as a function of the forward current density. It is seen that, the maximum current spreading length is less than 30 µm. As such, if the separation of the p-contact is on the order of several hundred µm, the limited current spreading in the vertical injection scheme can naturally isolate different devices. Metal bilayer Ni (7 nm)/Au (7 nm) was used as the p-contact, which was deposited by e-beam evaporator, following standard photolithography and patterning processes. Figure 5-3(c) shows a photo of the fabricated wafer. The squares denote p-contact, with a separation of around 300 µm.

Electrical performance of such LED devices was further tested. In this regard, the current-voltage (I-V) characteristics of the fabricated devices with different sizes were measured by Keithley 2400 source meter under a continuous-wave (CW) biasing. For the Mg doping range in the p-AlGaN layers in this study, we did not observe a significant change of the device electrical performance. Figure 5-3(d) and the inset of Figure 5-3(d) show the typical I-V characteristics of a device with a size of 1 mm × 1 mm in the linear and semi-logarithmic scale, respectively. The forward currents at 9 V and 12 V were around 2 mA and 10 mA, respectively. Further improvement on the electrical performance is expected by optimizing the electrical doping, as well as removing the Si substrate and the AlN buffer layer. Nearly uniform current injection is also found in the present devices. Figure 5-3(e) shows the forward current at a forward voltage of 12 V for devices with different sizes. It is seen that the increase of the current is proportional to the device size increase, indicating a uniform current injection.

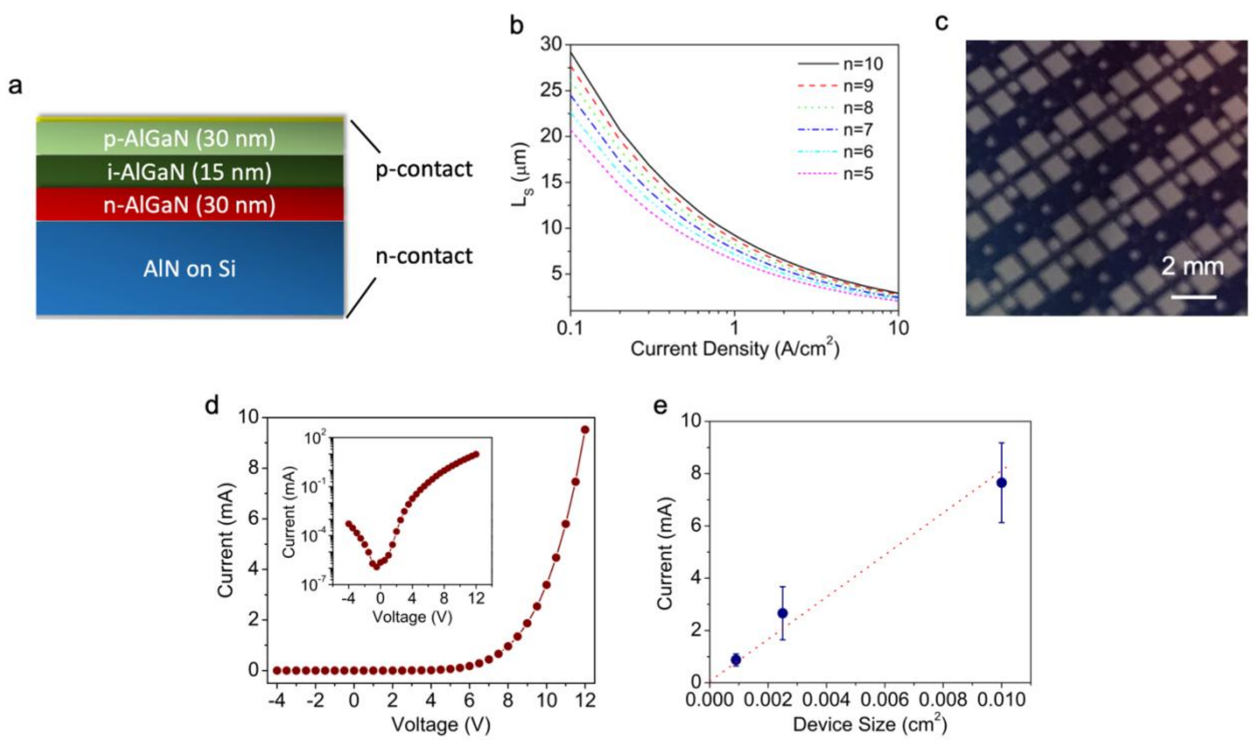

Figure 5-3 (a) Device schematic of AlGaN DH LEDs. (b) The current spreading length vs. the forward current density with various ideality factors (n). (c) A photo of fabricated wafer. The squares denote p-contact. (d) I-V characteristics of an AlGaN DH LED. The inset shows the I-V characteristics in a semi-logarithmic scale. (e) Forward currents at a forward voltage of 12 V for devices with different sizes. The error bars indicate the current variation for devices with the same size.

The light emission of such LED devices was studied in the end. In this regard, the electroluminescence (EL) spectra of the devices were collected from the device top surface with an optical fiber, which was further coupled to a deep UV spectrometer. Figure 5-4 shows the room temperature EL spectra. It is seen that devices emitting from 247 nm to 298 nm are obtained. The presence of the p-AlGaN related EL emission peak for devices emitting at 247 nm could be originated from the deep levels in high-Al content AlGaN alloys.[42-44]

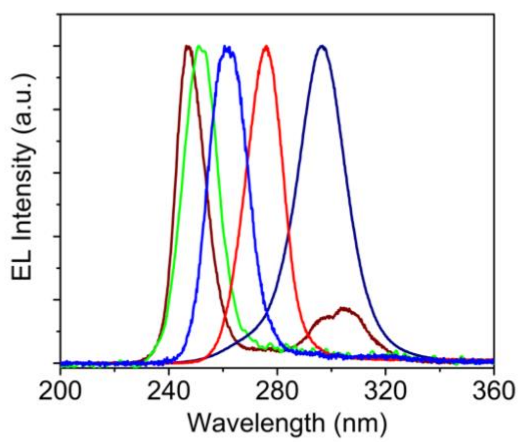

Figure 5-4 Room temperature EL spectra measured from AlGaN DH LEDs at different emission wavelengths.

For the present vertical AlGaN deep UV LEDs, the light output power has remained low, on the order of several hundred nano-watt. Besides the lack of complicated device designs such as multiple quantum wells (QWs) and electron blocking layers (EBLs), another reason is the light blocking by p-contact. This issue can be solved by using conventional dry etching to isolate devices and optimizing p-contact design.[45, 46] Moreover, the light output power can also be improved by using graphene electrode.[47] Separately, by removing Si substrate and the AlN buffer layer and transferring device structures to reflectors can also improve the light output power.

5.1.4 Conclusions

We have reported the MBE growth and characterization of AlGaN epilayers on nanowire-assisted AlN buffer layers on Si substrates. AlGaN epilayers with Al contents varying from ~35% to 70% have been obtained. Both SEM and AFM experiments indicate that such AlGaN epilayers have a smooth surface, with a rms roughness of around 0.4 nm. Vertical AlGaN deep UV LEDs down to 247 nm are further demonstrated. Today, despite of the advantages of vertical LEDs, AlGaN deep UV LEDs are mainly through lateral current injection. This work represents the first step toward high-efficiency, low-cost vertical AlGaN deep UV LEDs over a wide deep UV range.

References

1. H. Amano, R. Collazo, C. D. Santi, S. Einfeldt, M. Funato, J. Glaab, S. Hagedorn, A. Hirano, H. Hirayama, R. Ishii, Y. Kashima, Y. Kawakami, R. Kirste, M. Kneissl, R. Martin, F. Mehnke, M. Meneghini, A. Ougazzaden, P. J. Parbrook, S. Rajan, P. Reddy, F. Römer, J. Ruschel, B. Sarkar, F. Scholz, L. J. Schowalter, P. Shields, Z. Sitar, L. Sulmoni, T. Wang, T. Wernicke, M. Weyers, B. Witzigmann, Y.-R. Wu, T. Wunderer and Y. Zhang, *J. Phys. D: Appl. Phys.*, **53** (2020).
2. T. D. Moustakas, *MRS Commun*., **6**, 247 (2016).
3. E. Monroy, F. Omnes and F. Calle, *Semicond. Sci. Technol*., **18**, R33 (2003).
4. D. Li, K. Jiang, X. Sun and C. Guo, *Adv. Opt. Photonics*, **10** (2018).
5. M. Crawford, *Semicond. Semimet.*, **96**, 3 (2017).
6. F. Jiang, J. Zhang, Q. Sun and Z. Quan, *in Light-Emitting Diodes*, **4**, 133 (2019).
7. Q. Sun, W. Yan, M. Feng, Z. Li, B. Feng, H. Zhao and H. Yang, *J. Semicond.*, **37**, 044006 (2016).
8. Y. Zhang, S. Gautier, C.-Y. Cho, E. Cicek, Z. Vashaei, R. McClintock, C. Bayram, Y. Bai and M. Razeghi, *Appl. Phys. Lett.*, **102** (2013).
9. J. Shen, X. Yang, D. Liu, Z. Cai, L. Wei, N. Xie, F. Xu, N. Tang, X. Wang, W. Ge and B. Shen, *Appl. Phys. Lett.*, **117**, 022103 (2020).
10. Y. Li, W. Wang, X. Li, L. Huang, Y. Zheng, X. Chen and G. Li, *CrystEngComm*, **20**, 1483 (2018).
11. L. Niu, Z. Hao, Y. E, J. Hu, L. Wang and Y. Luo, *Appl. Phys. Express.*, **7**, 065505 (2014).
12. X.-Q. Shen, T. Takahashi, T. Ide and M. Shimizu, *CrystEngComm*, **19**, 1204 (2017).
13. M. A. Mastro, C. R. Eddy, D. K. Gaskill, N. D. Bassim, J. Casey, A. Rosenberg, R. T. Holm, R. L. Henry and M. E. Twigg, *J. Cryst. Growth*, **287**, 610 (2006).

14. A. S. Hussein, S. M. Thahab, Z. Hassan, C. W. Chin, H. Abu Hassan and S. S. Ng, *J. Alloys Compd.*, **487**, 24 (2009).

15. A. Bardhan, N. Mohan, H. Chandrasekar, P. Ghosh, D. V. Sridhara Rao and S. Raghavan, *J.Appl. Phys.*, **123** (2018).

16. Y. Li, W. Wang, Y. Lin, X. Li, L. Huang, Y. Zheng, Z. Zhang and G. Li, *Mater. Lett.*, **207**, 133 (2017).

17. Y. Huang, J. Liu, X. Sun, X. Zhan, Q. Sun, H. Gao, M. Feng, Y. Zhou, M. Ikeda and H. Yang, *CrystEngComm*, **22**, 1160 (2020).

18. Y. Robin, K. Ding, I. Demir, R. McClintock, S. Elagoz and M. Razeghi, *Mater. Sci. Semicond. Process.*, **90**, 87 (2019).

19. B. T. Tran and H. Hirayama, *Sci. Rep.*, **7**, 12176 (2017).

20. B. T. Tran, N. Maeda, M. Jo, D. Inoue, T. Kikitsu and H. Hirayama, *Sci. Rep.*, **6**, 35681 (2016).

21. T. Mino, H. Hirayama, T. Takano, K. Tsubaki and M. Sugiyama, *Appl. Phys. Express*, **4** (2011).

22. S. Fujikawa and H. Hirayama, *Appl. Phys. Express*, **4** (2011).

23. S. Zhao, J. Lu, X. Hai and X. Yin, *Micromachines (Basel)*, **11**, 125 (2020).

24. B. J. May, E. C. Hettiaratchy, C. Selcu, B. Wang, B. D. Esser, D. W. McComb and R. C. Myers, *J. Vac. Sci. Technol. B*, **37**, 031212 (2019).

25. J.-W. Min, D. Priante, M. Tangi, G. Liu, C. H. Kang, A. Prabaswara, C. Zhao, L. Al-Maghrabi, Y. Alaskar, A. M. Albadri, A. Y. Alyamani, T. K. Ng and B. S. Ooi, *J. Nanophotonics*, **12** (2018).

26. H. Sun, M. K. Shakfa, M. M. Muhammed, B. Janjua, K.-H. Li, R. Lin, T. K. Ng, I. S. Roqan, B. S. Ooi and X. Li, *ACS Photonics*, **5**, 964 (2017).

27. B. Janjua, H. Sun, C. Zhao, D. H. Anjum, F. Wu, A. A. Alhamoud, X. Li, A. M. Albadri, A. Y. Alyamani, M. M. El-Desouki, T. K. Ng and B. S. Ooi, *Nanoscale*, **9**, 7805 (2017).

28. Q. Zhang, X. Yin, E. Martel and S. Zhao, *Mater. Sci. Semicond. Process.*, **135**,106099 (2021).

29. X. Yin and S. Zhao, *ECS J. Solid State Sci. Technol.*, **10**, 076001 (2021).

30. X. Yin, Q. Zhang and S. Zhao, *Crystal Growth & Design*, **21**, 3645 (2021).

31. Q. Zhang, H. Parimoo, E. Martel and S. Zhao, *Sci. Rep.*, **12**, 1 (2022).

32. Q. Zhang, H. Parimoo, E. Martel, X. Yin and S. Zhao, *ECS J. Solid State Sci. Technol.* **11**, 066003 (2022).

33. J. Lu, Y. Zhong and S. Zhao, *J. Vac. Sci. Technol. B*, **38**, 062804 (2020).

34. F. Yun, M. A. Reshchikov, L. He, T. King, H. Morkoç, S. W. Novak and L. Wei, Journal of Applied Physics **92**, 4837 (2002).

35. J. Lu, Y. Zhong and S. Zhao, *J. Vac. Sci. Technol. B*, **39** (2) (2021).

36. Ž. Podlipskas, R. Aleksiejūnas, A. Kadys, J. Mickevičius, J. Jurkevičius, G. Tamulaitis, M. Shur, M. Shatalov, J. Yang and R. Gaska, *J. Phys. D: Appl. Phys.*, **49** (2016).

37. X. Yin and S. Zhao, *physica status solidi (b)*, **258**, 2100201 (2021).

38. J. M. Shah, Y. L. Li, T. Gessmann and E. F. Schubert, *J. Appl. Phys.*, **94**, 2627 (2003).

39. K. Lee, P. Parbrook, T. Wang, J. Bai, F. Ranalli, R. Airey and G. Hill, *physica status solidi (b)*, **247**, 1761 (2010).

40. Y. Liao, D. Li, Q. Guo, Y. Liu, H. Wang, W. Hu and Z. L. Wang, *AIP Adv.* **11**,105214 (2021).

41. Y. H. Liang and E. Towe, *J. Appl. Phys.* **123**, 095303 (2018).

42. K. B. Nam, M. L. Nakarmi, J. Y. Lin and H. X. Jiang, *Appl. Phys. Lett.* **86**, 222108 (2005).

43. N. Nepal, M. L. Nakarmi, J. Y. Lin and H. X. Jiang, *Appl. Phys. Lett.*, **89**, 092107 (2006).

44. M. L. Nakarmi, N. Nepal, J. Y. Lin and H. X. Jiang, *Appl. Phys. Lett.*, **94**, 091903 (2009).

45. W. S. Wong, T. Sands, N. W. Cheung, M. Kneissl, D. P. Bour, P. Mei, L. T. Romano and N. M. Johnson, *Appl. Phys. Lett.*, **77**, 2822 (2000).

46. W. S. Wong, T. Sands, N. W. Cheung, M. Kneissl, D. P. Bour, P. Mei, L. T. Romano and N. M. Johnson, *Appl. Phys. Lett.*, **75**, 1360 (1999).

47. H. Parimoo, J. Lu and S. Zhao, *Appl. Phys. Lett.*, **120**, 171108 (2022).

CHAPTER 6.

Polarization-Enhanced Vertical Deep Ultraviolet LEDs with Compositionally-Graded AlGaN Epilayers

As mentioned in Section 1.2, AlGaN alloy possesses unique electric polarization properties, which can further induce free charge carriers through linear grading of Al composition along the growth direction. Such a polarization doping technique provides an alternative approach to the realization of p-type conductivity in AlGaN alloys, compared to using Mg [65, 210, 211]. By utilizing such doping technique, AlGaN deep UV LEDs with polarization-induced p-AlGaN epilayers have been demonstrated in the past [65-67].

In this chapter [§], the growths and characterizations of compositionally-graded AlGaN epilayers on AlN-on-NW buffer layers are investigated. It has been established in previous chapters that AlGaN epilayers grown on AlN-on-NW buffer layers possess metal polarity. As such, reducing Al composition along the growth direction would lead to generations of free holes in the compositionally-graded AlGaN epilayers. Further utilizing such p-AlGaN epilayers, vertical AlGaN UV LEDs emitting at 278 nm are demonstrated. Such devices possess enhanced electrical performance with reduced device series resistance, compared to devices with p-AlGaN epilayers without compositional grading.

[§] Section 0 is from a manuscript that has been accepted for publication: Q. Zhang, H. Parimoo, E. Martel, X. Yin, and S. Zhao, "Vertical AlGaN Deep Ultraviolet Light Emitting Diodes with Polarization Enhanced p-AlGaN Epilayer on Si Substrate," *ECS J. Solid State Sci. Technol.*, vol. 11, no. 6, p. 066003, 2022, doi: 10.1149/2162-8777/ac7663.

6.1 Manuscript

Vertical AlGaN deep ultraviolet light emitting diodes with polarization enhanced p-AlGaN epilayer on Si substrate

Qihua Zhang, Heemal Parimoo, Eli Martel, Xue Yin, and Songrui Zhao

Department of Electrical and Computer Engineering, McGill University, 3480 University Street, Montreal, Quebec H3A 0E9, Canada

Email: songrui.zhao@mcgill.ca

Abstract

Despite of the technological importance of developing AlGaN deep UV LEDs on Si, there are only a few reports about AlGaN deep UV LEDs on Si based on AlGaN epilayers. Herein, we show vertical AlGaN deep UV LEDs on Si with polarization enhanced p-AlGaN epilayer. The devices emit at 278 nm, with uniform current injection. Compared to devices using standard p-AlGaN epilayer, the series resistance of devices with polarization enhanced p-AlGaN epilayer is reduced by a factor of 5. This work represents the first report of AlGaN deep UV LEDs on Si with polarization enhanced p-AlGaN epilayers.

6.1.1 Introduction

Developing III-nitride optoelectronics on silicon (Si) has been the efforts of the semiconductor community in the past decades.[1-10] However, hitherto, there are only countable reports of aluminum gallium nitride (AlGaN) deep ultraviolet (UV) light-emitting diodes (LEDs) on Si based on AlGaN epilayers.[4, 7, 11-13] This is in a sharp contrast to the development of AlGaN epilayer-based deep UV LEDs on other foreign substrates, such as sapphire and AlN-on-sapphire template. Today, the majority demonstrations of AlGaN deep UV LEDs on Si rely on the format of AlGaN nanowires.[14-22]

Multiple reasons account for this situation. Besides the well-known large lattice and thermal match issues between high Al content AlGaN alloys and Si, another primary cause is the poor p-type doping with magnesium (Mg). Despite that poor p-type doping in general is a challenge regardless of the choice of substrates – basically a fundamental limitation due to the large Mg activation energy,[23-27] this issue could be more severe for AlGaN thin films grown on Si.

Recent studies have shown that the presence of dislocations in thin films affect Mg dopant incorporation, as well as the device electrical behavior. The diffusion of Mg along dislocations,[28, 29] followed by the formation of Mg-Ga-O disordered layer on the surface of p-GaN, has been identified as an important factor that limits the free hole concentration in p-GaN.[29] Furthermore, Mg condensation at threading dislocations has been found, which leads to the formation of donor-type complex and leakage current in GaN p-n diodes.[30] Given the larger lattice mismatches between high Al content AlGaN alloys and Si, compared to other foreign substrates such as sapphire, such dislocation related effects could be more detrimental for the development of p-AlGaN thin films on Si. As such, lower free hole concentrations are often reported for AlGaN thin films on Si compared to those on sapphire and AlN-on-sapphire substrates.[7, 12, 31-35]

In addition, it is noted that, simply by adding more Mg dopants will create heavy doping effects, such as inversion domains, e.g., Ref. 36, even more asymmetric charge carrier transport due to the reduction of hole mobility.[27] The latter has been known as one of the major causes for the efficiency droop in AlGaN deep UV LEDs.[37, 38] The latter also limits the carrier injection efficiency into the active region, making the development of laser diodes difficult. It is also noted that high doping concentration is a potential source of internal optical loss for a laser cavity.[39]

With all the above considerations, it is strategically important to investigate alternative p-doping approach for high Al content p-type AlGaN thin films on Si. In fact, polarization doping has attracted interest in recent years, owing to the strong electric polarization fields in wurtzite structured III-nitrides.[18, 20, 21, 40-45] In a linear graded AlGaN with changing Al/Ga ratio, net polarization charges can be created, and three-dimensional electron or hole gases will be induced to due to the requirement of charge neutrality. As such, instead of relying on thermal activation of impurity dopants, free charge carriers can be generated by the polarization effect in the graded layer. Utilizing such polarization-induced p-AlGaN epilayers has led to the recent breakthrough in edge emitting AlGaN UV lasers in the deep UV range on bulk AlN substrate.[39]

In this work, we investigate AlGaN deep UV LEDs on Si with polarized enhanced p-type AlGaN epilayers through grading the Al content along the growth direction. Such LEDs are formed on a nanowire-assisted AlN buffer layer, following our recent development.[46, 47] The nanowire-assisted AlN buffer layer has led to the realization of vertically-injected LEDs emitting at 298 nm.[48] AlGaN deep UV LEDs in the present study are also vertically injected. It is found that, with the use of polarization enhanced p-AlGaN epilayers, the electrical performance is drastically improved compared to devices with standard p-AlGaN epilayers. The electrical performance is also improved compared to the previously reported laterally injected AlGaN UV LEDs on Si.[7]

6.1.2 Experimental Details

The molecular beam epitaxy (MBE) growth of the Al content graded AlGaN epilayers on the nanowire-assisted AlN buffer layer are studied first. In this regard, radio-frequency plasma-assisted MBE with a background pressure of 1×10^{-10} Torr was used for the growth. 3-inch highly conductive n-Si (111) were used as the substrates. Standard solvent cleaning was performed prior to loading wafers to the MBE chamber. The growth condition for the nanowire-assisted AlN buffer layer has been described elsewhere.[48] For the AlGaN epilayers, metal-rich conditions were used. The nitrogen flow rate was 0.3 standard cubic center meter (sccm). The substrate temperature was around 725 °C. The Al flux was varied from around 4×10^{-8} Torr to 2.5×10^{-8} Torr, whereas the Ga flux was adjusted accordingly, to ensure the metal-rich growth condition. The nitrogen flow rate limited growth rate was around 100 nm/hr. Reflection high-energy electron diffraction (RHEED) was used to monitor the growth in situ.

6.1.3 Results and Discussion

Shown in Figure 6-1a is the RHEED pattern during the growth of the graded AlGaN epilayer using the afore-mentioned growth condition. Streaky RHEED pattern is seen, suggesting a 2-dimensional (2D) growth mode and a smooth surface. The metal-rich condition was confirmed by the presence of RHEED intensity change when the metal shutter open/close test was performed. Figure 6-1b shows the scanning electron microscopy (SEM) image of the as-grown wafer, taken at a tiling angle of 45°, by an FEI Quanta FEG 450 system. A smooth surface can also be seen.

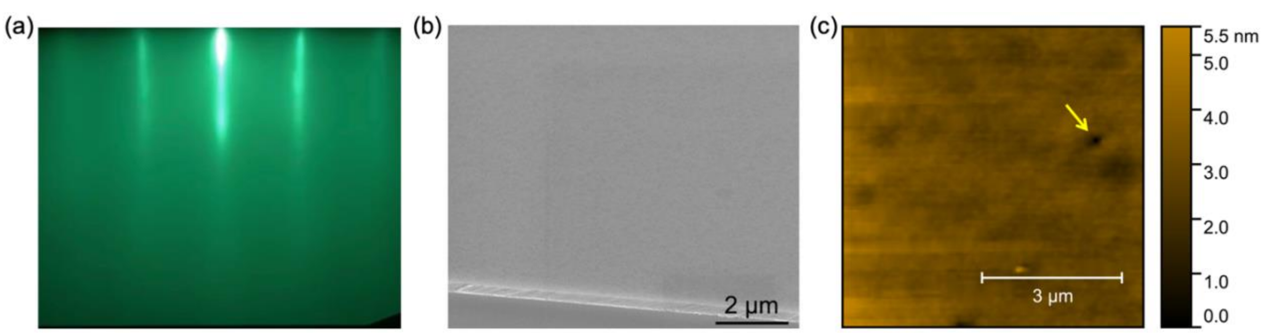

Figure 6-1 (a) RHEED pattern taken during the growth of the graded AlGaN epilayer. (b) SEM image of the graded AlGaN epilayer sample. (c) AFM image showing the surface of the graded AlGaN epilayer.

The surface of the as-grown wafer was further examined by Nanosurf C3000 atomic force microscopy (AFM) under dynamic non-contact mode. A typical scan is shown in Figure 6-1c, revealing a smooth surface. However, AFM image scans do show pits on the surface. A pit can be seen in Figure 6-1c (marked by arrow). In this study, a rms roughness of as low as 0.5 nm can be obtained from the graded AlGaN epilayer. This rms roughness is comparable to the typical values for AlGaN epilayers grown on sapphire and AlN-on-sapphire template.[49]

Photoluminescence (PL) experiments were further used to assess the Al contents in the AlGaN epilayers in this study. In this regard, the samples were excited by a 213 nm solid state laser, with a pulse width of 7 ns and a maximum pulse energy of 2 µJ. The emitted light was collected from the sample top surface by an optical fibre, which was further coupled to a deep UV spectrometer. It was further assumed that the PL peak position represented the bandgap energy and a bowing parameter of 1 eV was used in the Vegard's law.[50] For the graded AlGaN epilayer, the Al content variation estimated by the PL peak positions (not shown here) was from 70% to 30% (along the growth direction).

Using such graded AlGaN epilayers, we have further demonstrated vertical AlGaN deep UV LEDs on Si (Structure A in Figure 6-2a). Moreover, a reference device structure using non-graded AlGaN epilayer is also fabricated (Structure B in Figure 6-2a), to compare the device electrical performance. Both structures have the same nanowire-assisted AlN buffer layer and consist of AlGaN double-heterojunctions (DHs). Al contents in the n-AlGaN cladding and active region are 70% and 40%, respectively. The thickness for both n-AlGaN and p-AlGaN cladding layers is around 30 nm, whereas the thickness of the AlGaN active region is around 15 nm. The only difference is the p-AlGaN cladding layer: In Structure A, it uses a graded Mg-doped AlGaN cladding layer based on the afore-demonstrated graded AlGaN epilayer; whereas in Structure B, it uses a standard Mg-doped AlGaN cladding layer (i.e., no Al content grading, to be described below). Mg doping concentration was 6×10^{17} cm^{-3}, estimated by secondary ion mass spectroscopy (SIMS, EAG labs). Moreover, two types of samples (B-1 and B-2, to be described) were fabricated using Structure B to fully assess the role of the electric polarization field on the device electrical performance.

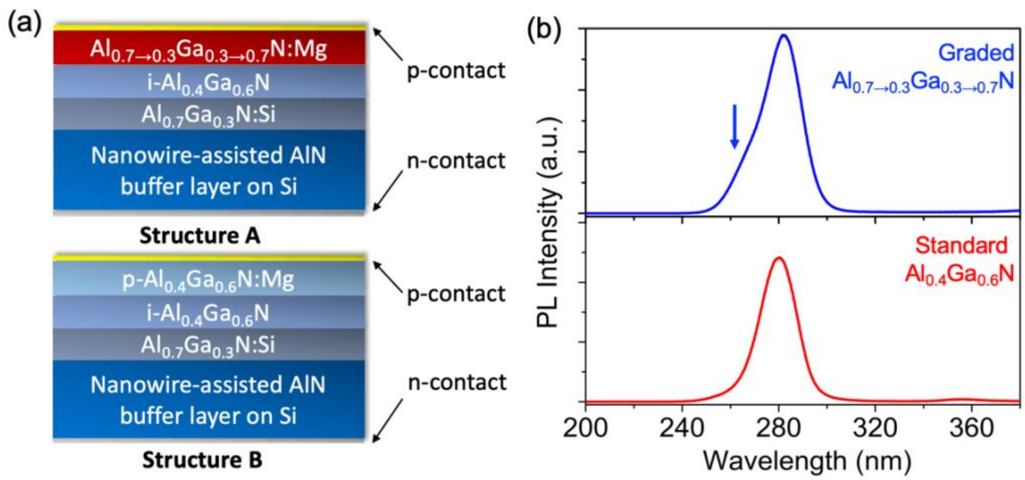

Figure 6-2 (a) Schematic of device structures used in this study. Structure B is a reference structure used for the device electrical performance comparison. (b) PL spectra measured from the graded AlGaN epilayer (top panel) and the standard AlGaN epilayer (bottom panel) used for the device structures.

For the device electrical performance comparison purpose, it is necessary to use a standard AlGaN epilayer that has the average Al content of the graded AlGaN in the p-AlGaN cladding layer. As such, knowing average Al content of the graded AlGaN is necessary. This can be evaluated by the PL peak position. Shown in Figure 6-2b (top panel) is the PL spectrum of the graded AlGaN. PL emission peak around 280 nm can be seen. This corresponds to an average Al content of ~40%. Using this Al content as a reference, the standard AlGaN epilayer was grown. The PL spectrum of the standard AlGaN is shown in the bottom panel of Figure 2b. PL emission peak around 280 nm is seen, confirming a similar Al content. It is noted, though, due to the Al content variation induced inhomogeneous broadening, the full-width-at-half-maximum (FWHM) of the graded AlGaN epilayer is slightly larger (19 nm) compared to that of the standard AlGaN epilayer (17 nm). Moreover, the graded AlGaN epilayer also shows an additional emission component around 265 nm (marked by arrow).

Electrical injection was realized by conventional metal bilayer nickel/gold (Ni/Au) as the p-contact and colloidal silver (Ag) adhesive as the n-contact on the backside of n-Si substrate. Compared to the conventional approach of device isolation with reactive ion etching, here we used the natural limitation of the current spreading in vertical injection scheme. Our estimations showed that in the best scenario the current spreading length was on the order of tens of micrometer. As such, by placing p-metal contact several hundred micrometer apart, devices can be isolated naturally.[48] The device size was determined by the p-metal size.

Figure 6-3a shows the I-V characteristics of a device with the graded p-AlGaN cladding layer under a continuous-wave (CW) biasing. At a forward voltage of 12 V, the forward current is 15 mA. In contrast, for a device with the standard p-AlGaN cladding layer (B1), the forward current is only about 5 mA (also shown in Figure 3a). Both devices show similar leakage current (inset of Figure 6-3a). The series resistance (R_s), estimated by the inverse of the slope shown in Figure 6-3a, for devices with the graded p-AlGaN cladding layer and the standard p-AlGaN cladding layer are around 146 Ω and 787 Ω, respectively. R_s is reduced roughly by a factor of 5 comparing the two types of devices. This could indicate that, by exploiting the Al content grading induced electric polarization field in the graded p-AlGaN cladding layer, the device electrical performance is enhanced.

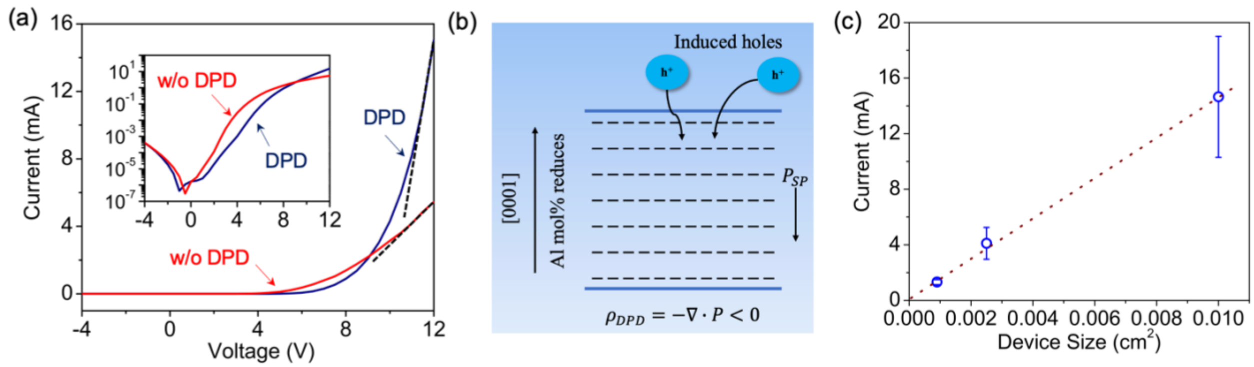

Figure 6-3 (a) I-V characteristics of the device with the graded p-AlGaN cladding layer (or distributed polarization doping, DPD) and the device with the standard p-AlGaN cladding layer. Device size: 1 mm × 1 mm. Dash lines are guide-for-eye. (b) Schematic of the polarization enhanced p-doping through Al content grading. (c) Forward currents at a voltage of 12 V for devices with the graded p-AlGaN cladding layer with different sizes. The error bars reflect the current variations for devices with the same size.

However, one should also note that in the graded p-AlGaN cladding layer, the last region was with low Al content. The improved electric performance thus could also be explained by the improved p-contact resistance due to the use of low Al content. To rule out this possibility, we further examined the device with standard Mg-doped p-AlGaN cladding layer but with an Al content of 30% (B-2). For such a device, all the rest employed the same growth conditions as structure B-1. It was found that the I-V characteristics of B-2 were inferior compared to the devices with graded p-AlGaN cladding layers (not shown). This therefore confirms that the improved I-V characteristics are due to the Al content grading induced electrical polarization field in the graded p-AlGaN cladding layer.

For the present graded AlGaN epilayer, our potassium hydroxide (KOH) etching experiments have confirmed a metal-polarity. As such, reducing Al content along the growth direction leads to negative bound polarization charges ρ_b, i.e., $\rho_b = -\nabla \cdot \boldsymbol{P} < 0$ (where $\boldsymbol{P}$ is the electric polarization vector and is in the opposite direction of the growth direction), inducing free holes or improved ionization of impurity acceptors, which can subsequently enhance the p-type conductivity. This is schematically shown in Figure 3b.

Theoretically, such an electric polarization field induced hole concentration can be estimated via $\sim 5\times10^{13}\times(\Delta x/\Delta \mathrm{d})$ cm^{-3}, where Δx and Δd (in cm) are the grading composition and thickness differences, respectively.[42, 44] It is noted that this estimation should be based on the strained p-AlGaN epilayer with composition grading within 30% and up to ~40%, due to the diminishment of piezoelectric polarization from relaxation.[42, 44, 51] By taking $\Delta x = 0.4$ and $\Delta d = 30\times10^{-7}$ cm of the graded AlGaN epilayer in the present study, the hole concentration upper limit is estimated to be around 6×10^{18} cm^{-3}.

As the present devices are through vertical injection, uniform current injection into the device active region is expected. This is indeed the case. Shown in Figure 6-3c is the forward currents at a forward voltage of 12 V for devices with the graded p-AlGaN cladding layer with different sizes. It is seen that the current increase is proportional to the device size increase, confirming a uniform current injection.

Electroluminescence (EL) characteristics are described in the end. In this regard, the EL emission was collected by an optical fiber from the device top surface. The devices were under continuous-wave (CW) biasing. EL emission spectra for a device with the graded p-AlGaN cladding layer under different injection currents are shown in Figure 6-4a. It is seen that a single emission peak at around 278 nm is measured, without a clear red or blueshift, suggesting the absence of heating effect and the quantum confined Stark effect. The relative light output power as a function of current density is shown in Figure 6-4b, a typical LED behavior is seen, i.e., the intensity increases linearly as the injection current increases. Figure 6-4c shows the relative external quantum efficiency (EQE), which was calculated by the integrated EL intensity divided by the injection current, as a function of the current density. The rising trend persists up to around 25 A/cm^2, and no efficiency droop is seen.

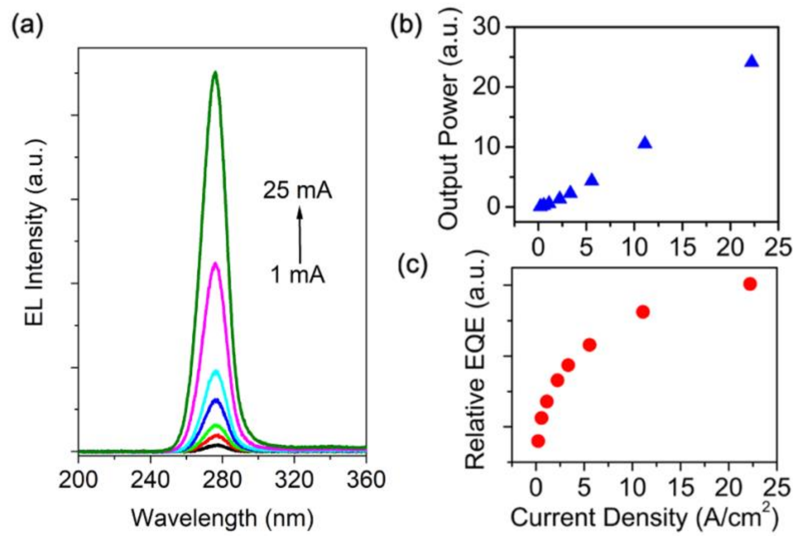

Figure 6-4 (a) EL spectra of a device with the graded p-AlGaN cladding layer under injection currents varying from 1 to 25 mA. (b) and (c) the light output power and relative EQE as a function of current density.

6.1.4 Conclusion

In summary, in this work we have first described the MBE growth of graded AlGaN epilayers on Si. A smooth surface is obtained, as suggested by RHEED, SEM, and AFM experiments. The rms roughness can be as low as 0.5 nm. The Al content grading also leads to a slightly broader PL emission and additional emission component, compared to non-graded AlGaN epilayers with a similar Al content. We have further demonstrated vertical AlGaN deep UV LEDs on Si using the graded p-AlGaN cladding layer. The device electrical performance is discussed first, in comparison with devices using standard p-AlGaN cladding layer. It is found that, with the use of graded p-AlGaN cladding layer, the device electrical performance is enhanced drastically, with the series resistance reduced by a factor of 5 compared to device with standard p-AlGaN. EL emission at 278 nm is measured from the device top surface, and no efficiency droop is seen for current densities up to 25 A cm^{-2}. Lastly, it is worth emphasizing that, today, despite of the advantages of vertical LEDs, AlGaN deep UV LEDs are mainly through lateral injection,[52] and this work paves a way for the fabrication of high-performance vertical AlGaN deep UV LEDs using low-cost Si substrate.

References

1. M. Feng, J. Liu, Q. Sun, and H. Yang, *Prog. Quantum Electronics*, **77,** 100323 (2021).
2. J. Shen, X. Yang, D. Liu, Z. Cai, L. Wei, N. Xie, F. Xu, N. Tang, X. Wang, W. Ge, and B. Shen, *Appl. Phys. Lett.*, **117**, 022103 (2020).
3. Y. Huang, J. Liu, X. Sun, X. Zhan, Q. Sun, H. Gao, M. Feng, Y. Zhou, M. Ikeda, and H. Yang, *CrystEngComm*, **22**, 1160 (2020).
4. Y. Robin, K. Ding, I. Demir, R. McClintock, S. Elagoz, and M. Razeghi, *Mater. Sci. Semicond. Process.*, **90**, 87 (2019).
5. F. Jiang, J. Zhang, Q. Sun, and Z. Quan, in *Light-Emitting Diodes*, **5**, 133 (2019).
6. Y. Li, W. Wang, X. Li, L. Huang, Y. Zheng, X. Chen, and G. Li, *CrystEngComm*, **20**, 1483 (2018).
7. B. T. Tran and H. Hirayama, *Sci. Rep.*, **7**, 12176 (2017).
8. Q. Sun, W. Yan, M. Feng, Z. Li, B. Feng, H. Zhao, and H. Yang, *J. Semicond.*, **37**, 044006 (2016).
9. T. Li, M. Mastro, and A. Dadgar, *III–V compound semiconductors: Integration with silicon-based microelectronics* (CRC Press, Boca Raton, FL) 1st edn ed. (2010).
10. A. Dadgar, M. Poschenrieder, J. Bläsing, K. Fehse, A. Diez, and A. Krost, *Appl. Phys. Lett.*, **80**, 3670 (2002).
11. Y. Zhang, S. Gautier, C.-Y. Cho, E. Cicek, Z. Vashaei, R. McClintock, C. Bayram, Y. Bai, and M. Razeghi, *Appl. Phys. Lett.*, **102**, 011106 (2013).
12. T. Mino, H. Hirayama, T. Takano, K. Tsubaki, and M. Sugiyama, *Appl. Phys. Express*, **4**, 092104 (2011).
13. S. Fujikawa and H. Hirayama, *Appl. Phys. Express*, **4** (2011).

14. S. M. Sadaf, S. Zhao, Y. Wu, Y. H. Ra, X. Liu, S. Vanka, and Z. Mi, *Nano Lett.*, **17**, 1212 (2017).

15. S. Zhao, S. M. Sadaf, S. Vanka, Y. Wang, R. Rashid, and Z. Mi, *Appl. Phys. Lett.*, **109**, 201106 (2016).

16. S. Zhao, M. Djavid, and Z. Mi, *Nano Lett.*, **15**, 7006 (2015).

17. S. Zhao, A. T. Connie, M. H. Dastjerdi, X. H. Kong, Q. Wang, M. Djavid, S. Sadaf, X. D. Liu, I. Shih, H. Guo, and Z. Mi, *Sci. Rep.*, **5**, 8332 (2015).

18. T. F. Kent, S. D. Carnevale, A. T. Sarwar, P. J. Phillips, R. F. Klie, and R. C. Myers, *Nanotechnol.*, **25**, 455201 (2014).

19. S. D. Carnevale, T. F. Kent, P. J. Phillips, M. J. Mills, S. Rajan, and R. C. Myers, *Nano Lett.*, **12**, 915 (2012).

20. H. Sun, D. Priante, J.-W. Min, R. C. Subedi, M. K. Shakfa, Z. Ren, K.-H. Li, R. Lin, C. Zhao, T. K. Ng, J.-H. Ryou, X. Zhang, B. S. Ooi, and X. Li, *ACS Photonics*, **5**, 3305 (2018).

21. A. T. M. Golam Sarwar, S. D. Carnevale, T. F. Kent, F. Yang, D. W. McComb, and R. C. Myers, *Appl. Phys. Lett.*, **106**, 32102 (2015).

22. H. Sun, M. K. Shakfa, M. M. Muhammed, B. Janjua, K.-H. Li, R. Lin, T. K. Ng, I. S. Roqan, B. S. Ooi, and X. Li, *ACS Photonics*, **5**, 964 (2017).

23. Y. Taniyasu, M. Kasu, and T. Makimoto, *Nature*, **441**, 325 (2006).

24. M. L. Nakarmi, N. Nepal, J. Y. Lin, and H. X. Jiang, *Appl. Phys. Lett.*, **94**, 091903 (2009).

25. M. L. Nakarmi, N. Nepal, C. Ugolini, T. M. Altahtamouni, J. Y. Lin, and H. X. Jiang, *Appl. Phys. Lett.*, **89**, 152120 (2006).

26. A. T. Connie, S. Zhao, S. M. Sadaf, I. Shih, Z. Mi, X. Du, J. Lin, and H. Jiang, *Appl. Phys. Lett.*, **106**, 213105 (2015).

27. N. H. Tran, B. H. Le, S. Zhao, and Z. Mi, *Appl. Phys. Lett.*, **110**, 32102 (2017).

28. S. Usami, N. Mayama, K. Toda, A. Tanaka, M. Deki, S. Nitta, Y. Honda, and H. Amano, *Appl. Phys. Lett.*, **114**, 232105 (2019).

29. L. Sang, B. Ren, R. Endo, T. Masuda, H. Yasufuku, M. Liao, T. Nabatame, M. Sumiya, and Y. Koide, *Appl. Phys. Lett.*, **115**, 172103 (2019).

30. T. Nakano, Y. Harashima, K. Chokawa, K. Shiraishi, A. Oshiyama, Y. Kangawa, S. Usami, N. Mayama, K. Toda, A. Tanaka, Y. Honda, and H. Amano, *Appl. Phys. Lett.*, **117**, 012105 (2020).

31. Y. H. Liang and E. Towe, *J. Appl. Phys.*, **123**, 95303 (2018).

32. B. P. Gunning, C. A. M. Fabien, J. J. Merola, E. A. Clinton, W. A. Doolittle, S. Wang, A. M. Fischer, and F. A. Ponce, *J. Appl. Phys.*, **117**, 45710 (2015).

33. X. Liu, A. Pandey, D. A. Laleyan, K. Mashooq, E. T. Reid, W. J. Shin, and Z. Mi, *Semicond. Sci. Technol.*, **33**, 85005 (2018).

34. T. Kinoshita, T. Obata, H. Yanagi, and S.-i. Inoue, *Appl. Phys. Lett.*, **102**, 12105 (2013).

35. Y. H. Liang and E. Towe, *Appl. Phys. Rev.*, **5**, 011107 (2018).

36. P. Kozodoy, H. Xing, S. P. DenBaars, U. K. Mishra, A. Saxler, R. Perrin, S. Elhamri, and W. C. Mitchel, *J. Appl. Phys.*, **87**, 1832 (2000).

37. J. H. Park, D. Y. Kim, E. F. Schubert, J. Cho, and J. K. Kim, *ACS Energy Lett.*, **3**, 655 (2018).

38. X. Hai, R. T. Rashid, S. M. Sadaf, Z. Mi, and S. Zhao, *Appl. Phys. Lett.*, **114**, 101104 (2019).

39. Z. Zhang, M. Kushimoto, T. Sakai, N. Sugiyama, L. J. Schowalter, C. Sasaoka, and H. Amano, *Appl. Phys. Express*, **12**, 124003 (2019).

40. H. Zhang, C. Huang, K. Song, H. Yu, C. Xing, D. Wang, Z. Liu, and H. Sun, *Rep. Prog. Phys.*, **84**, 044401 (2021).

41. Z. Zhang, M. Kushimoto, M. Horita, N. Sugiyama, L. J. Schowalter, C. Sasaoka, and H. Amano, *Appl. Phys. Lett.*, **117**, 152104 (2020).

42. L. Zhang, K. Ding, J. C. Yan, J. X. Wang, Y. P. Zeng, T. B. Wei, Y. Y. Li, B. J. Sun, R. F. Duan, and J. M. Li, *Appl. Phys. Lett.*, **97**, 062103 (2010).

43. H. Sun, J. Yin, E. F. Pecora, L. D. Negro, R. Paiella, and T. D. Moustakas, *IEEE Photonics J.*, **9**, 1 (2017).

44. J. Simon, C. L. Vladimir Protasenko, H. Xing, and D. Jena, *Science*, **327**, 60 (2010).

45. S. Li, T. Zhang, J. Wu, Y. Yang, Z. Wang, Z. Wu, Z. Chen, and Y. Jiang, *Appl. Phys. Lett.*, **102**, 062108 (2013).

46. X. Yin, Q. Zhang, and S. Zhao, *Cryst. Growth Des.*, **21**, 3645 (2021).

47. X. Yin and S. Zhao, *ECS J. Solid State Sci. Technol.*, **10**, 076001 (2021).

48. Q. Zhang, H. Parimoo, E. Martel, and S. Zhao, *Sci. Rep.*, **12**, 7230 (2022).

49. V. Jmerik, A. Toropov, V. Davydov, and S. Ivanov, *Phys. status solidi – Rapid Res. Lett.*, 2100242 (2021).

50. F. Yun, M. A. Reshchikov, L. He, T. King, H. Morkoç, S. W. Novak, and L. Wei, *J. Appl. Phys.*, **92**, 4837 (2002).

51. V. Fiorentini, F. Bernardini, and O. Ambacher, *Appl. Phys. Lett.*, **80**, 1204 (2002).

52. M. Crawford, *Semiconductors and Semimetals*, **96**, 3 (2017).

CHAPTER 7.

Towards Far-UVC Emitting LEDs on Si

Depending on the wavelength, deep UV light can be further categorized into far-UVC (λ < 240 nm) range and near-UVC (240 – 280 nm) range [21, 212]. While both far-UVC light and near-UVC light are highly effective in inactivating viruses and pathogens, far-UVC light is considered safe to human skin because such radiation can be largely absorbed in the uppermost cornified skin layers consisting of dead skin cells [213, 214]. As a result, far-UVC light sources pose very little threat to human health and are more favored to be used in for skin-tolerant disinfection systems.

Currently, commercial light sources emitting in the far-UVC range are still dominated by the conventional excimer-based (such as KrCl (222 nm) or KrBr (207 nm)) lamps, which are power-consuming and of high heat generation. Far-UVC emitting AlGaN deep UV LEDs using AlGaN quantum wells have been demonstrated, however, the EQE has remained below 1%, as discussed in Chapter 1.

As an alternative approach, using an active region consisting of multiple pairs of monolayer-thick GaN well and AlN barrier layers (abbreviated as ML-GaN/AlN), far-UVC LEDs with emission wavelengths down to 232 nm have also been demonstrated recently [215, 216]. The ML-GaN/AlN structure takes advantage of the extreme quantum confinement in the GaN quantum well from the large band offset of AlN barrier for emissions in the far-UVC range, as well as the band structure reconstruction that favors the light extraction from the device surface (more details are described in Section 7.2).

In this chapter, with the goal of designing vertical LEDs emitting in the far-UVC range, both high Al content AlGaN epilayers and GaN/AlN stacks have been studied on the AlN-on-NW buffer layers. PL emissions down to 229 nm have been demonstrated by investigating on the growth conditions of high Al content AlGaN epilayers. Further using the GaN/AlN stacks, room temperature PL emissions from 300 nm down to 218 nm have been realized. Additionally, substantial improvements in light polarization properties have also been observed with the use of GaN/AlN stacks, which is beneficial to the design of highly-efficient far-UVC LEDs.

7.1 High Al-Content AlGaN Epilayers on AlN-on-NW Buffer

In Chapter 5, the growths and characterizations of AlGaN epilayers are discussed in detail. It was shown from the PL spectra that shortest wavelength achieved from our current study in the AlGaN epilayers was 242 nm. The push towards even higher Al-content AlGaN epilayers is essential for developing AlGaN far-UVC emitting LEDs. Further attempts have been made toward realizing higher Al-content AlGaN epilayers. As demonstrated in the normalized PL spectra in Figure 7-1, emission peaks at 232 and 229 nm have been measured. By applying Vegard's law, including E_g(GaN) = 3.4 eV, E_g(AlN) = 6.2 eV, and a bowing parameter of 1 eV [217], the average Al contents for such AlGaN epilayers are calculated to be 76 mol% and 78 mol%, respectively.

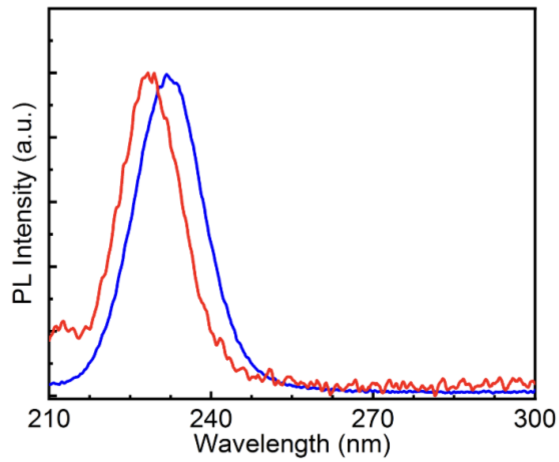

Figure 7-1 Normalized room temperature PL spectra for high Al-content AlGaN epilayers excited by a 193 nm ArF excimer laser with emission peaks at 232 nm and 229 nm, respectively.

To obtain these high Al content AlGaN epilayers, a very careful tuning of the III-N ratio during the MBE growth was performed. Owing to the larger bonding energy for Al-N bond than Ga-N bond, Al has a higher incorporation rate compared to Ga [218]. As such, in order for Ga adatoms to be incorporated during the growths of metal-rich AlGaN epilayers, Al adatoms need to be slightly deficient compared to N. On the other hand, for the growth of high Al-content AlGaN epilayers, the growth window between Al-deficient and Al-rich regime becomes extremely narrow. For example, corresponding to 0.3 sccm N flux, the Al flux used for the growth of 229 nm emitting AlGaN epilayers is 3.9×10^{-8} Torr; yet for the growth of Al-rich AlN epilayers at the same substrate temperature (745°C), the Al flux used is 4×10^{-8} Torr. As such, in order to further push the emission wavelength below 229 nm, Al flux requires rigorous adjustment to between Al-deficient for Ga incorporation and Al-rich regime.

Nonetheless, when the growth window becomes too narrow, the change in metal fluxes becomes too small to be adjusted by changing the cell temperatures. In this regard, introducing shutter interruption might be beneficial for adjusting the impinging fluxes by small increments and has the potential to realize AlGaN epilayers with higher Al content (beyond 80 mol%). Different shutter modulation techniques, including MME (where metal fluxes are periodically interrupted and nitrogen flux remains constant) [219-221], anion-modulated epitaxy (where nitrogen flux is periodically interrupted and metal fluxes remain constant) [222], and migration enhanced epitaxy (where metal fluxes and nitrogen flux are being alternately supplied) [223, 224], have been explored in the past for the growths of GaN and AlN epilayers as well as $Al_xGa_{1-x}N/Al_yGa_{1-y}N$ superlattice ($x \neq y$). For example, using MME, AlGaN epilayers with up to 70 mol% Al content have been demonstrated [221]. Similarly, studies of obtaining high Al-content AlGaN epilayers using different MBE shutter modulation approaches are being conducted by our group. Early preliminary results, such as AlGaN epilayer with a room temperature PL peak position of 228 nm, corresponding to an average Al content of 79 mol%, have been realized using anion-modulated epitaxy.

7.2 Investigations of GaN/AlN Stacks

ML-GaN/AlN structure recently emerges as an attractive candidate for far-UVC LED designs [215, 216, 224-226]. In general, each pair of ML-GaN/AlN consists of AlN barrier layer with thickness of 2 – 5 nm, and GaN well layer with thickness of a few monolayers. Studies of ML-GaN/AlN stacks have been conducted in the past on sapphire substrates [216, 224, 225, 227], and PL emission wavelength as short as 219 nm has been demonstrated at cryogenic temperature (5K) [224]. Multiple benefits have been reported for the use of ML-GaN/AlN. For example, the use of ML-GaN/AlN structure drastically increases the electron-hole wave function overlap in the confined QW structure, which mitigates quantum confined stark effect (QCSE) and improves radiative recombination efficiency. Another benefit of using ML-GaN/AlN structure, as compared to conventional high Al-content AlGaN epilayers, is the light polarization characteristics (TE) which is favored for light extraction from the surface of LED device on typical *c*-plane substrates. This can be explained by the difference in the valence band splitting between GaN (or low Al content AlGaN) and AlN (or high Al content AlGaN).

Shown in Figure 7-2 are the band structures for GaN and AlN [228]. For GaN, the crystal-field splitting energy (Δ_{CF}, energy difference between heavy hole band/ light hole band and crystal field split-off hole band) is a positive value (+37 meV) at Γ point, meaning that heavy hole band, within which the states have atomic orbitals perpendicular to *c*-axis, is the topmost valence band. In this case, the photons generated by the transition from conduction band minimum to heavy hole band are TE-polarized, thus are favored for being extracted from the device surface. On the other hand, Δ_{CF} becomes negative (-219 meV) in AlN, meaning that crystal field split-off hole band becomes the topmost valance band. The states within crystal field split-off hole band have atomic orbitals parallel to the *c*-axis. As such, the photons generated from conduction band minimum to crystal field split-off hole band transitions have TM polarization, which emit towards the edge of the device and remain in-plane coupled.

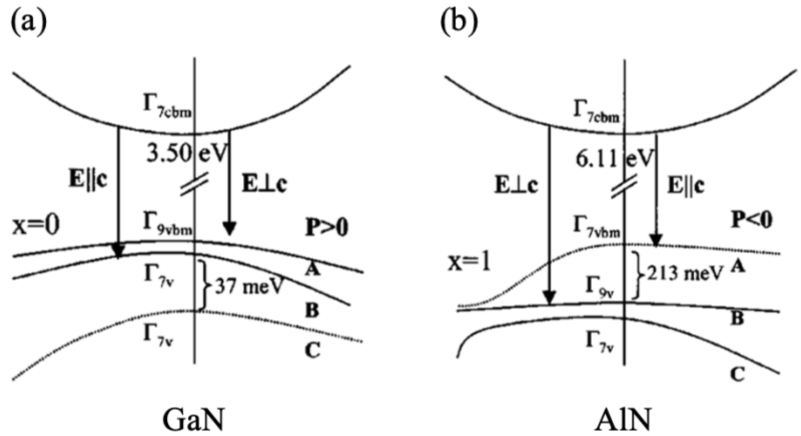

Figure 7-2 Schematics of band structure near the Γ point of (a) GaN and (b) AlN. A, B, C denote heavy-hole band, light-hole band, crystal field split-off band, respectively. (a-b) Reproduced with permission [228]. Copyright 2004, AIP Publishing.

For AlGaN alloy, as Al content increases, the crystal field split-off hole band becomes closer to heavy hole band and eventually becomes the topmost valence band. This indicates the switching from dominant TE-polarized emission to dominant TM-polarized emission. The crossover points at which the crystal field split-off hole band aligns with heavy hole band have been observed at AlGaN with 25 mol% to up 60 mol% Al content (i.e., λ ~ 260-320 nm), as reported by different research teams [228-231]. As a result, for the majority of AlGaN LEDs, the emission pattern is TM-polarized and has a "rabbit ear" like shape, where the intensity is weak along device surface normal but stronger on the side. This severely limits the LEE and further EQE of the LED devices. To date, the unfavorable light polarization property in AlGaN remains to be one of the fundamental challenges that hinder the development of highly efficient AlGaN deep UV LEDs.

7.2.1 Growth of GaN/AlN Stacks on AlN-on-NW Buffer Layer

Motivated by these benefits, preliminary MBE growth of GaN/AlN stacks was investigated in this thesis study. Schematically shown in Figure 7-3(a), 20 pairs of GaN/AlN stacks, consisting of AlN barrier layers with thickness around 4 nm and GaN well layers with various thicknesses depending on the growth time (t_{GaN}), have been grown on the AlN-on-NW buffer layers. Figure 7-3(b) further shows the HRXRD ω-2θ coupled scan on the GaN/AlN sample with t_{GaN} of 11 seconds. An AlN peak at 18.05° can be clearly observed. An additional peak at 17.37° is also observed besides the AlN peak, which is presumably attributed to GaN nanowires from the AlN-on-NW buffer layer.

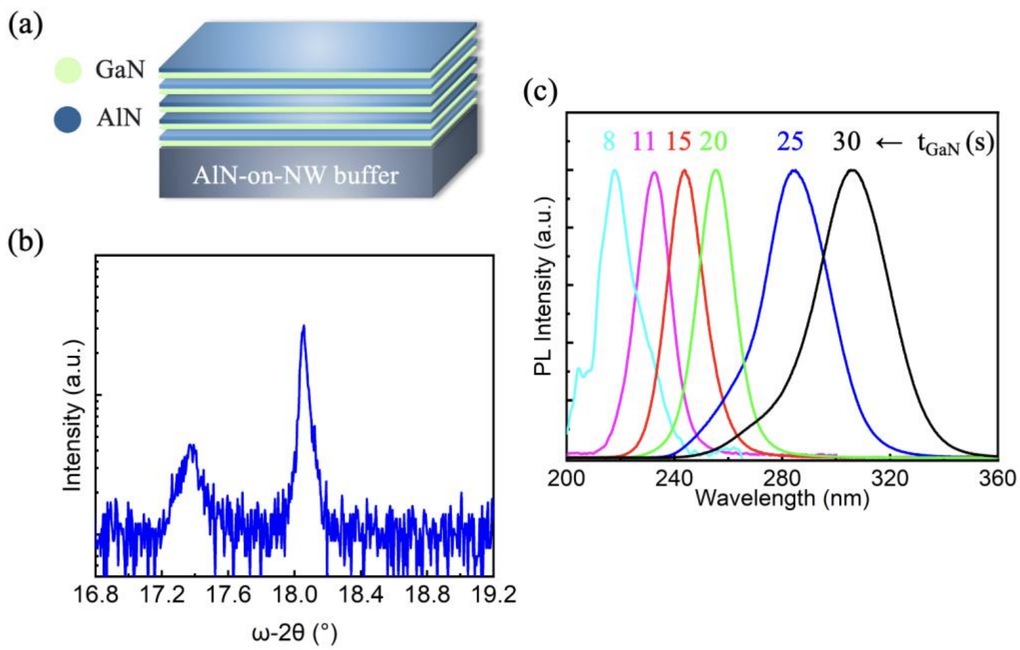

Figure 7-3 (a) Schematic structure for GaN/AlN stacks (20 pairs) grown on AlN-on-NW template on Si substrate. (b) HRXRD ω-2θ coupled scan for the GaN/AlN stacks. (c) Normalized PL spectra at room temperature with different t_{GaN}.

By adjusting the growth duration of GaN layer, GaN/AlN stacks with different emission wavelengths have been obtained. As shown in Figure 7-3(c), PL emission peaks from 300 nm down to 218 nm have been measured at room temperature.

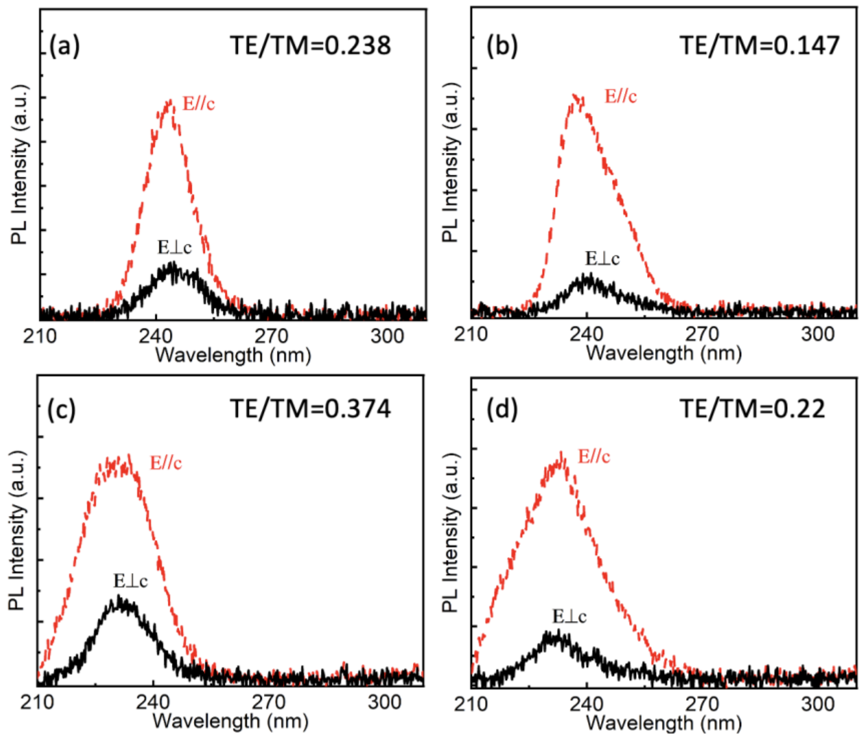

Figure 7-4 (a), (c) Polarization dependent PL spectra of GaN/AlN stacks with emission peaks at 240 nm, 230 nm. (b), (d) Polarization dependent PL spectra of AlGaN epilayers with similar respective emission wavelengths.

The use of GaN/AlN stacks are also seen to substantially improve the polarization characteristics (i.e., more TE over TM). Figure 7-4 shows the polarization measurements from GaN/AlN stacks, in comparison to bulk AlGaN epilayers. The ratio of the peak PL intensity of TE ($E \perp c$) emission component to the peak intensity of TM ($E \,//\, c$) emission component, i.e., TE/TM, are also indicated in the figure. In this experiment, a Glan-Taylor polarizer was inserted between the optical fiber and the emission edge of each sample. It is seen that for similar PL emission wavelengths, using GaN/AlN stacks leads to higher TE/TM ratios, as compared to using high Al content AlGaN epilayers. The improvement in light polarization property in the GaN/AlN stacks may well be suited for the design of far-UVC emitting LEDs with enhanced LEE and high EQE.

CHAPTER 8.

Conclusion and Future Work

8.1 Conclusion

In summary, AlN epilayers with excellent surface morphology were demonstrated on Si substrates using a nanowire template. A rms roughness as low as 0.4 nm from AFM experiment was obtained on the AlN surface at a nearly wafer scale. Moreover, the AlN epilayers were found to be Al-polar. Further utilizing such AlN-on-NW as buffer layers, AlGaN epilayers with a wide range of Al contents were grown. The IQE of the AlGaN epilayers, estimated by power dependent PL measurements and ABC models, was found to be in the range of 30% – 40% under low excitation power, which is higher compared to AlGaN epilayers on commercial AlN-on-sapphire templates. Using such AlGaN epilayers, vertical AlGaN LEDs emitting widely in the deep UV range down to 247 nm were demonstrated, with improved electrical performance compared to the previously reported lateral injection AlGaN UV LEDs on Si.

The role of nanowire template was also investigated by comparing the AlN epilayers grown with and without the nanowire layer, it was found that the use of the nanowire template drastically improved the crystalline quality of AlN epilayers by evaluating XRD rocking curves. The nanowire template was also found to be able to relax the tensile strain in AlN by PL and Raman studies. These improvements further translated to the improved Mg dopant incorporation and p-type conductivity of the AlGaN epilayers, as well as the diode characteristics of AlGaN p-i-n heterostructures.

In addition, the growths and characterizations of compositionally graded p-type AlGaN epilayers were investigated. Excellent surface morphology with a rms roughness as low as 0.5 nm was measured on such graded AlGaN epilayers. Vertical LEDs emitting at 278 nm were further demonstrated using such p-type AlGaN epilayers, and enhanced electrical performance was measured, compared to LEDs using conventional Mg-doped p-AlGaN epilayers.

In the end, the MBE growths and characterizations of both high Al content AlGaN epilayers and GaN/AlN stacks were investigated on the AlN-on-NW buffer layers, aiming for human-safe far-UVC emitting vertical LEDs. Room temperature PL emission wavelengths as low as 218 nm were measured from GaN/AlN stacks.

This thesis presents a viable path for vertical semiconductor LEDs across the entire deep UV range as well as a high quality ultrawide bandgap III-nitride semiconductor platform for both photonic and electronic devices.

8.2 Future Work

8.2.1 Improving the Crystallinity of AlN Using Multi-Step Growth Technique

In Chapter 4, a study on the growth temperature of AlN and its effect on the crystalline quality of the layer was conducted. It was found that as growth temperature increases from 750°C to 960°C, the FWHM of the AlN 002 XRD rocking curve reduces from 1960 arcsec down to 1300 arcsec. This observation is consistent with previous studies, suggesting the use of high temperature (HT) growth effectively reduces the dislocation densities [74, 232-234], which is largely attributed to the increased surface mobility of Al adatoms at high growth temperature that favors dislocation bending. On the other hand, the use of low growth temperature approach is often reported during the initial nucleation stage of AlN epilayers on sapphire or Si substrates, owing to the fact that 3D island growth mode at lower temperature (LT) effectively relaxes the strain on AlN. As such, two-step growth (LT/HT), or three-step growth (LT/MT/HT, MT: mid temperature) techniques for obtaining high crystal quality AlN epilayer on both sapphire and Si substrate have been reported [233, 234].

In this regard, similar growth techniques are currently being attempted on the growths of AlN epilayers on AlN-on-NW buffer layers. It is expected that lower FWHM will be measured from the AlN 002 RC scan, and AlN epilayers of higher crystal quality will be obtained.

8.2.2 Polarity Inversion

From Chapter 3, it was determined through KOH etching experiments that the polarity on the AlN epilayer surface was Al-polar. On the other hand, it was also suggested in the past that spontaneously formed GaN nanowires on Si substrate are of N-polarity, which was also confirmed in this thesis study. The switching from N polarity in the nanowire layer to metal polarity in the AlN epilayer hence suggested a polarity inversion. In the past, polarity inversion on the AlN epilayer was reported to be driven by growth kinetics and strongly dependent on the Al/N ratio, as well as the initial nucleation conditions [235-237]. Moreover, it was also suggested that the coalescence process could also lead to polarity inversion [238, 239]. Detailed TEM analysis is being conducted to examine the cause of the polarity inversion as well as to establish polarity control on such AlN epilayers.

8.2.3 Optimization on the Performance of AlGaN LEDs

<u>Electrical Performance</u>

Although the I-V characteristics of vertical AlGaN LEDs reported in this thesis were substantially improved compared to the previously reported lateral injection AlGaN UV LEDs on Si, they were not comparable to lateral injection AlGaN UV LEDs on sapphire. This could be attributed to the high series resistance in the AlN epilayer. As such, in order to enhance the electrical performance of the LED device, the AlN-on-NW buffer layer as well as Si substrate needs to be removed. Multiple fabrications steps will be involved. First, Si substrates can be removed using the wet etching process as discussed in Chapter 1. Next, GaN nanowires and AlN epilayers can be etched using KOH solution [240-242]. It is expected that, by removing of AlN-on-NW buffer layer as well as Si substrate and transferring the LED structure onto conductive substrates or metal plates, electrical performance will be further improved.

Optical Performance

The vertical AlGaN deep UV LEDs in this thesis had low light output powers, e.g., for devices emitting around 298 nm, the maximum output power measured was 0.3 μW. This could be attributed to various factors such as poor carrier confinement, light blocking by top metal electrode, light absorption by Si, and so on. As such, adopting more complex LED structures, such as single or multiple quantum wells, as well as electron blocking layers could substantially improve the optical output power [243-246]. Furthermore, using transparent electrode such as graphene can lead to enhancement in LEE [247, 248]. In the past, monolayer graphene had been successfully transferred to AlGaN nanowire deep UV LEDs by our group, and a two-fold improvement in light output power was measured from the LED devices with graphene contact layer compared to conventional metal contact layer [249]. Last but not least, transferring the LED structure onto UV reflective metal plates can also improve the device optical performance.

REFERENCES

[1] S. Strite and H. Morkoc, "GaN, AlN, and InN: a review," *J. Vac. Sci. Technol. B: Microelectron. Nanometer Struct.,* vol. 10, no. 4, pp. 1237-1266, 1992.

[2] O. Ambacher, "Growth and applications of Group III-nitrides," *J. Phys. D: Appl. Phys.,* vol. 31, no. 20, pp. 2653-2710, 1998.

[3] J. H. Edgar, Inspec, S. Strite, I. Akasaki, H. Amino, and C. Wetzel, *Properties, Processing and Applications of Gallium Nitride and Related Semiconductors* (EMIS datareviews series). INSPEC, 1999.

[4] H. Morkoç, "III--Nitride semiconductor growth by MBE: Recent issues," *J. Mater. Sci.: Mater. Electron.,* vol. 12, no. 12, pp. 677-695, 2001.

[5] I. Vurgaftman and J. R. Meyer, "Band parameters for nitrogen-containing semiconductors," *J. Appl. Phys.,* vol. 94, no. 6, pp. 3675-3696, 2003.

[6] M. Razeghi, "III-Nitride Optoelectronic Devices: From Ultraviolet Toward Terahertz," *IEEE Photonics J.,* vol. 3, no. 2, pp. 263-267, 2011.

[7] T. D. Moustakas and R. Paiella, "Optoelectronic device physics and technology of nitride semiconductors from the {UV} to the terahertz," *Rep. Prog. Phys.,* vol. 80, no. 10, p. 106501, 2017.

[8] E. F. Schubert, *Light-Emitting Diodes*, 2 ed. Cambridge: Cambridge University Press, 2006.

[9] S. J. Pearton *et al.*, "GaN-based diodes and transistors for chemical, gas, biological and pressure sensing," *J. Phys.: Condens. Matter,* vol. 16, no. 29, pp. R961-R994, 2004.

[10] K. T. Upadhyay and M. K. Chattopadhyay, "Sensor applications based on AlGaN/GaN heterostructures," *Mater. Sci. Eng.: B*, vol. 263, p. 114849, 2021.

[11] J. Ajayan *et al.*, "A critical review of AlGaN/GaN-heterostructure based Schottky diode/HEMT hydrogen (H2) sensors for aerospace and industrial applications," *Measurement,* vol. 186, p. 110100, 2021.

[12] H. Amano *et al.*, "The 2018 GaN power electronics roadmap," *J. Phys. D: Appl. Phys.,* vol. 51, no. 16, p. 163001, 2018.

[13] R. J. Kaplar *et al.*, "Review—Ultra-Wide-Bandgap AlGaN Power Electronic Devices," *ECS J. Solid State Sci. Technol.,* vol. 6, no. 2, pp. Q3061-Q3066, 2016.

[14] U. K. Mishra, P. Parikh, and W. Yi-Feng, "AlGaN/GaN HEMTs-an overview of device operation and applications," *Proc. IEEE,* vol. 90, no. 6, pp. 1022-1031, 2002.

[15] I. Akasaki, "Key inventions in the history of nitride-based blue LED and LD," *J. Cryst. Growth,* vol. 300, no. 1, pp. 2-10, 2007.

[16] Y. Liao *et al.*, "Recent progress of efficient deep UV-LEDs by plasma-assisted molecular beam epitaxy," *Phys. Status Solidi (c)*, vol. 9, no. 3-4, pp. 798-801, 2012.

[17] D. Zhu, D. J. Wallis, and C. J. Humphreys, "Prospects of III-nitride optoelectronics grown on Si," *Rep. Prog. Phys.,* vol. 76, no. 10, p. 106501, 2013.

[18] H. Hirayama, N. Maeda, S. Fujikawa, S. Toyoda, and N. Kamata, "Recent progress and future prospects of AlGaN-based high-efficiency deep-ultraviolet light-emitting diodes," *Jpn. J. Appl. Phys.,* vol. 53, no. 10, p. 100209, 2014.

[19] D. Li, K. Jiang, X. Sun, and C. Guo, "AlGaN photonics: recent advances in materials and ultraviolet devices," *Adv. Opt. Photon.,* vol. 10, no. 1, pp. 43-110, 2018.

[20] M. Kneissl, T.-Y. Seong, J. Han, and H. Amano, "The emergence and prospects of deep-ultraviolet light-emitting diode technologies," *Nature Photonics,* vol. 13, no. 4, pp. 233-244, 2019.

[21] H. Amano *et al.*, "The 2020 UV emitter roadmap," *J. Phys. D: Appl. Phys.,* vol. 53, no. 50, p. 503001, 2020.

[22] T. Wernicke, L. Sulmoni, C. Kuhn, G. Tränkle, M. Weyers, and M. Kneissl, "Group III-Nitride-Based UV Laser Diodes," M. Kneissl, A. Knorr, S. Reitzenstein, and A. Hoffmann Eds. Cham: Springer International Publishing, 2020, pp. 505-548.

[23] Q. Zhang, X. Yin, and S. Zhao, "Recent Progress on Aluminum Gallium Nitride Deep Ultraviolet Lasers by Molecular Beam Epitaxy," *phys. status solidi RRL,* vol. 15, p. 2100090, 2021.

[24] M. Feng, J. Liu, Q. Sun, and H. Yang, "III-nitride semiconductor lasers grown on Si," *Prog. Quantum Electron,* vol. 77, p. 100323, 2021.

[25] S. M. N. Hasan, W. You, M. S. I. Sumon, and S. Arafin, "Recent Progress of Electrically Pumped AlGaN Diode Lasers in the UV-B and -C Bands," *Photonics,* vol. 8, no. 7, p. 267, 2021.

[26] E. Monroy *et al.*, "AlGaN-based UV photodetectors," *J. Cryst. Growth,* vol. 230, no. 3, pp. 537-543, 2001.

[27] L. Sang, M. Liao, and M. Sumiya, "A Comprehensive Review of Semiconductor Ultraviolet Photodetectors: From Thin Film to One-Dimensional Nanostructures," *Sensors*, vol. 13, no. 8, 2013.

[28] Y. Zhang *et al.*, "Surface acoustic wave-based ultraviolet photodetectors: a review," *Sci. Bull.*, vol. 65, no. 7, pp. 587-600, 2020.

[29] Q. Cai *et al.*, "Progress on AlGaN-based solar-blind ultraviolet photodetectors and focal plane arrays," *Light: Sci. Appl.*, vol. 10, no. 1, p. 94, 2021.

[30] A. Costales, M. A. Blanco, Á. Martín Pendás, A. K. Kandalam, and R. Pandey, "Chemical Bonding in Group III Nitrides," *J. Am. Chem. Soc.*, vol. 124, no. 15, pp. 4116-4123, 2002.

[31] H. Kim *et al.*, "Design of high-efficiency GaN-based light emitting diodes with vertical injection geometry," *Appl. Phys. Lett.*, vol. 91, no. 2, 2007.

[32] V. Adivarahan *et al.*, "Vertical Injection Thin Film Deep Ultraviolet Light Emitting Diodes with AlGaN Multiple-Quantum Wells Active Region," *Appl. Phys. Express*, vol. 2, no. 9, p. 092102, 2009.

[33] L. Zhou *et al.*, "Vertical injection thin-film AlGaN/AlGaN multiple-quantum-well deep ultraviolet light-emitting diodes," *Appl. Phys. Lett.*, vol. 89, no. 24, p. 241113, 2006.

[34] D. W. Kim, H. Y. Lee, M. C. Yoo, and G. Y. Yeom, "Highly efficient vertical laser-liftoff GaN-based light-emitting diodes formed by optimization of the cathode structure," *Appl. Phys. Lett.*, vol. 86, no. 5, p. 052108, 2005.

[35] J.-T. Chu *et al.*, "Effects of Different n-Electrode Patterns on Optical Characteristics of Large-Area p-Side-Down InGaN Light-Emitting Diodes Fabricated by Laser Lift-Off," *Jpn. J. Appl. Phys.*, vol. 44, no. 11R, p. 7910, 2005.

[36] O. B. Shchekin *et al.*, "High performance thin-film flip-chip InGaN–GaN light-emitting diodes," *Appl. Phys. Lett.*, vol. 89, no. 7, p. 071109, 2006.

[37] M. Shimokawa *et al.*, "Fabrication of vertical AlGaN-based deep-ultraviolet light-emitting diodes operating at high current density (∼43 kA cm−2) using a laser liftoff method," *Appl. Phys. Express*, vol. 15, no. 4, p. 041006, 2022.

[38] D. Zhu, D. J. Wallis, and C. J. Humphreys, "Prospects of III-nitride optoelectronics grown on Si," *Rep Prog Phys*, Research Support, Non-U.S. Gov't vol. 76, no. 10, p. 106501, 2013.

[39] T. LI, M. MASTRO, and A. DADGAR, *III–V compound semiconductors: Integration with silicon-based microelectronics*. CRC Press, Taylor & Francis Group, 2011.

[40] G. W. Auner, F. Jin, V. M. Naik, and R. Naik, "Microstructure of low temperature grown AlN thin films on Si(111)," *J. Appl. Phys.*, vol. 85, no. 11, pp. 7879-7883, 1999.

[41] P. Chen *et al.*, "Growth of high quality GaN layers with AlN buffer on Si(1 1 1) substrates," *J. Cryst. Growth*, vol. 225, p. 150, 2001.

[42] G. F. Iriarte, J. G. Rodríguez, and F. Calle, "Synthesis of c-axis oriented AlN thin films on different substrates: A review," *Mater. Res. Bull.*, vol. 45, no. 9, pp. 1039-1045, 2010.

[43] A. Bardhan, N. Mohan, H. Chandrasekar, P. Ghosh, D. V. Sridhara Rao, and S. Raghavan, "The role of surface roughness on dislocation bending and stress evolution in low mobility AlGaN films during growth," *J. Appl. Phys.*, vol. 123, no. 16, p. 165108, 2018.

[44] Y. Li *et al.*, "Growth of high-quality AlGaN epitaxial films on Si substrates," *Mater. Lett.*, vol. 207, pp. 133-136, 2017.

[45] Y. Huang *et al.*, "Crack-free high quality 2 μm-thick Al0.5Ga0.5N grown on a Si substrate with a superlattice transition layer," *CrystEngComm*, vol. 22, no. 7, pp. 1160-1165, 2020.

[46] B. T. Tran, H. Hirayama, N. Maeda, M. Jo, S. Toyoda, and N. Kamata, "Direct Growth and Controlled Coalescence of Thick AlN Template on Micro-circle Patterned Si Substrate," *Sci. Rep.*, vol. 5, no. 1, p. 14734, 2015.

[47] B. T. Tran and H. Hirayama, "Growth and Fabrication of High External Quantum Efficiency AlGaN-Based Deep Ultraviolet Light-Emitting Diode Grown on Pattern Si Substrate," *Sci. Rep.*, vol. 7, no. 1, p. 12176, 2017.

[48] J. Shen *et al.*, "High quality AlN film grown on a nano-concave-circle patterned Si substrate with an AlN seed layer," *Appl. Phys. Lett.*, vol. 117, no. 2, p. 022103, 2020.

[49] Y. Robin, K. Ding, I. Demir, R. McClintock, S. Elagoz, and M. Razeghi, "High brightness ultraviolet light-emitting diodes grown on patterned silicon substrate," *Mater. Sci. Semicond. Process.*, vol. 90, pp. 87-91, 2019.

[50] S. Fujikawa and H. Hirayama, "284–300 nm Quaternary InAlGaN-Based Deep-Ultraviolet Light-Emitting Diodes on Si(111) Substrates," *Appl. Phys. Express*, vol. 4, no. 6, p. 061002, 2011.

[51] T. Mino, H. Hirayama, T. Takano, K. Tsubaki, and M. Sugiyama, "Realization of 256–278 nm AlGaN-Based Deep-Ultraviolet Light-Emitting Diodes on Si Substrates Using Epitaxial Lateral Overgrowth AlN Templates," *Appl. Phys. Express*, vol. 4, no. 9, p. 092104, 2011.

[52] M. Kneissl, J. Rass, and others, *III-nitride Ultraviolet Emitters*. Springer, 2016.

[53] A. Khan, K. Balakrishnan, and T. Katona, "Ultraviolet light-emitting diodes based on group three nitrides," *Nat. Photonics*, vol. 2, no. 2, pp. 77-84, 2008.

[54] M. A. Moram and M. E. Vickers, "X-ray diffraction of III-nitrides," *Rep. Prog. Phys.*, vol. 72, no. 3, p. 036502, 2009.

[55] J. F. Muth *et al.*, "Absorption coefficient, energy gap, exciton binding energy, and recombination lifetime of GaN obtained from transmission measurements," *Appl. Phys. Lett.*, vol. 71, no. 18, pp. 2572-2574, 1997.

[56] A. Sedhain *et al.*, "Photoluminescence properties of AlN homoepilayers with different orientations," *Appl. Phys. Lett.*, vol. 93, no. 4, p. 041905, 2008.

[57] J. Li *et al.*, "Band structure and fundamental optical transitions in wurtzite AlN," *Appl. Phys. Lett.*, vol. 83, no. 25, p. 5163, 2003.

[58] Y. Taniyasu and M. Kasu, "Origin of exciton emissions from an AlN p-n junction light-emitting diode," *Appl. Phys. Lett.*, vol. 98, no. 13, p. 131910, 2011.

[59] K. Hestroffer, C. Leclere, C. Bougerol, H. Renevier, and B. Daudin, "Polarity of GaN nanowires grown by plasma-assisted molecular beam epitaxy on Si(111)," *Phys. Rev. B*, vol. 84, no. 24, p. 245302, 2011.

[60] A. Roshko, M. Brubaker, P. Blanchard, T. Harvey, and K. Bertness, "The role of Si in GaN/AlN/Si(111) plasma assisted molecular beam epitaxy: polarity and inversion," *Jpn. J. Appl. Phys.*, vol. 58, no. SC, p. SC1050, 2019.

[61] A. Concordel *et al.*, "Polarity conversion of GaN nanowires grown by plasma-assisted molecular beam epitaxy," *Appl. Phys. Lett.*, vol. 114, no. 17, p. 172101, 2019.

[62] O. Ambacher *et al.*, "Role of Spontaneous and Piezoelectric Polarization Induced Effects in Group-III Nitride Based Heterostructures and Devices," *Phys. Status Solidi (b)*, vol. 216, no. 1, pp. 381-389, 1999.

[63] F. Bernardini, V. Fiorentini, and D. Vanderbilt, "Spontaneous polarization and piezoelectric constants of III-V nitrides," *Phys. Rev. B*, vol. 56, no. 16, pp. R10024-R10027, 1997.

[64] A. F. Wright, "Elastic properties of zinc-blende and wurtzite AlN, GaN, and InN," *J. Appl. Phys.*, vol. 82, no. 6, pp. 2833-2839, 1997.

[65] J. Simon, V. Protasenko, C. Lian, H. Xing, and D. Jena, "Polarization-Induced Hole Doping in Wide–Band-Gap Uniaxial Semiconductor Heterostructures," *Science*, vol. 327, no. 5961, pp. 60-64, 2010.

[66] D. Jena *et al.*, "Polarization-engineering in group III-nitride heterostructures: New opportunities for device design," *Phys. Status Solidi (a),* vol. 208, no. 7, pp. 1511-1516, 2011.

[67] J. Verma, S. M. Islam, V. Protasenko, P. Kumar Kandaswamy, H. Xing, and D. Jena, "Tunnel-injection quantum dot deep-ultraviolet light-emitting diodes with polarization-induced doping in III-nitride heterostructures," *Appl. Phys. Lett.,* vol. 104, no. 2, p. 21105, 2014.

[68] H. Zhang *et al.*, "Compositionally graded III-nitride alloys: building blocks for efficient ultraviolet optoelectronics and power electronics," *Rep. Prog. Phys.*, vol. 84, no. 4, p. 044401, 2021.

[69] Z. Zhang *et al.*, "A 271.8 nm deep-ultraviolet laser diode for room temperature operation," *Appl. Phys. Express,* vol. 12, no. 12, p. 124003, 2019.

[70] Z. Zhang *et al.*, "Space charge profile study of AlGaN-based p-type distributed polarization doped claddings without impurity doping for UV-C laser diodes," *Appl. Phys. Lett.,* vol. 117, no. 15, p. 152104, 2020.

[71] Z. Zhang *et al.*, "Continuous-wave lasing of AlGaN-based ultraviolet laser diode at 274.8 nm by current injection," *Appl. Phys. Express*, vol. 15, no. 4, p. 041007, 2022.

[72] T. Takano, T. Mino, J. Sakai, N. Noguchi, K. Tsubaki, and H. Hirayama, "Deep-ultraviolet light-emitting diodes with external quantum efficiency higher than 20% at 275 nm achieved by improving light-extraction efficiency," *Appl. Phys. Express*, vol. 10, no. 3, p. 031002, 2017.

[73] Y. Kashima *et al.*, "High external quantum efficiency (10%) AlGaN-based deep-ultraviolet light-emitting diodes achieved by using highly reflective photonic crystal on p-AlGaN contact layer," *Appl. Phys. Express,* vol. 11, no. 1, p. 012101, 2018.

[74] M. Shatalov *et al.*, "AlGaN Deep-Ultraviolet Light-Emitting Diodes with External Quantum Efficiency above 10%," *Appl. Phys. Express*, vol. 5, no. 8, p. 082101, 2012.

[75] M. Ichikawa *et al.*, "High-output-power deep ultraviolet light-emitting diode assembly using direct bonding," *Appl. Phys. Express*, vol. 9, no. 7, p. 072101, 2016.

[76] A. Pandey, W. J. Shin, J. Gim, R. Hovden, and Z. Mi, "High-efficiency AlGaN/GaN/AlGaN tunnel junction ultraviolet light-emitting diodes," *Photon. Res.,* vol. 8, no. 3, pp. 331-337, 2020.

[77] A. Pandey, J. Gim, R. Hovden, and Z. Mi, "An AlGaN tunnel junction light emitting diode operating at 255 nm," *Appl. Phys. Lett.*, vol. 117, no. 24, p. 241101, 2020.

[78] P. Wang *et al.*, "Graphene-assisted molecular beam epitaxy of AlN for AlGaN deep-ultraviolet light-emitting diodes," *Appl. Phys. Lett.,* vol. 116, no. 17, p. 171905, 2020.

[79] M. Ichikawa, T. Kemmochi, T. Mukai, M. Uomoto, and T. Shimatsu, "Fabrication of High Power Deep Ultraviolet Light-Emitting Diodes with Glass Lenses Using Atomic Diffusion Bonding," *ECS J. Solid State Sci. Technol.*, vol. 9, no. 1, p. 015004, 2020.

[80] N. Lobo-Ploch *et al.*, "Milliwatt power 233 nm AlGaN-based deep UV-LEDs on sapphire substrates," *Appl. Phys. Lett.,* vol. 117, no. 11, p. 111102, 2020.

[81] D. Liu *et al.*, "226 nm AlGaN/AlN UV LEDs using p-type Si for hole injection and UV reflection," *Appl. Phys. Lett.,* vol. 113, no. 1, 2018.

[82] D. Liu *et al.*, "229 nm UV LEDs on aluminum nitride single crystal substrates using p-type silicon for increased hole injection," *Appl. Phys. Lett.*, vol. 112, no. 8, p. 081101, 2018.

[83] M. Guttmann *et al.*, "Optical light polarization and light extraction efficiency of AlGaN-based LEDs emitting between 264 and 220 nm," *Jpn. J. Appl. Phys.,* vol. 58, no. SC, p. SCCB20, 2019.

[84] Y. Taniyasu, M. Kasu, and T. Makimoto, "An aluminium nitride light-emitting diode with a wavelength of 210 nanometres," (in eng), *Nature,* vol. 441, no. 7091, pp. 325-8, 2006.

[85] O. Reentilä *et al.*, "Effect of the AIN nucleation layer growth on AlN material quality," *J. Cryst. Growth,* vol. 310, no. 23, pp. 4932-4934, 2008.

[86] M. Imura *et al.*, "Dislocations in AlN Epilayers Grown on Sapphire Substrate by High-Temperature Metal-Organic Vapor Phase Epitaxy," *Jpn. J. Appl. Phys.,* vol. 46, no. 4A, pp. 1458-1462, 2007.

[87] C. Huang, H. Zhang, and H. Sun, "Ultraviolet optoelectronic devices based on AlGaN-SiC platform: Towards monolithic photonics integration system," *Nano Energy,* vol. 77, p. 105149, 2020.

[88] R. R. Sumathi, "Review—Status and Challenges in Hetero-epitaxial Growth Approach for Large Diameter AlN Single Crystalline Substrates," *ECS J. Solid State Sci. Technol.*, vol. 10, no. 3, p. 035001, 2021.

[89] S. Zhao *et al.*, "Aluminum nitride nanowire light emitting diodes: Breaking the fundamental bottleneck of deep ultraviolet light sources," *Sci. Rep.*, vol. 5, p. 8332, 2015.

[90] S. Zhao, M. Djavid, and Z. Mi, "Surface Emitting, High Efficiency Near-Vacuum Ultraviolet Light Source with Aluminum Nitride Nanowires Monolithically Grown on Silicon," *Nano Lett.*, vol. 15, no. 10, pp. 7006-7009, 2015.

[91] B. K. SaifAddin *et al.*, "AlGaN Deep-Ultraviolet Light-Emitting Diodes Grown on SiC Substrates," *ACS Photonics*, vol. 7, no. 3, pp. 554-561, 2020.

[92] H. Liang *et al.*, "Vertically conducting deep-ultraviolet light-emitting diodes with interband tunneling junction grown on 6H-SiC substrate," *Jpn. J. Appl. Phys.*, vol. 55, no. 3, p. 031202, 2016.

[93] Y. J. Sung, D.-W. Kim, G. Y. Yeom, and K. S. Kim, "Performance of vertical type deep UV light-emitting diodes depending on the Ga-face n-contact hole density," *Appl. Phys. Lett.*, vol. 118, no. 23, 2021.

[94] M. Takeuchi, T. Maegawa, H. Shimizu, S. Ooishi, T. Ohtsuka, and Y. Aoyagi, "AlN/AlGaN short-period superlattice sacrificial layers in laser lift-off for vertical-type AlGaN-based deep ultraviolet light emitting diodes," *Appl. Phys. Lett.*, vol. 94, no. 6, p. 061117, 2009.

[95] R. Collazo *et al.*, "Progress on n-type doping of AlGaN alloys on AlN single crystal substrates for UV optoelectronic applications," *Phys. Status Solidi (c)*, vol. 8, no. 7-8, pp. 2031-2033, 2011.

[96] F. Mehnke *et al.*, "Electronic properties of Si-doped Alx Ga1−xN with aluminum mole fractions above 80%," *J. Appl. Phys.*, vol. 120, no. 14, p. 145702, 2016.

[97] F. Mehnke *et al.*, "Highly conductive n-AlxGa1−xN layers with aluminum mole fractions above 80%," *Appl. Phys. Lett.*, vol. 103, no. 21, p. 212109, 2013.

[98] H. Ahmad, Z. Engel, C. M. Matthews, S. Lee, and W. A. Doolittle, "Realization of homojunction PN AlN diodes," *J. Appl. Phys.*, vol. 131, no. 17, p. 175701, 2022.

[99] T. D. Moustakas, "Ultraviolet optoelectronic devices based on AIGaN alloys grown by molecular beam epitaxy," *MRS Commun.*, vol. 6, no. 3, pp. 247-269, 2016.

[100] Y. H. Liang and E. Towe, "Progress in efficient doping of high aluminum-containing group III-nitrides," *Appl. Phys. Rev.*, vol. 5, no. 1, p. 011107, 2018.

[101] T. Xu, C. Thomidis, I. Friel, and T. D. Moustakas, "Growth and silicon doping of AlGaN films in the entire alloy composition by molecular beam epitaxy," *Phys. Status Solidi (c)*, vol. 2, no. 7, pp. 2220-2223, 2005.

[102] T. Ive, O. Brandt, H. Kostial, K. J. Friedland, L. Däweritz, and K. H. Ploog, "Controlled n-type doping of AlN:Si films grown on 6H-SiC(0001) by plasma-assisted molecular beam epitaxy," *Appl. Phys. Lett.*, vol. 86, no. 2, p. 024106, 2005.

[103] I. Bryan *et al.*, "Doping and compensation in Al-rich AlGaN grown on single crystal AlN and sapphire by MOCVD," *Appl. Phys. Lett.*, vol. 112, no. 6, p. 062102, 2018.

[104] K. B. Nam, M. L. Nakarmi, J. Y. Lin, and H. X. Jiang, "Deep impurity transitions involving cation vacancies and complexes in AlGaN alloys," *Appl. Phys. Lett.*, vol. 86, no. 22, p. 222108, 2005.

[105] N. Nepal, M. L. Nakarmi, J. Y. Lin, and H. X. Jiang, "Photoluminescence studies of impurity transitions in AlGaN alloys," *Appl. Phys. Lett.*, vol. 89, no. 9, p. 092107, 2006.

[106] C. G. Van de Walle and J. Neugebauer, "First-principles calculations for defects and impurities: Applications to III-nitrides," *J. Appl. Phys.*, vol. 95, no. 8, pp. 3851-3879, 2004.

[107] S. Petit, R. Jones, M. J. Shaw, P. R. Briddon, B. Hourahine, and T. Frauenheim, "Electronic behavior of rare-earth dopants in AlN: A density-functional study," *Phys. Rev. B*, vol. 72, no. 7, p. 073205, 2005.

[108] R. Zeisel *et al.*, "DX-behavior of Si in AlN," *Phys. Rev. B*, vol. 61, no. 24, pp. R16283-R16286, 2000.

[109] M. L. Nakarmi, K. H. Kim, K. Zhu, J. Y. Lin, and H. X. Jiang, "Transport properties of highly conductive n-type Al-rich AlxGa1−xN(x⩾0.7)," *Appl. Phys. Lett.*, vol. 85, no. 17, pp. 3769-3771, 2004.

[110] J. Li, T. N. Oder, M. L. Nakarmi, J. Y. Lin, and H. X. Jiang, "Optical and electrical properties of Mg-doped p-type AlxGa1−xN," *Appl. Phys. Lett.*, vol. 80, no. 7, pp. 1210-1212, 2002.

[111] K. B. Nam, M. L. Nakarmi, J. Li, J. Y. Lin, and H. X. Jiang, "Mg acceptor level in AlN probed by deep ultraviolet photoluminescence," *Appl. Phys. Lett.*, vol. 83, no. 5, pp. 878-880, 2003.

[112] N. Nepal, M. L. Nakarmi, H. U. Jang, J. Y. Lin, and H. X. Jiang, "Growth and photoluminescence studies of Zn-doped AlN epilayers," *Appl. Phys. Lett.*, vol. 89, no. 19, p. 192111, 2006.

[113] A. Sedhain, T. M. A. Tahtamouni, J. Li, J. Y. Lin, and H. X. Jiang, "Beryllium acceptor binding energy in AlN," *Appl. Phys. Lett.*, vol. 93, no. 14, p. 141104, 2008.

[114] J. C. Zolper, R. G. Wilson, S. J. Pearton, and R. A. Stall, "Ca and O ion implantation doping of GaN," *Appl. Phys. Lett.*, vol. 68, no. 14, pp. 1945-1947, 1996.

[115] T. Mattila and R. M. Nieminen, "Ab initio study of oxygen point defects in GaAs, GaN, and AlN," *Phys. Rev. B*, vol. 54, no. 23, pp. 16676-16682, 1996.

[116] T. Mattila and R. M. Nieminen, "Point-defect complexes and broadband luminescence in GaN and AlN," *Phys. Rev. B*, vol. 55, no. 15, pp. 9571-9576, 1997.

[117] C. Stampfl and C. G. de Walle, "Theoretical investigation of native defects, impurities, and complexes in aluminum nitride," *Phys. Rev. B*, vol. 65, no. 15, p. 155212, 2002.

[118] M. L. Nakarmi, N. Nepal, J. Y. Lin, and H. X. Jiang, "Photoluminescence studies of impurity transitions in Mg-doped AlGaN alloys," *Appl. Phys. Lett.*, vol. 94, no. 9, p. 091903, 2009.

[119] Y. Nakagawa *et al.*, "Hydrogen Dissociation from Mg-doped {GaN}," *Jpn. J. Appl. Phys.*, vol. 43, no. 1, pp. 23-29, 2004.

[120] Y. Liao *et al.*, "Development of Milliwatt Power AlGaN-based Deep UV-LEDs by Plasma-assisted Molecular Beam Epitaxy," *MRS Proceedings*, vol. 1202, pp. 1202-I10-01, 2009.

[121] B. P. Gunning *et al.*, "Comprehensive study of the electronic and optical behavior of highly degenerate p-type Mg-doped GaN and AlGaN," *J. Appl. Phys.*, vol. 117, no. 4, p. 45710, 2015.

[122] B. Gunning, J. Lowder, M. Moseley, and W. Alan Doolittle, "Negligible carrier freeze-out facilitated by impurity band conduction in highly p-type GaN," *Appl. Phys. Lett.*, vol. 101, no. 8, p. 82106, 2012.

[123] Y. H. Liang and E. Towe, "Heavy Mg-doping of (Al,Ga)N films for potential applications in deep ultraviolet light-emitting structures," *J. Appl. Phys.*, vol. 123, no. 9, p. 95303, 2018.

[124] P. Bagheri *et al.*, "Doping and compensation in heavily Mg doped Al-rich AlGaN films," *Appl. Phys. Lett.*, vol. 120, no. 8, p. 082102, 2022.

[125] Y. Chen *et al.*, "High hole concentration in p-type AlGaN by indium-surfactant-assisted Mg-delta doping," *Appl. Phys. Lett.*, vol. 106, no. 16, p. 162102, 2015.

[126] P. Kozodoy *et al.*, "Heavy doping effects in Mg-doped GaN," *J. Appl. Phys.*, vol. 87, no. 4, pp. 1832-1835, 2000.

[127] A. Chakraborty *et al.*, "Electrical and structural characterization of Mg-doped p-type Al0.69Ga0.31N films on SiC substrate," *J. Appl. Phys.*, vol. 101, no. 5, p. 053717, 2007.

[128] R. Kirste *et al.*, "Compensation effects in GaN:Mg probed by Raman spectroscopy and photoluminescence measurements," *J. Appl. Phys.*, vol. 113, no. 10, p. 103504, 2013.

[129] S. Usami *et al.*, "Direct evidence of Mg diffusion through threading mixed dislocations in GaN p–n diodes and its effect on reverse leakage current," *Appl. Phys. Lett.*, vol. 114, no. 23, p. 232105, 2019.

[130] T. Nakano *et al.*, "Screw dislocation that converts p-type GaN to n-type: Microscopic study on Mg condensation and leakage current in p–n diodes," *Appl. Phys. Lett.*, vol. 117, no. 1, p. 012105, 2020.

[131] S. Usami *et al.*, "Correlation between dislocations and leakage current of p-n diodes on a free-standing GaN substrate," *Appl. Phys. Lett.*, vol. 112, no. 18, p. 182106, 2018.

[132] S. R. Jeon *et al.*, "Investigation of Mg doping in high-Al content p-type AlxGa1−xN (0.3<x<0.5)," *Appl. Phys. Lett.*, vol. 86, no. 8, p. 82107, 2005.

[133] T. Kinoshita, T. Obata, H. Yanagi, and S.-i. Inoue, "High p-type conduction in high-Al content Mg-doped AlGaN," *Appl. Phys. Lett.*, vol. 102, no. 1, p. 12105, 2013.

[134] H. Ahmad, J. Lindemuth, Z. Engel, C. M. Matthews, T. M. McCrone, and W. A. Doolittle, "Substantial P-Type Conductivity of AlN Achieved via Beryllium Doping," *Adv. Mater.*, vol. 33, no. 42, p. 2104497, 2021.

[135] Y. S. Wu, J.-H. Cheng, W. C. Peng, and H. Ouyang, "Effects of laser sources on the reverse-bias leakages of laser lift-off GaN-based light-emitting diodes," *Appl. Phys. Lett.*, vol. 90, no. 25, 2007.

[136] W. H. Chen *et al.*, "Study of the structural damage in the (0001) GaN epilayer processed by laser lift-off techniques," *Appl. Phys. Lett.*, vol. 91, no. 12, p. 121114, 2007.

[137] Y. Sun *et al.*, "Microanalyses of the reverse-bias leakage current increase in the laser lift off GaN-based light emitting diodes," *J. Appl. Phys.*, vol. 106, no. 1, p. 013101, 2009.

[138] F. Jiang, J. Zhang, Q. Sun, and Z. Quan, "GaN LEDs on Si Substrate," in *Light-Emitting Diodes*, (Solid State Lighting Technology and Application Series, 2019, ch. Chapter 4, pp. 133-170.

[139] Q. Sun *et al.*, "GaN-on-Si blue/white LEDs: epitaxy, chip, and package," *J. Semicond.* , vol. 37 p. 044006, 2016.

[140] M. Hochberg and T. Baehr-Jones, "Towards fabless silicon photonics," *Nat. Photonics,* vol. 4, no. 8, pp. 492-494, 2010.

[141] A. Rickman, "The commercialization of silicon photonics," *Nat. Photonics,* vol. 8, no. 8, pp. 579-582, 2014.

[142] M. Fraga, M. Bosi, and M. Negri, "Silicon Carbide in Microsystem Technology — Thin Film Versus Bulk Material," 2015.

[143] K. M. Lau, K. M. Wong, X. Zou, and P. Chen, "Performance improvement of GaN-based light-emitting diodes grown on patterned Si substrate transferred to copper," *Opt. Express,* vol. 19, no. S4, pp. A956-A961, 2011.

[144] X. Zou, X. Zhang, W. C. Chong, C. W. Tang, and K. M. Lau, "Vertical LEDs on Rigid and Flexible Substrates Using GaN-on-Si Epilayers and Au-Free Bonding," *IEEE Trans. Electron Devices,* vol. 63, no. 4, pp. 1587-1593, 2016.

[145] Y. Li *et al.*, "High-performance vertical GaN-based near-ultraviolet light-emitting diodes on Si substrates," *J. Mater. Chem. C,* vol. 6, no. 42, pp. 11255-11260, 2018.

[146] W. Wang *et al.*, "High-efficiency vertical-structure GaN-based light-emitting diodes on Si substrates," *J. Mater. Chem. C,* vol. 6, no. 7, pp. 1642-1650, 2018.

[147] D. E. Aspnes and A. A. Studna, "Dielectric functions and optical parameters of Si, Ge, GaP, GaAs, GaSb, InP, InAs, and InSb from 1.5 to 6.0 eV," *Phys. Rev. B,* vol. 27, no. 2, pp. 985-1009, 1983.

[148] M. A. Green, "Self-consistent optical parameters of intrinsic silicon at 300K including temperature coefficients," *Sol. Energy Mater. Sol. Cells,* vol. 92, no. 11, pp. 1305-1310, 2008.

[149] Y. Li *et al.*, "Nucleation layer design for growth of a high-quality AlN epitaxial film on a Si(111) substrate," *CrystEngComm,* vol. 20, no. 11, pp. 1483-1490, 2018.

[150] T. Szymański, M. Wośko, M. Wzorek, B. Paszkiewicz, and R. Paszkiewicz, "Origin of surface defects and influence of an in situ deposited SiN nanomask on the properties of

strained AlGaN/GaN heterostructures grown on Si(111) using metal–organic vapour phase epitaxy," *CrystEngComm*, vol. 18, no. 45, pp. 8747-8755, 2016.

[151] Y. Feng *et al.*, "Competitive growth mechanisms of AlN on Si (111) by MOVPE," *Sci. Rep.*, vol. 4, no. 1, p. 6416, 2014.

[152] L. Niu, Z. Hao, Y. E, J. Hu, L. Wang, and Y. Luo, "MBE-grown AlN-on-Si with improved crystalline quality by using silicon-on-insulator substrates," *Appl. Phys. Express*, vol. 7, no. 6, p. 065505, 2014.

[153] S. S. Sharofidinov *et al.*, "On a reduction in cracking upon the growth of AlN on Si substrates by hydride vapor-phase epitaxy," *Semiconductors*, vol. 50, no. 4, pp. 541-544, 2016.

[154] X.-Q. Shen, T. Takahashi, T. Ide, and M. Shimizu, "High quality thin AlN epilayers grown on Si(110) substrates by metal-organic chemical vapor deposition," *CrystEngComm*, vol. 19, no. 8, pp. 1204-1209, 2017.

[155] B. T. Tran, N. Maeda, M. Jo, D. Inoue, T. Kikitsu, and H. Hirayama, "Performance Improvement of AlN Crystal Quality Grown on Patterned Si(111) Substrate for Deep UV-LED Applications," *Sci. Rep.*, vol. 6, p. 35681, 2016.

[156] A. S. Hussein, S. M. Thahab, Z. Hassan, C. W. Chin, H. Abu Hassan, and S. S. Ng, "High Al-content AlxGa1−xN epilayers grown on Si substrate by plasma-assisted molecular beam epitaxy," *J. Alloys Compd.*, vol. 487, no. 1, pp. 24-27, 2009.

[157] T. D. Moustakas, "Molecular Beam Epitaxy: Thin Film Growth and Surface Studies," *MRS Bull.*, vol. 13, no. 11, pp. 29-36, 1988.

[158] X. Wang and A. Yoshikawa, "Molecular beam epitaxy growth of GaN, AlN and InN," *Prog. Cryst. Growth Charact. Mater.*, vol. 48-49, pp. 42-103, 2004.

[159] M. M. Oye *et al.*, "Effects of different plasma species (atomic N, metastable N2*, and ions) on the optical properties of dilute nitride materials grown by plasma-assisted molecular-beam epitaxy," *Appl. Phys. Lett.*, vol. 91, no. 19, p. 191903, 2007.

[160] Z. Sitar, M. J. Paisley, B. Yan, and R. F. Davis, "Structural Defects in GaN Epilayers Grown by Gas Source Molecular Beam Epitaxy," *MRS Online Proc. Libr.*, vol. 162, no. 1, pp. 537-541, 1989.

[161] K. Yasutake, A. Takeuchi, H. Kakiuchi, and K. Yoshii, "Molecular beam epitaxial growth of AlN single crystalline films on Si (111) using radio-frequency plasma assisted nitrogen radical source," *J. Vac. Sci. Technol. A,* vol. 16, no. 4, pp. 2140-2147, 1998.

[162] V. A. Grant, R. P. Campion, C. T. Foxon, W. Lu, S. Chao, and E. C. Larkins, "Optimization of RF plasma sources for the MBE growth of nitride and dilute nitride semiconductor material," *Semicond. Sci. Technol.,* vol. 22, no. 2, p. 15, 2007.

[163] S. Agarwal, B. Hoex, M. C. M. van de Sanden, D. Maroudas, and E. S. Aydil, "Absolute densities of N and excited N2 in a N2 plasma," *Appl. Phys. Lett.,* vol. 83, no. 24, pp. 4918-4920, 2003.

[164] Q. Zhuang, "1 - Molecular beam epitaxy (MBE) growth of nitride semiconductors," in *Nitride Semiconductor Light-Emitting Diodes (LEDs) (Second Edition)*, J. Huang, H.-C. Kuo, and S.-C. Shen Eds.: Woodhead Publishing, 2018, pp. 3-23.

[165] R. A. Kubiak, S. M. Newstead, and P. Sullivan, "1 - The Technology and Design of Molecular Beam Epitaxy Systems," in *Molecular Beam Epitaxy*, R. F. C. Farrow Ed. Park Ridge, NJ: William Andrew Publishing, 1995, pp. 1-113.

[166] E. J. Tarsa, B. Heying, X. H. Wu, P. Fini, S. P. DenBaars, and J. S. Speck, "Homoepitaxial growth of GaN under Ga-stable and N-stable conditions by plasma-assisted molecular beam epitaxy," *J. Appl. Phys.,* vol. 82, no. 11, pp. 5472-5479, 1997.

[167] A. R. Smith, R. M. Feenstra, D. W. Greve, J. Neugebauer, and J. E. Northrup, "Reconstructions of the $\mathrm{GaN}(000\overline{1})$ Surface," *Phys. Rev. Lett.,* vol. 79, no. 20, pp. 3934-3937, 1997.

[168] A. R. Smith *et al.*, "Determination of wurtzite GaN lattice polarity based on surface reconstruction," *Appl. Phys. Lett.,* vol. 72, no. 17, pp. 2114-2116, 1998.

[169] C. D. Lee, Y. Dong, R. M. Feenstra, J. E. Northrup, and J. Neugebauer, "Reconstructions of the AlN(0001) surface," *Phys. Rev. B,* vol. 68, no. 20, p. 205317, 2003.

[170] T. Lei, M. Fanciulli, R. J. Molnar, T. D. Moustakas, R. J. Graham, and J. Scanlon, "Epitaxial growth of zinc blende and wurtzitic gallium nitride thin films on (001) silicon," *Appl. Phys. Lett.,* vol. 59, no. 8, pp. 944-946, 1991.

[171] T. Lei and T. D. Moustakas, "A Comparative Study of GaN Epitaxy on Si(001) and SI(111) Substrates," *MRS Online Proc. Libr.,* vol. 242, no. 1, pp. 433-439, 1992.

[172] T. Lei, K. F. Ludwig, and T. D. Moustakas, "Heteroepitaxy, polymorphism, and faulting in GaN thin films on silicon and sapphire substrates," *J. Appl. Phys.*, vol. 74, no. 7, pp. 4430-4437, 1993.

[173] K. S. Stevens, A. Ohtani, A. F. Schwartzman, and R. Beresford, "Growth of group III nitrides on Si(111) by plasma‐assisted molecular beam epitaxy," *J. Vac. Sci. Technol., B: Microelectron. Nanometer Struct.--Process., Meas., Phenom.*, vol. 12, no. 2, pp. 1186-1189, 1994.

[174] A. Ohtani, K. S. Stevens, and R. Beresford, "Microstructure and photoluminescence of GaN grown on Si(111) by plasma‐assisted molecular beam epitaxy," *Appl. Phys. Lett.*, vol. 65, no. 1, pp. 61-63, 1994.

[175] M. Miyauchi, Y. Ishikawa, and N. Shibata, "Growth of Aluminum Nitride Films on Silicon by Electron-Cyclotron-Resonance-Assisted Molecular Beam Epitaxy," *Jpn. J. Appl. Phys.*, vol. 31, no. Part 2, No. 12A, pp. L1714-L1717, 1992.

[176] E. Calleja *et al.*, "Growth kinetics and morphology of high quality AlN grown on Si(111) by plasma-assisted molecular beam epitaxy," *J. Appl. Phys.*, vol. 82, no. 9, pp. 4681-4683, 1997.

[177] M. A. Sanchez-Garcia *et al.*, "The effect of the III/V ratio and substrate temperature on the morphology and properties of GaN- and AlN-layers grown by molecular beam epitaxy on Si(1 1 1)," *J. Cryst. Growth*, vol. 183, no. 1, pp. 23-30, 1998.

[178] S. Guha and N. A. Bojarczuk, "GaN based light emitting diodes grown on Si(111) by molecular beam epitaxy," *Electronics Letters*, vol. 33, no. 23, pp. 1986-1987

[179] S. Guha and N. A. Bojarczuk, "Multicolored light emitters on silicon substrates," *Appl. Phys. Lett.*, vol. 73, no. 11, pp. 1487-1489, 1998.

[180] S. Guha and N. A. Bojarczuk, "Ultraviolet and violet GaN light emitting diodes on silicon," *Appl. Phys. Lett.*, vol. 72, no. 4, pp. 415-417, 1998.

[181] E. Calleja *et al.*, "Growth of III-nitrides on Si(111) by molecular beam epitaxy Doping, optical, and electrical properties," *J. Cryst. Growth*, vol. 201-202, pp. 296-317, 1999.

[182] M. A. Sánchez-García *et al.*, "MBE growth of GaN and AlGaN layers on Si(111) substrates: doping effects," *J. Cryst. Growth*, vol. 201-202, pp. 415-418, 1999.

[183] S. A. Nikishin, N. N. Faleev, A. S. Zubrilov, V. G. Antipov, and H. Temkin, "Growth of AlGaN on Si(111) by gas source molecular beam epitaxy," *Appl. Phys. Lett.,* vol. 76, no. 21, pp. 3028-3030, 2000.

[184] S. Nikishin *et al.*, "Gas source molecular beam epitaxy of high quality AlxGa1−xN (0⩽x⩽1) on Si(111)," *J. Vac. Sci. Technol., B: Microelectron. Nanometer Struct.--Process., Meas., Phenom.,* vol. 19, no. 4, pp. 1409-1412, 2001.

[185] M. A. Sánchez-García, F. B. Naranjo, J. L. Pau, A. Jiménez, E. Calleja, and E. Muñoz, "Ultraviolet electroluminescence in GaN/AlGaN single-heterojunction light-emitting diodes grown on Si(111)," *J. Appl. Phys.,* vol. 87, no. 3, pp. 1569-1571, 2000.

[186] K. A. Bertness, A. Roshko, L. M. Mansfield, T. E. Harvey, and N. A. Sanford, "Mechanism for spontaneous growth of GaN nanowires with molecular beam epitaxy," *J. Cryst. Growth,* vol. 310, no. 13, pp. 3154-3158, 2008.

[187] J. Ristić *et al.*, "On the mechanisms of spontaneous growth of III-nitride nanocolumns by plasma-assisted molecular beam epitaxy," *J. Cryst. Growth,* vol. 310, no. 18, pp. 4035-4045, 2008.

[188] A. Pierret *et al.*, "Growth, structural and optical properties of {AlGaN} nanowires in the whole composition range," *Nanotechnology,* vol. 24, no. 11, p. 115704, 2013.

[189] R. K. Debnath, R. Meijers, T. Richter, T. Stoica, R. Calarco, and H. Lüth, "Mechanism of molecular beam epitaxy growth of GaN nanowires on Si(111)," *Appl. Phys. Lett.,* vol. 90, no. 12, p. 123117, 2007.

[190] S. Fan, S. Zhao, X. Liu, and Z. Mi, "Study on the coalescence of dislocation-free GaN nanowires on Si and SiOx," *J. Vac. Sci. Technol., B: Microelectron. Nanometer Struct.--Process., Meas., Phenom.,* vol. 32, no. 2, p. 02C114, 2014.

[191] G. Calabrese *et al.*, "Molecular beam epitaxy of single crystalline GaN nanowires on a flexible Ti foil," *Appl. Phys. Lett.,* vol. 108, no. 20, p. 202101, 2016.

[192] B. J. May, A. T. M. G. Sarwar, and R. C. Myers, "Nanowire LEDs grown directly on flexible metal foil," *Appl. Phys. Lett.,* vol. 108, no. 14, p. 141103, 2016.

[193] C. Zhao *et al.*, "III-nitride nanowires on unconventional substrates: From materials to optoelectronic device applications," *Prog. Quantum Electron,* vol. 61, pp. 1-31, 2018.

[194] T. Araki *et al.*, "Radio-frequency plasma-excited molecular beam epitaxy growth of GaN on graphene/Si(100) substrates," *Appl. Phys. Express,* vol. 7, no. 7, p. 071001, 2014.

[195] I. M. Høiaas *et al.*, "GaN/AlGaN Nanocolumn Ultraviolet Light-Emitting Diode Using Double-Layer Graphene as Substrate and Transparent Electrode," *Nano Lett.*, vol. 19, no. 3, pp. 1649-1658, 2019.

[196] A. Liudi Mulyo, M. K. Rajpalke, P. E. Vullum, H. Weman, K. Kishino, and B.-O. Fimland, "The influence of AlN buffer layer on the growth of self-assembled GaN nanocolumns on graphene," *Sci. Rep.*, vol. 10, no. 1, p. 853, 2020.

[197] S. Zhao, S. M. Sadaf, S. Vanka, Y. Wang, R. Rashid, and Z. Mi, "Sub-milliwatt AlGaN nanowire tunnel junction deep ultraviolet light emitting diodes on silicon operating at 242 nm," *Appl. Phys. Lett.*, vol. 109, no. 20, p. 201106, 2016.

[198] S. Zhao, X. Liu, Y. Wu, and Z. Mi, "An electrically pumped 239 nm AlGaN nanowire laser operating at room temperature," *Appl. Phys. Lett.*, vol. 109, no. 19, p. 191106, 2016.

[199] K. H. Li, X. Liu, Q. Wang, S. Zhao, and Z. Mi, "Ultralow-threshold electrically injected AlGaN nanowire ultraviolet lasers on Si operating at low temperature," *Nat. Nanotechnol.*, vol. 10, no. 2, pp. 140-144, 2015.

[200] S. Zhao and Z. Mi, "AlGaN Nanowires: Path to Electrically Injected Semiconductor Deep Ultraviolet Lasers," *IEEE J. Quantum Electron.*, vol. 54, no. 6, pp. 1-9, 2018.

[201] K. L. Averett, J. E. Van Nostrand, J. D. Albrecht, Y. S. Chen, and C. C. Yang, "Epitaxial overgrowth of GaN nanocolumns," *J. Vac. Sci. Technol., B: Microelectron. Nanometer Struct.--Process., Meas., Phenom.*, vol. 25, no. 3, pp. 964-968, 2007.

[202] P. Dogan *et al.*, "Formation of High-Quality GaN Microcrystals by Pendeoepitaxial Overgrowth of GaN Nanowires on Si(111) by Molecular Beam Epitaxy," *Crys. Growth Des.*, vol. 11, no. 10, pp. 4257-4260, 2011.

[203] A. Aiello, D. Das, and P. Bhattacharya, "InGaN/GaN Quantum Dot Light-Emitting Diodes on Silicon with Coalesced GaN Nanowire Buffer Layer," *ACS Appl. Nano Mater.*, vol. 4, no. 2, pp. 1825-1830, 2021.

[204] X. Yin, Q. Zhang, and S. Zhao, "Molecular Beam Epitaxial Growth of AlN Thin Films on Si through Exploiting Low Al Adatom Migration and the Nitrogen-Rich Environment on a Nanowire Template," *Crys. Growth Des.*, vol. 21, no. 7, pp. 3645-3649, 2021.

[205] Q. Zhang, X. Yin, E. Martel, and S. Zhao, "Molecular beam epitaxy growth and characterization of AlGaN epilayers in nitrogen-rich condition on Si substrate," *Mater. Sci. Semicond. Process.*, vol. 135, p. 106099, 2021.

[206] X. Yin and S. Zhao, "High Internal Quantum Efficiency AlGaN Epilayer Grown by Molecular Beam Epitaxy on Si Substrate," *ECS J. Solid State Sci. Technol.*, vol. 10, no. 7, p. 076001, 2021.

[207] G. Koblmüller, F. Wu, T. Mates, J. S. Speck, S. Fernández-Garrido, and E. Calleja, "High electron mobility GaN grown under N-rich conditions by plasma-assisted molecular beam epitaxy," *Appl. Phys. Lett.*, vol. 91, no. 22, p. 221905, 2007.

[208] H. Tang, S. M. Sadaf, X. Wu, and W. Jiang, "Highly efficient p-type doping of GaN under nitrogen-rich and low-temperature conditions by plasma-assisted molecular beam epitaxy," *AIP Advances*, vol. 9, no. 5, p. 55008, 2019.

[209] M. Zhang, P. Bhattacharya, W. Guo, and A. Banerjee, "Mg doping of GaN grown by plasma-assisted molecular beam epitaxy under nitrogen-rich conditions," *Appl. Phys. Lett.*, vol. 96, no. 13, p. 132103, 2010.

[210] L. Zhang *et al.*, "Three-dimensional hole gas induced by polarization in (0001)-oriented metal-face III-nitride structure," *Appl. Phys. Lett.*, vol. 97, no. 6, p. 062103, 2010.

[211] S. Li *et al.*, "Polarization induced hole doping in graded \$Al_xGa_{1-x}N\$ (x = 0.7 ~ 1) layer grown by molecular beam epitaxy," *Appl. Phys. Lett.*, vol. 102, no. 6, p. 62108, 2013.

[212] J. Glaab *et al.*, "Skin tolerant inactivation of multiresistant pathogens using far-UVC LEDs," *Sci. Rep.*, vol. 11, no. 1, p. 14647, 2021.

[213] I. R. M. Barnard, E. Eadie, and K. Wood, "Further evidence that far-UVC for disinfection is unlikely to cause erythema or pre-mutagenic DNA lesions in skin," *Photodermatol., Photoimmunol. Photomed.*, vol. 36, no. 6, pp. 476-477, 2020.

[214] R. P. Hickerson *et al.*, "Minimal, superficial DNA damage in human skin from filtered far-ultraviolet C," *Br. J. Dermatol.*, vol. 184, no. 6, pp. 1197-1199, 2021.

[215] C. Liu, Y. K. Ooi, S. M. Islam, H. Xing, D. Jena, and J. Zhang, "234 nm and 246 nm AlN-Delta-GaN quantum well deep ultraviolet light-emitting diodes," *Appl. Phys. Lett.*, vol. 112, no. 1, p. 011101, 2018.

[216] S. M. Islam *et al.*, "MBE-grown 232–270 nm deep-UV LEDs using monolayer thin binary GaN/AlN quantum heterostructures," *Appl. Phys. Lett.*, vol. 110, no. 4, p. 41108, 2017.

[217] F. Yun *et al.*, "Energy band bowing parameter in AlxGa1−xN alloys," *J. Appl. Phys.*, vol. 92, no. 8, pp. 4837-4839, 2002.

[218] E. Iliopoulos and T. D. Moustakas, "Growth kinetics of AlGaN films by plasma-assisted molecular-beam epitaxy," *Appl. Phys. Lett.*, vol. 81, no. 2, pp. 295-297, 2002.

[219] M. Moseley, D. Billingsley, W. Henderson, E. Trybus, and W. A. Doolittle, "Transient atomic behavior and surface kinetics of GaN," *J. Appl. Phys.*, vol. 106, no. 1, p. 014905, 2009.

[220] H. Ahmad, K. Motoki, E. A. Clinton, C. M. Matthews, Z. Engel, and W. A. Doolittle, "Comprehensive Analysis of Metal Modulated Epitaxial GaN," *ACS Appl. Mater. Interfaces*, vol. 12, no. 33, pp. 37693-37712, 2020.

[221] Z. Engel, E. A. Clinton, K. Motoki, H. Ahmad, C. M. Matthews, and W. A. Doolittle, "Adlayer control for tunable AlGaN self-assembled superlattices," *J. Appl. Phys.*, vol. 130, no. 16, p. 165304, 2021.

[222] L. E. Goff, C. T. Foxon, C. R. Staddon, A. J. Kent, and R. P. Campion, "Anion modulation epitaxy (AME), an alternative growth strategy for group III-nitrides," *Phys. Status Solidi (c)*, vol. 9, no. 3-4, pp. 530-533, 2012.

[223] Y. Horikoshi, M. Kawashima, and H. Yamaguchi, "Migration-Enhanced Epitaxy of GaAs and AlGaAs," *Jpn. J. Appl. Phys.*, vol. 27, no. 2R, p. 169, 1988.

[224] S. M. Islam *et al.*, "Deep-UV emission at 219 nm from ultrathin MBE GaN/AlN quantum heterostructures," *Appl. Phys. Lett.*, vol. 111, no. 9, p. 91104, 2017.

[225] Y. Taniyasu and M. Kasu, "Polarization property of deep-ultraviolet light emission from C-plane AlN/GaN short-period superlattices," *Appl. Phys. Lett.*, vol. 99, no. 25, p. 251112, 2011.

[226] K. Kamiya, Y. Ebihara, K. Shiraishi, and M. Kasu, "Structural design of AlN/GaN superlattices for deep-ultraviolet light-emitting diodes with high emission efficiency," *Appl. Phys. Lett.*, vol. 99, no. 15, p. 151108, 2011.

[227] V. Jmerik, A. Toropov, V. Davydov, and S. Ivanov, "Monolayer‐Thick GaN/AlN Multilayer Heterostructures for Deep‐Ultraviolet Optoelectronics," *Phys. Status Solidi RRL*, vol. 15, p. 2100242, 2021.

[228] K. B. Nam, J. Li, M. L. Nakarmi, J. Y. Lin, and H. X. Jiang, "Unique optical properties of AlGaN alloys and related ultraviolet emitters," *Appl. Phys. Lett.*, vol. 84, no. 25, pp. 5264-5266, 2004.

[229] J. Zhang, H. Zhao, and N. Tansu, "Effect of crystal-field split-off hole and heavy-hole bands crossover on gain characteristics of high Al-content AlGaN quantum well lasers," *Appl. Phys. Lett.*, vol. 97, no. 11, p. 111105, 2010.

[230] J. E. Northrup *et al.*, "Effect of strain and barrier composition on the polarization of light emission from AlGaN/AlN quantum wells," *Appl. Phys. Lett.*, vol. 100, no. 2, p. 021101, 2012.

[231] S. H. Park, "Theoretical study of optical properties in deep ultraviolet Al-rich AlGaN/AIN quantum wells," *Semicond. Sci. Technol.*, vol. 24, no. 3, p. 035002, 2009.

[232] P. Saengkaew *et al.*, "Low-temperature/high-temperature AlN superlattice buffer layers for high-quality AlxGa1−xN on Si (111)," *J. Cryst. Growth*, vol. 311, no. 14, pp. 3742-3748, 2009.

[233] M. L. Nakarmi, B. Cai, J. Y. Lin, and H. X. Jiang, "Three-step growth method for high quality AlN epilayers," *Phys. Status Solidi (a)*, vol. 209, no. 1, pp. 126-129, 2012.

[234] P. Xiang *et al.*, "Improving the Quality of GaN on Si(111) Substrate with a Medium-Temperature/High-Temperature Bilayer AlN Buffer," *Jpn. J. Appl. Phys.*, vol. 52, no. 8S, p. 08jb18, 2013.

[235] A. Yoshikawa and K. Xu, "In situ investigation for polarity-controlled epitaxy processes of GaN and AlN in MBE and MOVPE growth," *Opt. Mater.*, vol. 23, no. 1-2, pp. 7-14, 2003.

[236] K. Xu, N. Yano, A. W. Jia, A. Yoshikawa, and K. Takahashi, "Kinetic Process of Polarity Selection in GaN Growth by RF-MBE," *Phys. Stat. Sol. (b)*, vol. 228, p. 523, 2001.

[237] V. Lebedev, B. Schroter, G. Kipshidze, and W. Richter, "The polarity of AlN films grown on Si(111)," *J. Cryst. Growth*, vol. 207 p. 266, 1999.

[238] T. Auzelle *et al.*, "The influence of AlN buffer over the polarity and the nucleation of self-organized GaN nanowires," *J. Appl. Phys.*, vol. 117, no. 24, p. 245303, 2015.

[239] Z. de Souza Schiaber *et al.*, "Polarity-Induced Selective Area Epitaxy of GaN Nanowires," *Nano Lett.*, vol. 17, no. 1, pp. 63-70, 2017.

[240] E. S. Hellman, "The Polarity of GaN: a Critical Review," *MRS Internet J. Nitride Semicond. Res.*, vol. 3, p. e11, 1998.

[241] W. Guo *et al.*, "KOH based selective wet chemical etching of AlN, AlxGa1−xN, and GaN crystals: A way towards substrate removal in deep ultraviolet-light emitting diode," *Appl. Phys. Lett.,* vol. 106, no. 8, 2015.

[242] D. Zhuang and J. H. Edgar, "Wet etching of GaN, AlN, and SiC: a review," *Mater. Sci. Eng.: R,* vol. 48, no. 1, pp. 1-46, 2005.

[243] Ž. Podlipskas *et al.*, "Dependence of radiative and nonradiative recombination on carrier density and Al content in thick AlGaN epilayers," *J. Phys. D: Appl. Phys.,* vol. 49, no. 14, p. 145110, 2016.

[244] Z. Bryan, I. Bryan, J. Xie, S. Mita, Z. Sitar, and R. Collazo, "High internal quantum efficiency in AlGaN multiple quantum wells grown on bulk AlN substrates," *Appl. Phys. Lett.,* vol. 106, no. 14, p. 142107, 2015.

[245] K. Ban *et al.*, "Internal Quantum Efficiency of Whole-Composition-Range AlGaN Multiquantum Wells," *Appl. Phys. Express,* vol. 4, no. 5, p. 052101, 2011.

[246] Y. Liao, C. Thomidis, C.-k. Kao, and T. D. Moustakas, "AlGaN based deep ultraviolet light emitting diodes with high internal quantum efficiency grown by molecular beam epitaxy," *Appl. Phys. Lett.,* vol. 98, no. 8, p. 81110, 2011.

[247] X. Huang, Z. Zeng, Z. Fan, J. Liu, and H. Zhang, "Graphene-Based Electrodes," *Adv. Mater.,* vol. 24, no. 45, pp. 5979-6004, 2012.

[248] G. Jo, M. Choe, S. Lee, W. Park, Y. H. Kahng, and T. Lee, "The application of graphene as electrodes in electrical and optical devices," *Nanotechnology,* vol. 23, no. 11, p. 112001, 2012.

[249] H. Parimoo, Q. Zhang, M. Vafadar, J. Sivasundarampillai, and S. Zhao, "AlGaN nanowire deep ultraviolet light emitting diodes with graphene electrode," *Appl. Phys. Lett.,* vol. 120, no. 17, p. 171108, 2022.